TREE TRANSPIRATION MAPPING FROM UPSCALED SAP FLOW IN THE BOTSWANA KALAHARI

DIANA CHAVARRO-RINCON
February 2009

TREE TRANSPIRATION MAPPING FROM UPSCALED SAP FLOW IN THE
BOTSWANA KALAHARI

DISSERTATION

to obtain
the degree of doctor at the University of Twente,
on the authority of the rector magnificus,
prof.dr. H. Brinksma,
on account of the decision of the graduation committee,
to be publicly defended
on Thursday February 26, 2009 at 15:00 hrs

by

Diana Chavarro-Rincón

born on 23 December 1965

in Bogotá , Colombia

To my dearest friend Jean Roy

Summary

In arid and semi-arid environments such as the Kalahari, where groundwater represents the main source of water supply, water extraction by vegetation from unsaturated and saturated soil must be carefully identified. Previous studies in the Kalahari have shown that groundwater can be discharged from more than 60m depth in the form of transpiration by deep rooted vegetation. Investigations carried out by the Botswana Government concluded that most of the tree species in the eastern Kalahari make predominant use of soil water from depths of more than 3m, *i.e.* below the root zone of shrubs and grasses. These findings shed light on how certain species remain green during the dry season, but they also raised concerns on the significance of tree transpiration compared to the potential groundwater recharge, thus highlighting the importance of tree transpiration mapping.

This study presents a methodology for the mapping of tree transpiration based on the upscaling of sap flow measurements during the dry season. For that purpose, nine Kalahari tree species namely, *Acacia fleckii, Acacia erioloba, Acacia luederitzii, Boscia albitrunca, Lonchorcarpus nelsii, Terminalia sericea, Burkea Africana, Ochna pulchra* and *Dichrostachys cinerea* were investigated. The selection of these species was based on their frequency of occurrence in the study area. The methodology is presented in two major steps: *i)* sap flow investigations and *ii)* upscaling and mapping. The former was based on ground measurements and follow-up laboratory experiments, and the latter on GIS and RS techniques. This approach is considered adequate for savanna ecosystems in which different species coexist, as it allows the identification of species-dependent transpiration dynamics based on the examination of inherent sap flow patterns. The method was developed for the particular conditions of the Kalahari but it can be used in its general form in other environments

In the first step, sap flow measurements were acquired using thermal dissipation probes (TDP), in which the effect of natural thermal gradients (NTG) was analyzed. Complementary, the issue of conductive sapwood area determination was reviewed at the light of laboratory experiments using X-ray computed tomography (CT) and nuclear magnetic resonance (NMR). Sap flow was calculated as the product of sap flux densities measured with TDP, and sapwood area in groups of 18 to 24 specimens per species. The obtained sap flow patterns suggested unusual water-use habits *e.g.* nocturnal sap flow, downwards stem flow and air moisture harvesting, in four out of the nine species investigated. Such events had to be considered before the upscaling process.

In the second step, mean sap flow of each measured tree was correlated directly or indirectly with a RS-measurable parameter, namely canopy area (CA), for the establishment of species-specific upscaling functions. Five multi-spectral airborne

images at three different resolutions, together with an IKONOS satellite image of the study area were classified using object-oriented approach to allow species differentiation. Accuracy assessment of the classification determined the best resolution in which tree species can be discriminated. Species-specific upscaling functions based on the correlation between CA and sap flow were applied to the classified images, resulting in transpiration maps.

The results showed that among the nine measured species, the presence of the evergreen *Boscia albitrunca* defines areas of high water extraction. The total dry-season transpiration flux in the five images ranged from 0.021mm/day for the image with predominant occurrence of *Dichrostachys cinerea* and *Terminalia sericea*, to 0.165mm/day for the image where *Boscia Albitrunca* was abundant. Transpiration fluxes obtained from the RS-based upscaling approach yielded more realistic values than energy balance methods previously applied in the same area and during the same season. The results presented in this study showed that the combination of ground measurements, laboratory experiments and GIS/RS procedures constitutes a robust approach for the mapping of natural processes such as tree transpiration.

Keywords: GIS/RS, sap flow patterns, TDP, transpiration flux, upscaling.

Acknowledgements

Table of Contents

Chapter 3

Conductive Sapwood Area **43**

An overview of xylem functioning based on NMR

Abstract...**43**

Chapter 4

Dry Season Sap Flow Patterns in the Kalahari **61**

Abstract...**61**

Chapter 7

Appendix

Abbreviations and Acronyms

ADAS	Automatic Data Acquisition System
ADC	Agricultural Digital Camera
AMH	Air Moisture Harvesting
CT	Computed Tomography
CA	Canopy Area
BGS	Botswana Geological Survey
DCA	Digital Compressed Archive
DSF	Downwards Sap Flow
GIS	Geographic Information System
GRES	Groundwater Recharge and Evaluation Study
HL	Hydraulic Lift
HR	Hydraulic Redistribution
ITC	International Institute for Geo-information Science and Earth Observations
KRP	Kalahari Research Project
m.a.s.l.	meters above sea level
MAP	Mean Annual Precipitation
MRI	Magnetic Resonance Imaging
NIR	Near Infra Red
NMR	Nuclear Magnetic Resonance
NTG	Natural Thermal Gradients
PMCC	Pearson's Product-Moment Correlation Coefficient
RS	Remote Sensing
RSE	Residual Standard Error
SGC	Swedish Geological Company
SA	Stem Area
SD	Stem Diameter
SF	Sap Flow
SW	Sapwood Area
STD	Standard Deviation
TDP	Thermal Dissipation Probes
VPD	Vapor Pressure Deficit

When a tree has had part of its bark stripped off,
nature in order to provide for it, supplies to the stripped portion a far
greater quantity of nutritive moisture than to any other part.
So that because of the first scarcity which has been referred to,
the bark there grows much more thickly than in any other place.

And this moisture has such power of movement
that after having reached the spot where its help is needed,
it raises itself partly up like a ball rebounding,
and makes various buddings and sproutings,
somewhat after the manner of water when it boils.

Leonardo da Vinci

x

Chapter 1

General Introduction

The Kalahari is not an easy place to know.
It is still less easy to understand.

E.J. Wayland (1953)

1.1   General framework

The Kalahari Desert stretches across north-western South Africa, south eastern Namibia and approximately 75% of southern Botswana; between the Orange and the Zambezi rivers. It is part of an extensive area of contiguous sub-basins into which continental sediments have been deposited for millions of years. The Kalahari Sand, the most common surface of this group of sediments, extends from latitude 1°N to 29°S constituting the largest continuous stretch of sand in the world (Dennis *et al*. 1999; Heritage 2002; Thomas and Shaw 1991). The term Kalahari is a derivation of the Setswana word *Kgalagadi* meaning "always dry" or "a waterless place". As the name implies, the Kalahari Desert has scarce permanent or episodic water courses. Nevertheless, the denomination "desert" may be inappropriate given its ecological diversity and relatively well-developed vegetation. On the other hand, the term desert lacks rigorous scientific meaning and it has been applied to a wide range of environments. The Kalahari Desert embraces numerous vegetation types including a mix of Acacia trees, Acacia scrub and grasslands. Figure 1.1 shows a scene typical of the Kalahari landscape. The extent of vegetation in the Kalahari Desert indicates that the area should preferably be labeled a 'dry savanna', rather than a desert. The Kalahari Desert is referred to simply as the Kalahari for the remainder of this work.

Thomas and Shaw (1991), described the Kalahari as a *"delicate environment of considerable contrast, where differences in the landscape arise in response to marked changes in the rainfall characteristics"*. It is the gradient character of the precipitation (considered an organizing concept), together with the relatively undisturbed wilderness, that makes the Kalahari attractive for research on vegetation's distribution, water-use and astounding coping mechanisms in this coarse and thirsty environment (Caylor et al. 2003; Dowty et al. 2000; Scholes et al. 2002)

Figure 1.1 Typical Kalahari landscape. Trees and shrub species can be leafless while others remain green during the dry season.

In recent years initiatives such as the Kalahari Transect and the SAFARI2000 have greatly contributed to the understanding of links between climate-biogeochemistry and ecosystem structure and functioning in the Kalahari (Caylor *et al*. 2003; Dowty *et al*. 2000; Privette *et al*. 2004; Ringrose *et al*. 2003; Scholes *et al*. 2002). These studies have shown that in the Kalahari's harsh conditions, the survival of such a wide range of vegetation is ensured only if individual species or species associations are able to implement mechanisms at a local scale to overcome constraints at the regional or global scale. As such, unusual water extraction habits are observed in certain vegetation species of the Kalahari. These strategies, operating at a local scale, contribute to overcoming regional water scarcity and global increases in CO_2 due to climate change, both of which force vegetation to use water more efficiently (Caylor *et al*. 2003; Dowty *et al*. 2000; Privette *et al*. 2004; Ringrose *et al*. 2003; Scholes *et al*. 2002). These amazing mechanisms are, however, complex and highly variable in space and time and therefore are not completely understood or even fully identified.

From the hydrological and water management perspective, authorities such as the Botswana government have increased awareness that vegetation dynamics influence the response of groundwater to climate variability (Caylor and Shugart

2006). Groundwater is the main source of water in Botswana. For this reason the government has promoted studies focusing on the influence of vegetation on groundwater recharge in the Botswana Kalahari. The Groundwater Recharge and Evaluation Study (GRES), carried out by the Botswana Geological Survey (BGS), the University of Botswana and the Vrije Universiteit Amsterdam, investigated recharge mechanisms in areas of Botswana with thick sand cover and deep groundwater tables. The GRES project was undertaken in two phases between 1987 and 1997. Since 2000, the Kalahari Research Project (KRP), a collaboration of the BGS and ITC has followed-up on the groundwater recharge investigation (as well as the groundwater discharged by trees) with a spatio-temporal assessment of sub-surface fluxes in the eastern Kalahari (Obakeng 2007). This study analyzes recharge and discharge issues and highlights the importance of investigating groundwater use by vegetation. The hypothesis of groundwater abstraction by vegetation root uptake in the Botswana Kalahari was first presented by De Vries *et al.* (2000), as one of the conclusions of the GRES project. De Vries *et al.* undertook intensive research of the groundwater recharge in the eastern fringe of the Kalahari. His premise was supported by the existence of green leaves in large trees at the end of the dry season, evidence of transpiration at a time when most of the vegetation has a brownish appearance (De Vries *et al.* 2000). Later, Obakeng (2007) implemented comprehensive monitoring of the water balance components, while simultaneously investigating rooting depths and possible groundwater extraction by vegetation. From chemical and natural tracers in deep boreholes, Obakeng (2007) concluded that some of the Kalahari species can develop roots as deep as 70m. The same study revealed that most of the tree species in the eastern Botswana Kalahari made predominant use of soil water from depths of more than 3m, i.e. below the root zone of shrubs and grasses.

The conclusions presented by De Vries *et al.* (2000) and Obakeng (2007), confirm that some of the Kalahari tree species make use of groundwater for survival during the dry season. However several questions remain unanswered: Do these tree species use *only* groundwater during the dry season? Is the water removed from deep soil layers actually *lost* by transpiration? How should tree survival strategies be numerically analyzed in order to realistically quantify tree transpiration during the critical dry season? How do sap flow and transpiration patterns vary throughout the vegetative year and how they are related to hydro-climatic conditions? Lastly, from the tree physiology perspective, why do certain tree species enter into a dry-season-dormancy while others remain active and strive for water? These questions encompass a broad research topic within the fields of ecohydrology and ecophysiology. Their definite answers likely require further high resolution spatio-temporal monitoring of soil-vegetation-atmosphere processes. However, the results and discussions presented in this thesis provide answers to some of these questions and aim to make a contribution towards better understanding of intriguing environments such as the Kalahari.

1.2   Scope of the study

Given the uncertainties of vegetation water-use prevalent in the Kalahari, the author presents an attempt to identify transpiration patterns and to quantify water abstraction by the predominant species in the eastern Kalahari. The study focuses on the eco-hydrological conditions at the end of the dry season of 2004 and was executed in the experimental Serowe site of the KRP (Obakeng 2007).

1.2.1   Objective

The main objective of this study is to develop a methodology for the quantification and mapping of tree transpiration fluxes to be used in hydrological balances. To achieve this objective the study was carried out in two major steps: *i)* sap flow investigations and *ii)* upscaling and mapping. The former was based on ground measurements and follow-up laboratory experiments, and the latter on geographic information systems (GIS) and remote sensing (RS) techniques. This methodology was developed for the particular conditions of the Kalahari, however it can be used in its general form in other environments where tree transpiration constitutes an unidentified component of the water balance.

1.2.2   Approach

The identification of vegetation water-use habits in Kalahari species was based on an investigation of sap flow patterns in the most abundant woody species of the eastern Kalahari. Sap flow was estimated from direct measurements of sap flux densities in tree trunks and from conductive sapwood area assessment. Once sap flow patterns were identified and carefully analyzed, the quantity of sap was expressed in terms of individual-tree transpiration fluxes. These fluxes were correlated directly or indirectly with a RS-measurable parameter that allowed the establishment of upscaling functions to be applied in RS imagery. Considering the variability of transpiration dynamics in the species investigated, upscaling functions are species-dependent and therefore species separation had to be carried-out in the RS images. The final product of the study is therefore a transpiration map per RS image, which represents the amount of water that is lost to the atmosphere in the form of transpiration fluxes. Tree transpiration maps thus obtained correspond to the mean 24-hour flux of the period from which sap flow measurements were collected.

1.3   Outline of the thesis

The research is presented in 7 chapters, briefly outlined below.

Chapter 1: General introduction to the problem and to the research approach.

Chapters 2 to 4: Results and conclusions of the ground measurements. Chapter 2 discusses technical aspects of the method used to measure sap flux densities, including its limitations and adaptations to environments such as the Kalahari. Chapter 3 presents an overview of the concept of conductive sapwood (xylem) area. A short review of the different methods for its determination is presented. Chapter 4 describes the sap flow patterns identified in the Kalahari species at the end of the dry season. This chapter also discusses the effect of vegetation water-use habits on the quantification of transpiration from upscaled sap flow.

Chapter 5 and 6: GIS and RS components. Chapter 5 describes the procedure for image classification (species discrimination) suitable for mixed forest such as the Kalahari savanna. In Chapter 6, upscaling functions based on the results of Chapter 4 are presented and applied to classified images resulting in transpiration maps.
Finally, Chapter 7 presents a summary of the results and general conclusions of the study.

1.4   Description of the study area

The area is located in the Central District of Botswana, at the eastern fringe of the Kalahari basin. This study was carried out within the framework of the KRP, which covers a total area of *ca.* 2700km². However, the investigation of transpiration patterns was concentrated in a 100 km²-polygon (S 22°20', E 26°20') within this area, approximately 40 km west of Serowe in the *sandveld*[1] (Figure 1.2). The KRP included a portion of the eastern *hardveld*[2] which also embraces species typical of savanna vegetation. However, considering that the *hardveld* hydrological, geomorphologic and geological characteristics are substantially different from those of the *sandveld*, such species are not included in this study although they merit additional investigation. Figure 1.2 shows the location of the KRP project and the area selected for the sap flow and transpiration patterns investigation. This 100 km²-polygon is referred to as the study area.

1.4.1   Geomorphology, climate and hydrology

The study area is a gently undulating sand plateau sloping towards the west without prominent drainage lines. The area is characterised by permeable sands

---

[1]Afrikaans name for the area covered by the Kalahari sand mantle
[2]Afrikaans name for the most eastern Kalahari covered by 0-5m of superficial deposits and where some rock outcrops can be found.

Modified from Obakeng, 2007 and SGC, 1988
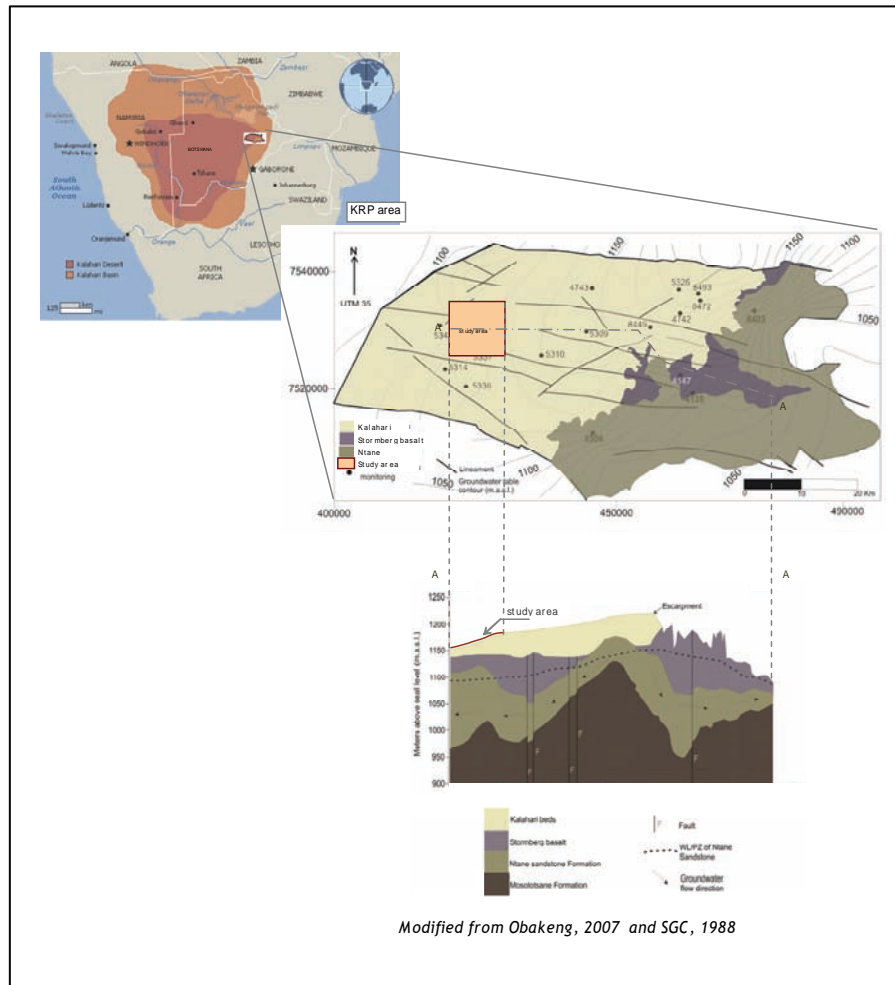
Figure 1.2 Localization of study area

with high infiltration rates, high retention capacity due to the thick sand layer and consequently negligible surface runoff. The sand mantle of the Kalahari lies over rocks of the Karoo formation (sandstone, shale and basalt) and reaches depths of 0-5m on the eastern fringe to 60-100m towards the center (Obakeng 2007; Thomas and Shaw 1991)

The climate is semi-arid with a mean annual temperature of 20°C. During the summer season (from November to March) day-time temperatures can reach up to 35°C, while during winter (June to August) temperature at midday can reach 30°C but it might drop below freezing point at night. However, the main seasonal contrasts in the study area (as throughout the Kalahari) result from variations in precipitation rather than in temperature. It is therefore more appropriate

to talk in terms of a wet and dry season rather than summer and winter, though the latter terms are also commonly used.

The area receives a mean annual precipitation (MAP) of 400mm. Rainfall is seasonal, occurring mainly in summer and transitional autumn (April to May). During these seasons cloud coverage and rain might decrease the ambient temperature considerably, although usually only for a short period of time. The dry season begins in June, coinciding with the beginning of the winter season and continues until the early spring (October). During these months only about 10% of the annual rainfall occurs. It is not only the low rainfall that gives the study area the character of a desert, but also the high potential evapotranspiration (PET). Obakeng (2007), found that PET is highly temporally but less spatially variable in the KRP area, ranging from 0.1 to 6.3mm/day. The estimated mean annual PET for the years 2002 to 2004 was 1,035mm, showing that in the Kalahari there is potential to evaporate more than four times the annual rainfall

Surface water streams in the area are non-existent, making groundwater reserves the main source of water supply. Ephemeral surface streams exist about 15km east of the study area in the *hardveld*, but they flow east and therefore have no influence on the available moisture of the area. Groundwater is mainly found in the Karoo rocks below the thick layer of Kalahari sands. The Ntane formation (Aeolian sandstones) is considered the main aquiferous unit, favored by a system of fractures that enhances its porosity. In the area selected for this study, a structurally controlled groundwater system flows west with a gentle gradient. According to Obakeng (2007), the groundwater table in this location can be found at depths between 60 and 100m. The high-intensity rains occurring during the summer are the main source of groundwater replenishment in the area.

1.4.2   Vegetation

The vegetation of the study area was investigated during the KRP (Demisse 2006; Obakeng 2007) and the conclusions were in agreement with the findings reported by the Safari2000 project. Areas of less than 400mm MAP are characterised by woody species belonging mainly to the *Mimosaceae* family represented by the *Acacia* and *Dichrostachys* genera, while areas with MAP ranging from 400mm to 600mm are characterized by woody species of the *Combretaceae* family, represented by the *Terminalia* genus (Scholes *et al.* 2002). The vegetation cover of the study area is accordingly a mosaic of open savanna grassland and low thorny trees, many of them with a marked seasonal variation in leaf cover. Among the most abundant species in the area, nine were selected for this study based on their frequency of occurrence and phenological distinctiveness. These are (Figure 1.3): *Acacia fleckii, Acacia erioloba, Acacia luederitzii, Boscia albitrunca, Lonchorcarpus nelsii, Terminalia sericea, Burkea Africana, Ochna*

pulchra and *Dichrostachys cinerea*. The local and English names of the species are presented in Table 1.1.

One of the remarkable characteristics of some of these Kalahari species is their ability to tap groundwater during the dry season when surface moisture is unavailable. This attribute is connected with rooting system morphology and physiology, aspects that been investigated in previous studies in the Kalahari (Cole and Brown 1976; Seymour and Milton 2003). Such studies have revealed significant differences in the rooting habits between trees species. Some of the Kalahari species, mainly those belonging to the *Acacia* genus, have been portrayed as having both large tap roots and well developed lateral rooting systems which enable them to make use of available soil moisture (Burke 2006; Canadell *et al.* 1996; Cole and Brown 1976; Leistner 1967; Ludwig 2001; Otieno *et al.* 2005; Roupsard *et al.* 1999; Sekhwela 2003; Seymour and Milton 2003). Obakeng, 2007, found traces of LiCl in *Boscia albitrunca* leaves one day after insertion in a borehole at 40m depth, and in *Acacia erioloba* leaves three days after injection at 70m depth.

Table 1.1 tree species investigated

scientific name	local name	English name	Afrikaans name
Burkea africana	Monato	Wild syringa	Wildesering
Lonchocarpus nelssi	Mahata	Kalahari apple-leaf	Kalahari appelblaar
Acacia fleckii	Mohahu	Plate thorn	Bladdoring
Ochna pulchra	Monyelenyele	Peeling plane	Lekkerbreek
Dichrostachys cinerea	Moselesele	Sickle bush	Sekelbos
Acacia erioloba	Mogothlo	Camel thorn	kameeldoring
Acacia luederitzii	Mokha	False umbrella thorn	Basterhaak-en-steek
Boscia albitrunca	Motopi	Shepherd's tree	Witgat
Terminalia sericea	Mogonono	Silver cluster-leaf	Vaalboom

Besides rooting system characteristics, another important feature related to the water-use habits of woody species is their phenological variation during the vegetative year. Observations during the KRP and information from published literature has shown that the schedule of pheno-phases in the Kalahari species is variable, and that moisture availability and air temperature variations are the main environmental cues (Childes 1989). Such studies conclude that some deep-rooting species in the Kalahari flower and come into leaf before the rains, showing independence from the available moisture in the upper soil layers and marked response to the rise in temperature (Childes 1989; Curtis and Mann-heimer 2005; Wyk van and Wyk van 1997). After the rains, these species maintain their leaves during part of the dry season and start defoliating as temperature drops according to the degree of resistance to frost. On the other hand, species with a shallow root system only begin vegetative growth after the appearance of the rains. A comprehensive description of the rooting characteristics

and phenological behaviour of the Kalahari species, based on available published literature and direct observations is presented in Chapter 4.
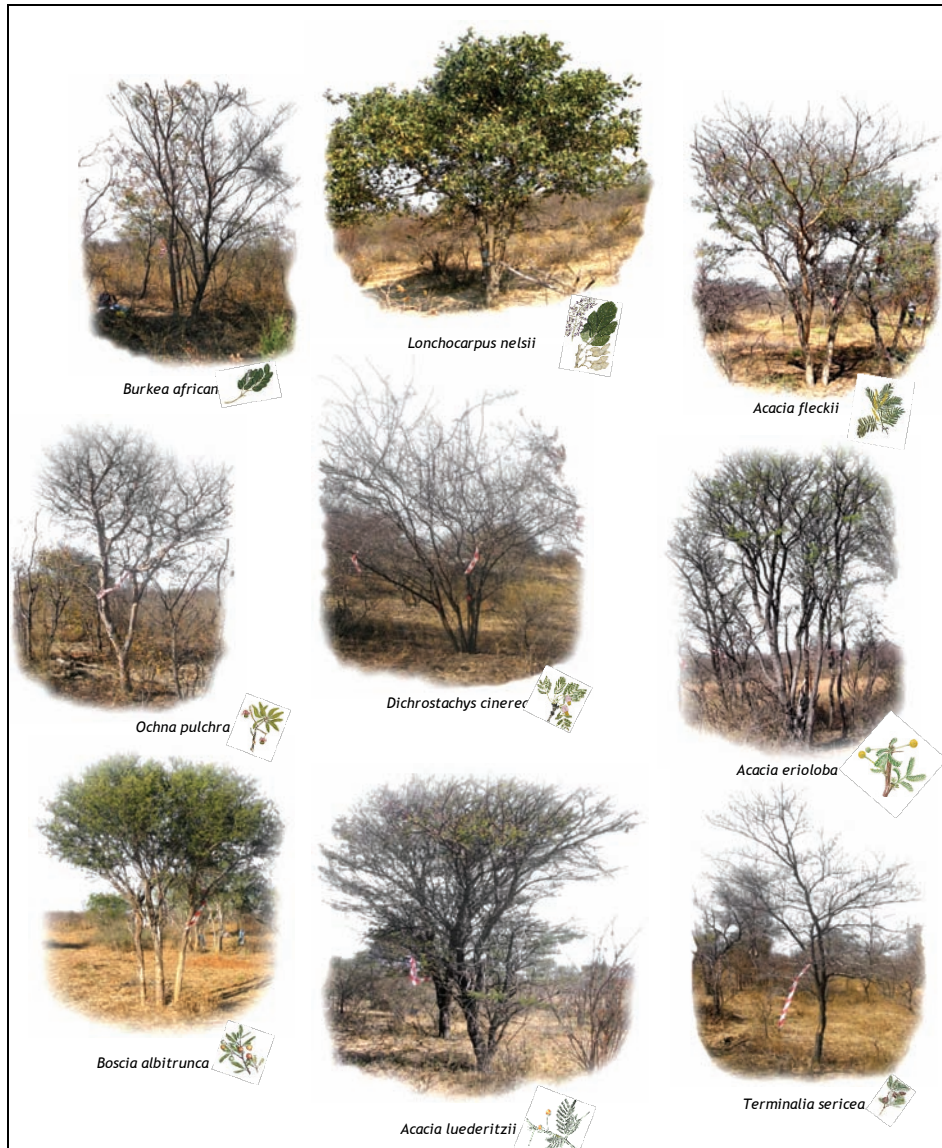
Figure 1.3 Tree species investigated in this study (appearance during the dry season).

References

Burke, A. 2006. Savanna trees in Namibia - Factors controlling their distribution at the arid end of the spectrum. Flora. 201:189-201.

Canadell, J., R. Jackson, J. Ehleringer, H. Mooney, O. Sala and E. Schulze 1996. Maximum rooting depth of vegetation types at the global scale. Oecologia. 108:583-595.

Caylor, K. and H. Shugart 2006. Pattern and process in savanna ecosystems. *In* Dryland Ecohydrology Eds. P. D'Odorico and A. Porporato. Springer Netherlands, p. 231.

Caylor, K., H. Shugart, P. Dowty and T.M. Smith 2003. Tree spacing along the Kalahari transect in southern Africa. Journal of Arid Environment. 54:281-296.

Childes, S.L. 1989. Phenology of nine common woody species in semi-arid, deciduous Kalahari Sand vegetation. Vegetatio. 79:151-163.

Cole, M. and R. Brown 1976. The vegetation of the Ghanzi area of western Botswana. Journal of Biogeography. 3:169-196.

Curtis, B. and C. Mannheimer 2005. Tree Atlas of Namibia Ed. N.B.R. Institute, Windhoek. 674 p.

De Vries, J., E. Selaolo and H. Beekman 2000. Groundwater recharge in the Kalahari, with reference to paleo-hydrologic conditions. Journal of Hydrology. 238:110-123.

Demisse, G. 2006. Spatial distribution of savannah woody species biodiversity in Serowe, Botswana. Unpublished MSc thesis. International Institute for Geo-Information Science and Earth Observations, ITC. Esnchede, The Netherlands., Enschede.

Dennis, N., M. Knight and P. Joyce 1999. The Kalahari: Survival in a Thirstland Wilderness. New Holland Publishers.

Dowty, P., K. Caylor, H. Shugart and W. Emanuel 2000. Approaches for the estimation of primary productivity and vegetation structure in the Kalahari region. *In* Towards Sustainable Natural Resource Management in the Kalahari Region Eds. S. Ringrose and R. Chanda. University of Botswana Press. .

Heritage, A. 2002. The Great World Atlas Ed. D.K. DK, London.

Leistner, O. 1967. The Plant Ecology of the Southern Kalahari. *In* Memoirs of the Botanical Survey of South Africa. Department of Agricultural Technical Research, Pretoria. 172 p.

Ludwig, F. 2001. Tree-grass Interactions on an East African Savanna: the effects of competition, facilitation and hydraulic lift. Wageningen University and Research Centre, sub-department of Nature Conservation, Wageningen.

Obakeng, O.T. 2007. Soil moisture dynamics and evapotranspiration at the fringe of the Botswana Kalahari. Vrije Universiteit, Amsterdam, NL.

Otieno, D., M. Schmidt, J. Kinyamario and J. Tenhunen 2005. Responses of *Acacia tortillis* and *Acacia xanthophloea* to seasonal changes in soil water

availability in the savanna region of Kenia. Journal of Arid Environments. 62:377-400.

Privette, J., Y. Tian, R. Roberts, R.J. Scholess, Y. Wang, K. Caylor, P. Frost and M. Mukelabai 2004. Vegetation structure characteristics and relationships of Kalahari woodlands and savannas. Global Change Biology. 10:281-291.

Ringrose, S., W. Matheson, P. Wolski and P. Huntsman-Mapila 2003. Vegetation cover trends along the Botswana Kalahari transect. Journal of Arid Environment. 54:297-317.

Roupsard, O., A. Ferhi, A. Granier, F. Pallo, D. Depommier, B. Mallet, H. Joly and E. Dreyer 1999. Reverse Phenology and Dry-Season Water Uptake by Faidherbia albida (Del.) A. Chev. in an Agroforestry Parkland of Sudanese West Africa Functional Ecology. 13:460-472.

Scholes, R., P. Dowty, K. Caylor, D. Parsons, P. Frost and H. Shugart 2002. Trends in savanna structure and composition along the aridity gradient in the Kalahari. Journal of Vegetation Sciences. 13:419-428.

Sekhwela, M. 2003. Woody vegetation resource changes around selected settlement along aridity gradient in the Kalahari, Botswana. Journal of Arid Environments. 54:469-482.

Seymour, C. and S. Milton 2003. A collation and overview of research information on Acacia erioloba (Camelthorn) and identification of relevant research gaps to inform protection of the species. Department of Water Affairs and Forestry, Pretoria, South Africa.

Thomas, D.S.G. and P.A. Shaw 1991. Kalahari environment. Cambridge University Press, Cambridge etc. 284 p.

Wyk van, B. and P. Wyk van 1997. Field Guide to Trees of Southern Africa. Struik Publishers.

Sap Flux Densities

Technical aspects of TDP method

Abstract

An intensive sap flow campaign was carried out during the 2004 dry season in the Serowe study area. Sap flux densities were collected using Thermal Dissipation Probes (TDP) sensors in nine Kalahari species: *Acacia fleckii, Acacia erioloba, Acacia luederitzii, Boscia albitrunca, Lonchorcarpus nelsii, Terminalia sericea, Burkea Africana, Ochna pulchra* and *Dichrostachys cinerea*. In spite of the evidence that TDP is an effective tool for estimations of tree transpiration in tropical or boreal forest, previous studies in semi-arid environments reported the vulnerability of TDP to natural thermal gradients (NTG). In the past, a cyclic ON&OFF-power mode which included a new calibration was proposed to compensate for NTG in the TDP operation. However, such correction is not universal as it was developed for specific conditions and therefore its application in different species or environments would require additional verification. With this antecedent and motivated by the observations of the 2004 campaign, a second survey was carried out in May 2005. During this campaign, a new multi-step approach for the correction of NTG in TDP sensors was tested in four species out of the nine measured in 2004. The proposed method also introduces an ON&OFF-power mode (commutated signal), but it simulates the constant heating conditions in which the Granier method was originally developed. First, the existence of NTG in the Kalahari species was confirmed; next, a commutated power mode was implemented and finally, the TDP raw signal was corrected by modeling to steady-state to allow the use of the original calibration. The validity of the results was confirmed by a novel verification scheme that allowed simultaneous volumetric measurement of tree water consumption and sap flow estimations. The two main advantages of the proposed method are *i)* its species-independent applicability and *ii)* the low power requirements that might account for 50% less energy consumption compared with the standard Granier method.

Keywords: commutated-power mode, NTG, sap flow, steady-state, TDP.

2.1 *Introduction*

The quantification of tree transpiration in regions with arid and semi-arid climates where there is often reliance on groundwater supply, is essential for good water management. Such is the case in the Kalahari where the vast open savanna vegetation competes with the human population for water supply. Among other methods, sap flow method from direct measurements of sap flux densities in trees is considered an effective approach for transpiration estimations. The common acceptability of sap flow methods results mainly from their simplicity, and good suitability for automatization (Granier *et al.* 1996; Oren *et al.* 1999; Vertessy *et al.* 1995; Wullschleger *et al.* 2001). Sap flow can be calculated from sap flux density S_f, and conductive sapwood area A_x (also termed xylem area), both susceptible to uncertainties in their determination (see Chapter 3 for considerations of sapwood area). For stand transpiration assessment, sap flow of individual trees can be upscaled using biometric parameters that are correlated to rates of sap flow, as presented in Chapter 6. There is general agreement that the greatest errors in the transpiration assessment from upscaled sap flow occur in the determination of S_f rather than in the process of upscaling itself (Hatton *et al.* 1995; Lu *et al.* 2004; Wullschleger *et al.* 1998).

Thermal-based sap flow methods, which quantify water transport using heat as a tracer, have been the most widely used. In their review on whole-plant water use in trees, Wullschleger *et al.* (1998), presented the results of 52 studies published between 1970 and 1998. The study includes 92 observations of 67 tree species, of which more than 50% (51 out of 92) used thermal-based sap flow techniques i.e. heat pulse velocity, trunk segment heat balance, stem heat balance, or heat dissipation methods. In the recent years, heat field deformation and laser heat pulse methods have been added to the list of thermal-based possibilities. Though widely accepted, thermal-based methods have two main disadvantages. Firstly, they are invasive as they require probes to be inserted into the tree xylem, and secondly they rely on precise determination of xylem depth for proper sensor installation. Detailed discussions on the advantages and drawbacks of sap flow methods are found in Bauerle *et al.* (2002), Čermák, *et al.* (2004), Köstner, *et al.* (1998), Lundblad, *et al.* (2001), Smith, (1996) and Wullschleger *et al.* (2001).

Among the thermodynamic methods for sap flow determination, the Thermal Dissipation Probes method (TDP) has been widely used due to its technical simplicity and low implementation cost. Originally the TDP method was empirically calibrated in segments of trunks of three species, namely Douglas-fir (*Pseudotsuga menziesii*), European blank pine (*Pinus nigra*) and Oak (*Quercus pedunculata*). The TDP calibration parameters according to its developer, do not depend on the characteristics of the tree wood and therefore their use could be extended to other species, provided the original probe design remains unmodified (Granier et al. 1990). Confirmation of TDP original calibration was presented by Clearwater *et al.* (1999) and Meinzer *et al.* (2004) in tropical tree species. Since its

introduction in 1985, TDPs have been widely used in temperate, boreal and tropical climates. Their use in arid or semi-arid environments appears less frequently in published work *e.g.* Do and Rocheteau (2002 a&b), and Roupsard *et al.* (1998) who have presented results of studies in the African Sahel.

One of the most challenging problems of TDP (and of most thermodynamic methods) is the assumption that the combination wood-sap is in thermal equilibrium along the tree trunk and therefore the only cause of difference in temperature between the two probes is the applied heat. This supposition has proved to be incorrect, especially in sparse vegetation where the stems are subject to direct sun radiation or in semi-arid areas where the range of temperature variations between day and night results in trunk heat storage. The effect of NTG is emphasized when sap flow measurements are taken close to soil surface and in species with low sap flow rates (Do and Rocheteau 2002; Köstner *et al.* 1998). NTG mislead the TDP signal, which in turn can lead to large errors in transpiration accounts (Do and Rocheteau 2002; Lundblad *et al.* 2001). The problem has been tackled by some researchers including the creator of the method and possible solutions have been proposed. Köstner *et al.* (1998) recommended the scheduling of thermal gradients monitoring between measuring periods and the posterior correction of TDP induced gradients. This solution however was later debated by Do and Rocheteau (2002), who demonstrated that natural thermal gradients are variable over time and consequently have to be acquired simultaneously with sap flow measurements. In the same study, a different approach was presented using a cyclic signal. Although Do and Rocheteau's method takes into account the effect of natural thermal gradients, it has the disadvantage of introducing a new species-dependent calibration due to the shortened cycles not allowing the temperature to reach steady state. The method was tested in *Acacia tortillis trees*, but the applicability of the new calibration in other species or environments remained subject to verification. Although TDP sensors are still vulnerable to NTG and other environmental problems, they remain one of the most common methods of sap flow quantification.

This chapter presents a brief description of the sap flow campaign carried out during the Kalahari dry season of 2004 using TDP method. A detailed discussion on the water-abstraction habits of the species investigated, represented by the sap flow patterns, is presented in Chapter 4. The emphasis of this chapter is on technical aspects of the TDP sensors and the influence of ambient thermal gradients on TDP signal. Considering the frequency of such gradients in open savannah vegetation (the subject of this research), the author proposes a corrective method to compensate for its distorting effect. Finally, a verification experiment to validate the proposed method is presented.

2.2 Methods and Instrumentation

2.2.1   Sap flow related nomenclature

The expression *sap flow* is used in this study to refer to the volume of water with dissolved nutrients (sap) flowing through the tree stem per unit of time normally given in l/h. Sap flux density (S_f) denotes sap flow per unit of conducting sapwood area per unit of time and is given in $cm^3/(cm^2h)$. The term sapwood area or xylem area (A_x) represents the portion of the tree trunk cross section that allows the flowing of sap. According to the TDP method, sap flow is calculated by the product of S_f which is obtained from the TDP sensor and A_x. Finally, the expression *natural thermal gradients* refers to temperature differences between the two TDP measuring points resulting from any process different from the heat applied by the TDP heating element. Natural thermal gradients will be denoted hereafter with the abbreviation NTG.

2.2.2   TDP method

Developed by the French scientist André Granier in 1985, TDP method is based on the measurable temperature difference between a reference unheated probe, 20mm long, and a second probe constantly heated. Both probes are inserted parallel to each other in the sapwood at a vertical separation of approximately 10cm (Figure 2.1). The difference in temperature ΔT, between the two probes is measured with copper constantan thermocouples located inside each probe. When sap flow takes place, this difference is reduced due to the cooling effect of the upwards moving sap (heat convection). For more detailed description of the TDP method see Granier (1985) and Lu (2004).

A basic assumption of the method is that under conditions of stable thermal regime between the heating element, the wood and the sap, the constant heat input is equal to the heat dissipated by convection and conduction at the wall of the probe (Granier 1985; Lu *et al.* 2004). At zero flow, heat losses by convection do not occur and therefore the applied heat will be dissipated only by conduction through the sapwood until equilibrium is obtained. Temperature difference, ΔT, between the probes is maximum at this moment and will decrease proportionally to the increase of sap flow rate. Granier found an empirical calibration between S_f and the variability of ΔT called flow index K:

$$K= (\Delta T_{max} - \Delta T)/\Delta T \tag{2.1}$$

Where ΔT_{max} = maximum temperature difference (zero flow), ΔT temperature difference for a given sap flux density S_f. From his calibration, sap flux density is defined as:

$$S_f = 0.0119 \, K^{1.231} \qquad [cm^3/(cm^2 xh)] \qquad\qquad [2.2]$$
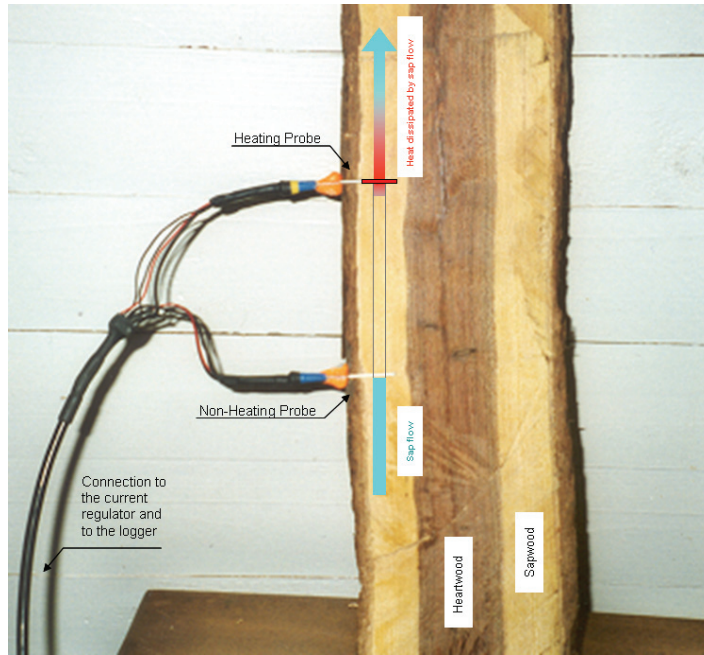
Figure 2.1 TDP installation (modified from Mapanda 2003)

2.2.3   Standard TDP campaign

Sap measurements were acquired during the dry season (July to September) of 2004 in the Serowe study area, Central District of Botswana, using thermal dissipation probes (TDP) (UP Gmbh, Germany). Based on their frequency of occurrence, nine tree species were selected and measured, namely: *Acacia fleckii, Acacia erioloba, Acacia luederitzii, Boscia albitrunca, Lonchorcarpus nelsii, Terminalia sericea, Burkea Africana, Ochna pulchra* and *Dichrostachys cinerea*. Continuous records of sap flux densities were collected every 30min during 3 or 4 days at each site and stored in multi channel data loggers (DataHog2, Skye instruments Ltd, UK). Sap sensors were installed ensuring that the measuring spot on the stem experienced minimal sun exposure by proper azimuth selection and adequate sun shielding.

2.2.4   Meteorological measurements

The microclimatic monitoring network established in 2001 by the KRP (Obakeng 2007), consisted of eleven Automatic Data Acquisition Systems, ADAS towers, (named GS00 to GS10), conceived to measure parameters for evapotranspiration assessment, precipitation and soil moisture characterization. Such measurements were acquired continuously from 2001 to the beginning of 2005. Ten of the ADAS stations were installed at fixed locations in the Serowe area and the remaining one, a mobile station, was used for the 2004 dry season sap flow campaign at different sites according to the coincidence of number of trees of the same species. The mobile ADAS system collected solar radiation, air temperature, relative humidity and wind speed measurements at each sap flow-related site. Figure 2.2 shows an example of sap flow measurements setup.
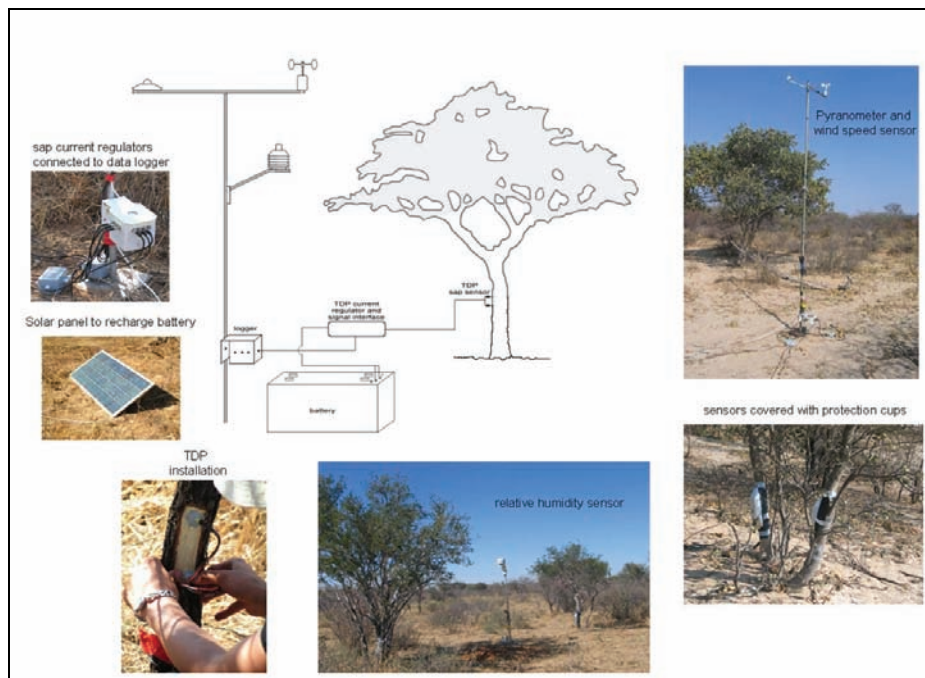
Figure 2.2 Sap flow measurements setup

2.2.5   Correction of Natural Thermal Gradients

After the data processing of the 2004 dry-season campaign, several recurrent features characteristic of each species were observed and sap flow patterns were identified. These patterns are presented and discussed in detail in Chapter

4. However, the presence of ambient thermal gradients in TDP measurements in ecosystems similar to the Kalahari, made it imperative to investigate their occurrence in the Serowe species. As a result a new campaign was carried out, this time at the end of the growing season when the Kalahari trees are still in leaf. This would normally result in enhanced sap flows and therefore easier interpretation of the TDP signal.

The second sap flow campaign took place from the second week of May 2005 (early autumn) when most of the Kalahari tree species have not started defoliation, to the first week of June 2005. The emphasis of this second campaign was on the testing of the proposed NTG compensation method, rather than on the quantification of sap flow (the sap flow calculated from the corrected signal could not be compared with the results of the 2004 campaign as it did not take place during the dry season). This correction strategy was based on the earlier suggestion of Köster *et al.* (1988) and first implemented by Do and Rocheteau, (2002). However, the methodology presented here differs from previous attempts of NTG correction in three major aspects: first, it considers the temporal variability of NTGs, second, it allows the original calibration presented by Granier (1987) and third, it is species and environment independent and therefore applicable without additional laboratory validation.

The schedule of measurements was designed with the following three objectives: verification of NTG existence, collection of standard TDP measurements following detection of NTG, and implementation of a commutated power scheme that allows sap flux densitiy correction. To achieve these objectives the measuring scheme was divided into 3 steps of variable duration, ranging from 24 to 48h, but with a fixed sampling time interval of 30sec. For all the measurements, standard TDP systems (UP Gmbh, Germany) were used and data were recorded by a multi channel data logger (DataHog2, Skye instruments Ltd, UK). Sap flow sensors were powered by a rechargeable battery and its voltage was permanently monitored by a Hobo logger (Onset Computer Corporation). Probes were inserted in the trunk after removal of the bark at a vertical separation of 10cm. The description of each measuring step is presented below.

Step#1: NTG were monitored using three non-powered standard TDP sensors (identified hereafter as sap1, sap2, and sap3), installed at different azimuths. Special care was taken to isolate the probes from direct solar radiation through the use of protection shields properly sealed off.

Step#2: normal sap velocity measurements were collected by connecting the TDP sensors to the power supply according to the standard Granier TDP method.

Step#3: TDP measurements in a commutated power mode were acquired at 15min heating (power ON) and 15min cooling (power OFF) intervals allowing

two samples per hour. The switching ON and OFF of the power was implemented by a sequencer based on a Hobo logger constructed in-house.

2.2.6 Verification experiment

In order to verify the proposed methodology for NTG compensation, a cut-tree experiment was implemented immediately after step#3 of the 2005 campaign. Cut-tree experiments have been widely used for quantification of tree water uptake, either by partial or total stem severing (Green and Clothier 1988; Olbrich 1991; Roberts 1977; Vertessy *et al.* 1997). The complexity of conductive sapwood tissue, as described in Chapter 3, led to the conclusion that the testing of the new method in a piece of the trunk subject to pressurized fluid in laboratory conditions was not appropriate.

In this case, the experiment was conducted in a live tree and was based on the procedure presented by Roberts (1977) with the following modifications: after step#3 the sap flow sensors were temporally removed, the tree was cut with a normal saw and immediately immersed in a container filled with water. Next, a second cut was made a few centimeters above the first, this time under water to avoid air induced embolism in the sapwood. For this purpose, a specially designed underwater saw was used. The saw-assembly consisted of a small chain-saw adapted to the shaft of an electric drill. The drill was tightly attached to a wooden handle in such a way that the blade could go under the water while being powered and maneuvered from above (Figure 2.3). The maneuver and hoisting of the severed tree was assisted by a mast assembled from a pair of rafters bolted together and fitted with a pulley and anchor points for supporting cables (Figure 2.4). A plastic bag filled with water was then wrapped around the bottom of the tree while it was still underwater inside the container, taking care not to expose the cut sapwood to air. Immediately the ensemble was moved and placed in a transparent acrylic cylinder filled with water, followed by the removal of the plastic bag with a tiny cutter. Once the tree was in the transparent cylinder, the whole assembly – tree with its trunk sitting in the cylinder with water - was lifted and tightly fixed to the mast preventing it from swaying in the wind.

For the water consumption monitoring, a programmable digital metering pump was used (KNF STEPDOS). The selection of this type of pump was based on its repeatability, programmability, possibility for hardware interface and connection with data loggers. The pump itself does not include a volumetric measurement function but this was custom-implemented through the recording of the number of pump revolutions using full capacity (80ml/min) programmed flow rate.
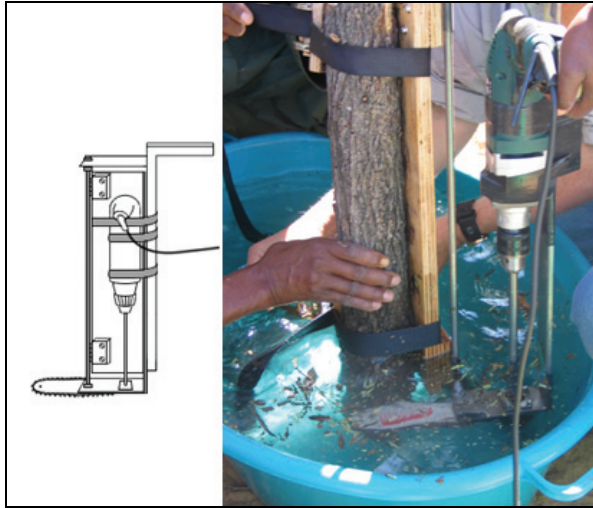
Figure 2.3 Underwater saw
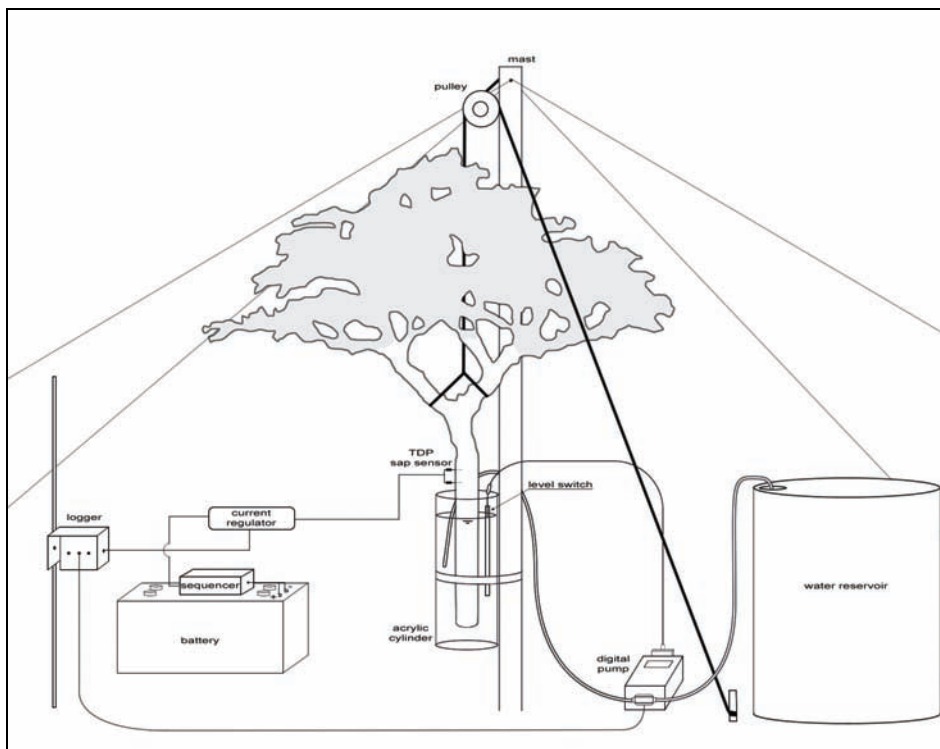
Figure 2.4 Verification experiment setup

The automatic measurement of the water consumed by the tree was made possible by the installation of a level switch that generated signals of turn-ON and turn-OFF in the pump. The pump was connected to a reservoir which supplied water on demand to the cylinder. Water level detection in the level switch was based on the contrast between the dielectric properties of air and water. As such, the pump provided precisely the quantity of water depleted by transpiration. Once the setting was complete, the TDP sensors were reinstalled in the original position and operated under commutated ON&OFF power mode. A few hours before dismantling the installation, a small amount of Eosine-B (MERCK) was added to the water in the cylinder, staining it red. The water then stained the sapwood red during transpiration, approximately revealing the sap conductive area later verified in a cut disk by X-rays tomography.

The verification experiment in both standard TDP and commutated method was implemented in four of the nine tree species measured in the 2004-dry-season campaign.

2.3 The model

The application of the original TDP calibration presented by Granier (1985) in the ON-OFF signal, obtained from the commutated power mode, was possible after the implementation of a simple model. The commutated cycles (15min ON&OFF) are usually not long enough to reach thermal equilibrium. To compensate for the insufficient time in the system to reach steady state, every cycle ON and OFF is fitted to a multi-exponential function which simulates the thermal response of the wood. Once the fitting parameters are obtained, the function is extrapolated to infinite time and the steady state ΔT retrieved. Extrapolated ΔT thus obtained is used to calculate sap velocity from equations [2.1] and [2.2]. The asymptotic ΔT value of the function corresponds to the thermal equilibrium that would be established in the wood if that specific heating or cooling condition was maintained

For modeling purposes, an imaginary cylinder of sapwood is considered in the tree (Figure 2.5).The active part of the sensor *i.*e. the heating probe inserted in an aluminum tube is at the cylinder center, and the reference probe is located tangentially at its bottom. The woody body is in fact, a hollow cylinder with internal radius $r_i = 1$mm (equivalent to the radius of the aluminum tube in which the needle of the sensor is actually inserted), external radius $r_o = 100$mm (the recommended separation between the two TDP needles) and $l = 20$mm equivalent to both the TDP needle and aluminum tube length. To consider the heat spatial distribution in radial direction, the cylinder is discretised in a series of concentric cylinders, each 1mm thick (dr) at its own temperature response.
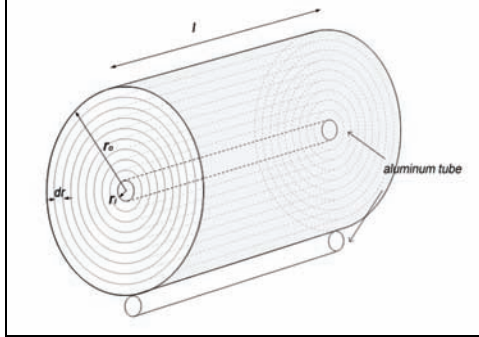
Figure 2.5 Imaginary cylinder of sapwood

The thermal sub-system is composed of *a)* a source of heat (heating filament plus aluminum tube) which under the proposed power scheme is considered as a commutated source of heat, *b)* a heat sink (the tree as a whole), and *c)* a volume of material between the source and the sink across which heat flow is occurring *i.e.* the investigated woody cylinder with volume V_w. It is assumed that the thermal properties of the tree wood are isotropic and that heat flow occurs only in a radial direction. The hypothetical wood cylinder is characterized by two relevant thermal parameters: thermal resistance (R_w)[3], inversely proportional to thermal conductivity (K_w) of the material and thermal capacitance (C_w). C_w is a function of density (δ_w) and specific heat capacity (c_w), which is water content and temperature dependent and therefore variable between periods of sap flow and no sap flow due to its convective effect. R_w is defined as the ratio between ΔT at steady state across the investigated volume to the heat flow rate, h_{Rw}, used to maintain that temperature difference (in the TDP operation, h_{Rw} is equal to 0.2W during 'ON' periods and 0 during 'OFF' periods):

$$R_w = \Delta T / h_{Rw} \hspace{5cm} [2.3]$$

Thermal capacitance, C_w, is the ratio between the amount of heat h_{Cw} needed to bring to the steady state temperature the system (initially thermally homogeneous) to the steady state ΔT:

$$C_w = h_{Cw} / \Delta T \hspace{5cm} [2.4]$$

Defining *t* as instantaneous time and ΔT as the temperature above or below the temperature at initial (starting) condition, the impulse response of the system can be evaluated as:
$$H = h_{Rw} + h_{Cw} \quad \text{[Watts]} \hspace{4cm} [2.5]$$

---

[3] In this chapter the sub index *w* refers to wood.

where h_{Rw} and h_{Cw} are respectively the instantaneous heat flow consumed by the heat conduction and by the heat capacity components. With the same ΔT across R_w and C_w in equations [2.3] and [2.4]:

$$R_w h_{R_w} = \int_0^t \frac{h_{C_w}}{C_w} dt \qquad [2.6]$$

Multiplying both sides of [2.5] by R_w and inserting [2.6] into [2.5]:

$$R_w H = \int_0^t \frac{h_{C_w}}{C_w} dt + h_{C_w} R_w \qquad [2.7]$$

Which results in:

$$R_w H = \frac{h_{C_w(t)}}{C_w} t + h_{C_w} R_w \qquad [2.8]$$

Solving for $h_{cw(t)}$:

$$h_{C_w(t)} = H \frac{R_w C_w}{t + R_w C_w} = H e^{\frac{-t}{R_w C_w}} \qquad [2.9]$$

Replacing [2.9] in [2.5] and solving for h_{Rw} :

$$h_{R_W} = H(1 - e^{\frac{-t}{R_w C_w}}) \qquad [2.10]$$

Equation [2.10] can be introduced in [2.3] to evaluate steady state ΔT:

$$\Delta T = R_w H(1 - e^{\frac{-t}{R_w C_w}}) \qquad [2.11]$$

where the factor $R_w C_w$ is the thermal time constant T_w of the sapwood cylinder under investigation and $R_w H$ is the peak amplitude A_w. Equation [2.11] can be then written as:

$$\Delta T = A_w (1 - e^{\frac{-t}{T_w}}) \qquad\qquad [2.12]$$

However, the solution to equation [2.12] would determine the fitting parameters *T* and *A* as if the thermal process took place in a single material. To account for the different media across which heat flow occurs, equation [2.12] is therefore split in more than one term. From this perspective, three different thermal responses are identified in the TDP operation. They are attributed to: *i-* the heater filament and all the components wrapped by this filament (i.e. isolation layer and thermo-couple assembly) represented by T_1, *ii-* the assembly of aluminum tube and silicone compound, T_2, (used to improve thermal contact between heating filament and aluminum tube if needed) and *iii-* the sapwood itself, T_3. Equation [2.12] takes a 3rd-order exponential form as follows

$$\Delta T = A_1 (1 - e^{\frac{-t}{T_1}}) + A_2 (1 - e^{\frac{-t}{T_2}}) + A_3 (1 - e^{\frac{-t}{T_3}}) \qquad\qquad [2.13]$$

Where A_1, A_2, A_3 are amplitudes and T_1, T_2 and T_3 time constants for the sub thermal circuits in consideration. To account for the small time difference between the logger and the sequencer clocks, a time offset *(t-t₀)* is incorporated in place of *t*. Steady state *ΔT* at the end of an ON cycle is then calculated as:

$$\Delta T_{ON} = \Delta T_{OFF-last} + A_1 (1 - e^{\frac{-(t-t_0)}{T_1}}) + A_2 (1 - e^{\frac{-(t-t_0)}{T_2}}) + A_3 (1 - e^{\frac{-(t-t_0)}{T_3}}) \qquad\qquad [2.14]$$

where *ΔT$_{OFF-last}$* is the measured temperature difference at the end of the previous OFF cycle and $t = t_\infty$. In an equivalent manner, steady state *ΔT* at the end of an OFF cycle was calculated as:

$$\Delta T_{OFF} = \Delta T_{ON-last} - \left[A_1 (1 - e^{\frac{-(t-t_0)}{T_1}}) + A_2 (1 - e^{\frac{-(t-t_0)}{T_2}}) + A_3 (1 - e^{\frac{-(t-t_0)}{T_3}}) \right] \qquad\qquad [2.15]$$

where *ΔT$_{ON-last}$* is the temperature difference at the end of the previous ON cycle.

The corrected *ΔT$_{ON}$* for a given cycle *(i)* is calculated as:

$$\Delta T_{(i)\ ON\ corrected} = \Delta T_{(i)\ ON\ extrap.} - (\Delta T_{(i-1)\ OFF\ extrap.} + \Delta T_{(i+1)\ OFF\ exrap.})/2 \qquad\qquad [2.16]$$

where $\Delta T_{(i-1)\ OFF\ extrap.}$ and $\Delta T_{(i+1)\ OFF\ extrap.}$ are the ΔT_{OFF} values taken to steady state before and after the ΔT_{ON} to be corrected.

Once ΔTs are corrected according to [2.16], the original Granier calibration presented in equation [2.2] can be applied.

2.4   Results

2.4.1   Standard TDP measurements in nine Kalahari species

In order to establish patterns and identify possible measurement from faulty sensors, groups of 18 to 24 individuals of each species were simultaneously measured during the 2004 dry season, using TDP standard method. Sap flux densities thus collected are shown in Figure 2.6. Sap flow patterns observed in some species show atypical water absorption habits, specifically nocturnal sap flow at the stem level in which the TDP signal was apparently enhanced compared to the daylight[4] hours activity. TDP results might be affected by NTG, for which the compensation method was not developed at the time of the 2004 campaign. However, the magnitude and synchrony of the TDP signal suggest additional physical phenomena besides the effect of NTG.

A detailed discussion on the sap flow patterns observed during the 2004 campaign and its implication in transpiration quantification is presented in Chapter 4. The following sections of this chapter give attention to the issue of a NTG compensation method in TDP measurements.

2.4.2 Correction for the effect of natural thermal gradients

The commutated power mode in the TDP operation implemented in the May 2005 campaign was carried out in four species: *Boscia albitrunca*, *Acacia fleckii*, *Dichrostachys cinerea* and *Acacia luederitzii*. Similar experiments in the other five species measured in the 2004 campaign remain the subject of further investigation. The schedule of measurements is presented in Table 2.1 and the results of the proposed method are presented step-by-step thereafter

---

[4] In this study the expression *daylight hours* refers to the time between sunrise and sunset *i.e.* hours of active solar radiation. In the month of May in the Kalahari, such period extends from ~6h00 to ~18h00. Conversely, *nighttime* designates the hours between sunset and sunrise in absence of solar radiation.
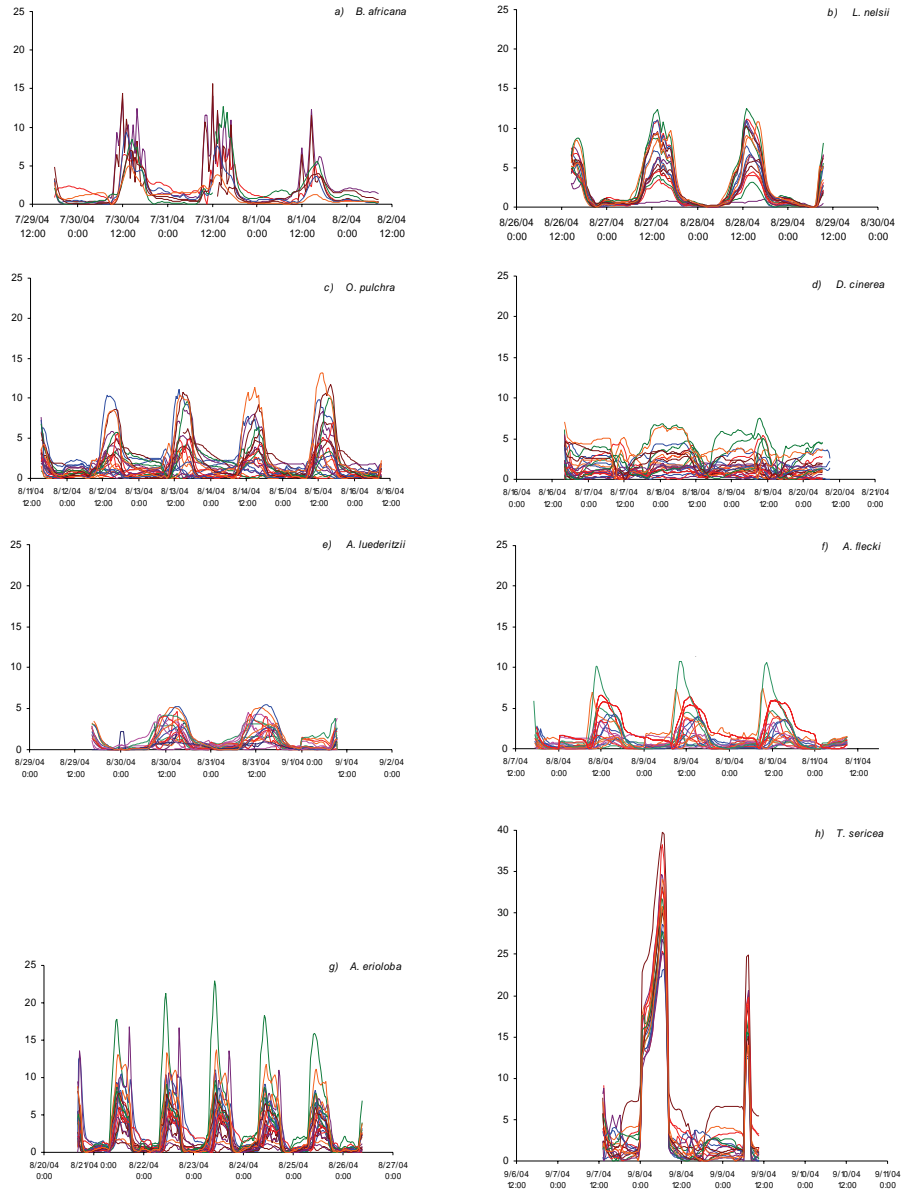
Figure 2.6 (a-h) Sap flux densities collected during the 2004 dry-season campaign. Y-axes: sap flux densities in $cm^3/(cm^2xh)$.
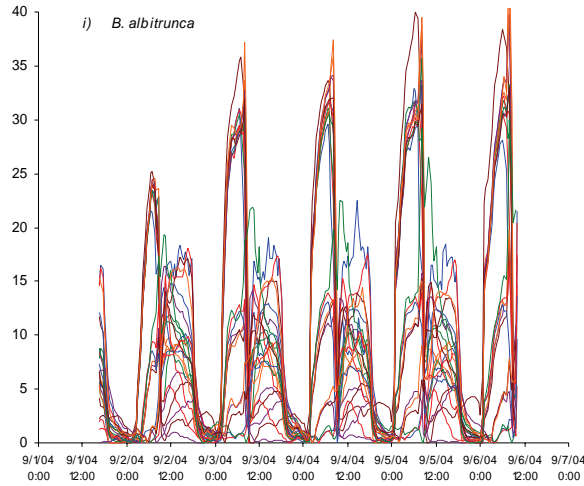
Figure 2.6 (i) Sap flux densities collected during the 2004 dry-season campaign. Y-axes: sap flux densities in cm³/(cm²xh)

Table 2.1 Schedule of measurements, 2005 campaign.

species	step#1	step#2	step#3
Boscia albitrunca	11 May, 13h00 - 12 May, 14h30	12 May, 14h30 - 13 May, 16h00	13 May, 16h00 - 15 May, 13h30
Dichrostachys cinerea	18 May, 13h00 - 19 May, 22h30	19 May, 22h30 - 20 May, 23h30	20 May, 23h30 - 22 May, 10h00
Acacia fleckii	24 May, 11h00 - 25 May, 11h00	25 May, 11h00 - 26 May, 11h00	26 May, 11h00 - 29 May, 11h00
Acacia luederitzii	26 May, 18h30 - 28 May, 18h00	28 May, 18h00 - 30 May, 18h30	30 May, 18h30 - 31 May, 14h30

2.4.2.1 Measurements of NTG - Step#1

Temperature differences between the two non-powered probes monitored by three TDP systems showed negative temperature gradients during the daylight hours (temperatures increasing from the upper stem towards the ground), with peaks ranging from -0.75°C in the case of *Boscia albitrunca* down to -5.15°C for *Dichrostachys cinerea* (Figure 2.7). During the night, when gradients tend to be positive, NTG were smaller and in some cases close to 0°C except for *Acacia Luederitzii* with a peak gradient of 0.70°C. NTG were similar in magnitude and diurnal pattern in the three systems of every tree except for *Dichrostachys cinerea* which showed a big gradient in sap1 on May 19th during daylight hours. Sap1 measurements in this tree resulted not only in differences in magnitude but also in pattern compared with sap2 and sap3.

Similar behavior is observed in the portion of the day measured on May 18th, suggesting that it was not the result of malfunctioning of the sensor but rather a local factor *e.g.* insufficient thermal shielding area of the stem (Lu *et al.* 2004

recommended that under certain conditions this effect can be attenuated by shading the exposed roots and extending the insulation to the ground surface).
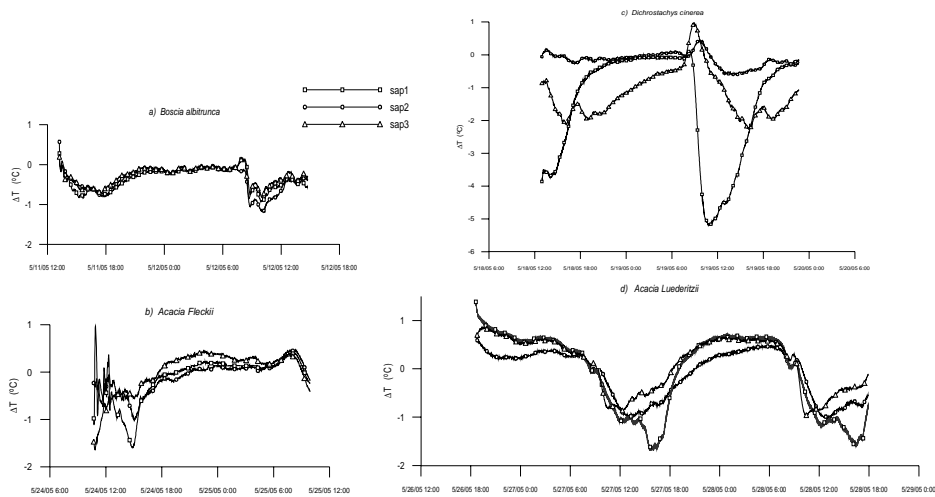
2.7 Natural thermal gradients in four species studied in the 2005 campaign.

Measurements from the closest meteorological station showed particularly low values of solar radiation (Ra) on the previous three days: daily average Ra: 143, 168 and 126W/m^2 on May 15th, 16th and 17th respectively. Average Ra in May in Serowe area is 210W/m^2 (calculated from continuous records presented in Figure 2.8). Air temperature T_a, measured at 2m height at the same station showed that the largest daily T_a difference during the month of May occurred on the 19th, ΔT_a=13.93°C. The occurrence of both a change in average Ra and a large T_a difference, may have led to heat storage resulting in a large NTG on May 18th and 19th.

Daily patterns of NTG in the four species were in agreement with the findings reported by Do and Rocheteau (2002) *i.e.* negative during the day and positive (or with positive trend) during the night. Applying the criteria presented by those authors, NTG for the four species investigated were to a large extent non-negligible (NTG>>0.20 °C).
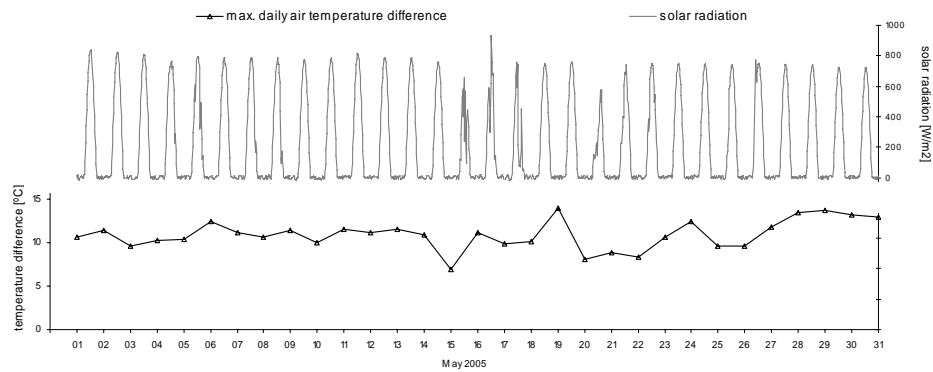
Figure 2.8 Solar radiation and maximum daily air temperature difference at 2m height from GS05 station.Data from May 2005 (Obakeng, 2007).

2.4.2.2 Standard TDP measurements – Step#2

Standard TDP sap velocity measurements were acquired immediately after the monitoring of NTG in the same tree. Resulting daily averages of the four species reported similar values compared with long term records obtained during the KRP in May 2003 and May 2004. To illustrate, for *Boscia albitrunca* the average sap velocity in the GS03 station (~10 kilometres from the experimental site) in May 2004 was 5.21 cm/h. During this step of the experiment average velocity from three TDP sensors in the same species was 6.31cm/h on May 13th of 2005.

2.4.2.3 TDP measurements in commutated power mode- Step#3

An example of commutated power mode with 15 min ON/15 min OFF is presented in Figure 2.9. Two cycles arbitrarily selected during daylight hours and nighttime show the range of temperature variation and the different exponential behavior of $\varDelta T$. A feature observed in these plots is the similarity of the rates at which the tree wood reaches thermal equilibrium according to the time of the day. In the four species such rate is lower during the daylight hours *e.g.* during the most active period of sap flow. Another aspect is the difference between the $\varDelta T$_OFF and NTG recorded during step#1. To illustrate, on May 14th in *B.albitrunca*, $\varDelta T$ at the end of the OFF cycle at about 6h00 *was 1.26°C*. This differs in magnitude and polarity from $\varDelta T$= -0.11°C registered during step#1 at an equivalent time of the day (Figure 2.7a). The discrepancy is attributed to the daily variation of NTG that would not necessarily correspond to $\varDelta T$_OFF, even in the eventuality that the system reached thermal equilibrium. Figure 2.9 also shows that 15min power ON interval is not sufficient for the wood to reach thermal equilibrium (this would be represented in the graph by an asymptote rather than a curved line at the end of every interval). Hence the use of exponential extrapolation to estimate steady-state values.
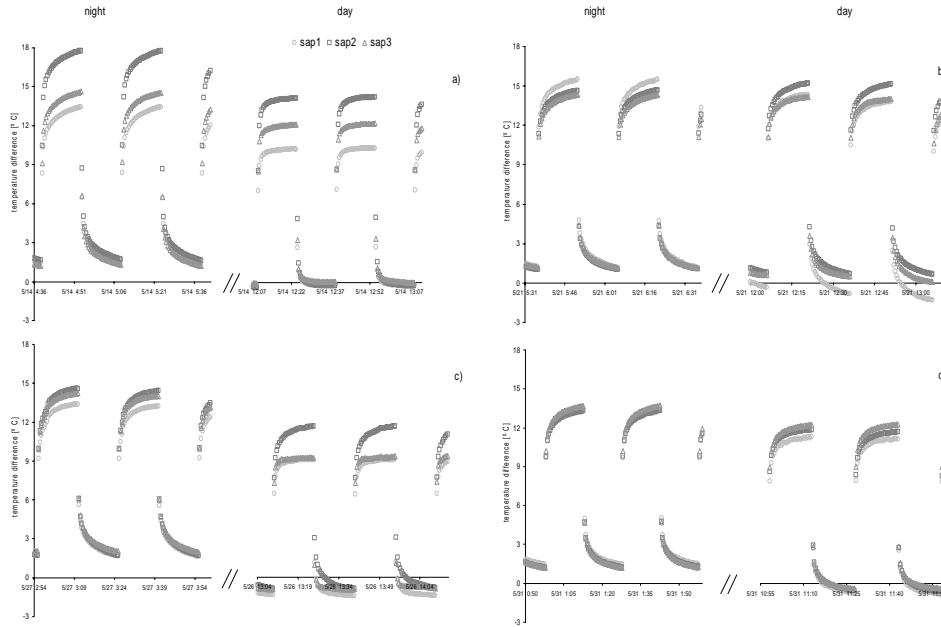
Figure 2.9. Example of cycles ON and OFF in commutated power mode (step#3) during day and night time for a) *B. albitrunca*, b) *D. cinerea*, c) *A. fleckii* and d) *A. luederitzii*

2.4.2.4 Modeled TDP signal

Equations [2.14] and [2.15] were applied to the data set and the unknown parameters were obtained through a least-square fitting routine. In this fitting, T1 and T2 parameters were considered as time-independent constants, whereas A1, A2, A3 and T3 were calculated for each cycle. In this way for example, the processing of the 177 cycles ON&OFF, corresponding to *B. albitrunca* resulted in the fitting parameters presented in Table 2.2 (mean values and standard deviation), with fitted accuracy within 4 or 5 significant figures.

Figure 2.10 presents an example of single ON and OFF cycles extrapolated to steady state. In this figure, the TDP signal at the end of the ON cycle (a) on May 14th at about midnight shows $\Delta T= 13.19°C$ and after extrapolation $\Delta T= 13.57°C$. In the OFF cycle (b) the difference is bigger, $\Delta T= 1.22°C$ after 15min and $\Delta T= 0.74°C$ after extrapolation. Differences between ΔT measured and ΔT extrapolated in the four species studied accounted for differences of up to 0.7°C, with a marked tendency to be larger during the night. The good fitting between model and measured data as observed in Figure 2.10 confirms that the 3-exponential model is suitable (up to 5 significant figures accuracy) to model the thermal response of the combination sensor-wood-sap.

31

$$\Delta T_{ON} = 1.221 + \{ 8.063(1-e^{-((t-11.430)/12)}) + 1.914(1-e^{-((t-11.430)/80)}) + 2.367(1-e^{-((t-11.430)/466.238)}) \}$$

$$\Delta T_{OFF} = 13.263 - \{ 8.069(1-e^{-((t-11.390)/12)}) + 2.084(1-e^{-((t-11.390)/80)}) + 2.375(1-e^{-((t-11.39)0/563.896)}) \}$$
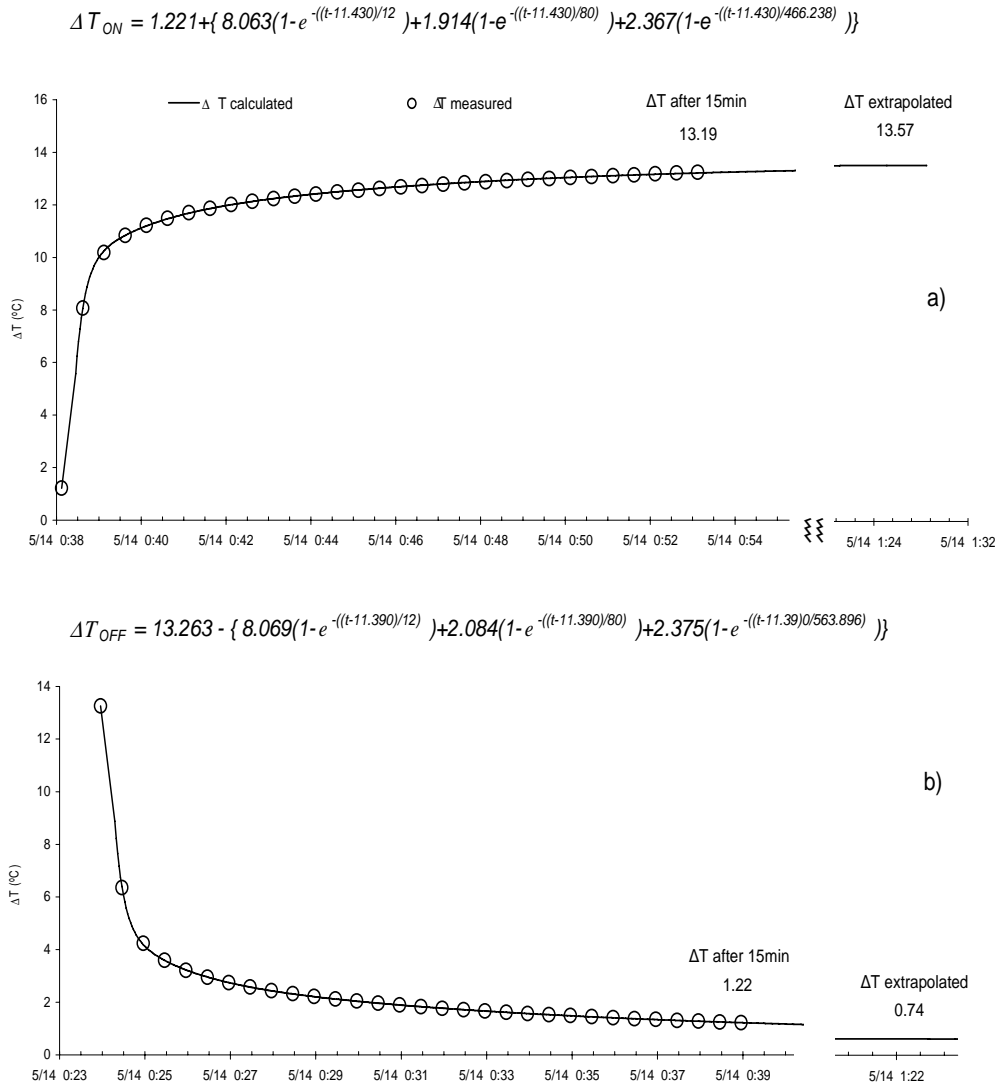
Figure 2.10. Example of multi-exponential extrapolation. a) ON and b) OFF cycles. Data from *B. albitrunca* sap1 on May 14th at approximately midnight

Table 2.2 Average fitting parameters of multi-exponential function for extrapolation of ΔT. Data from *B. albitrunca*, 177 cycles, 30 samples per cycle.

T_1=12 sec	T_2=80 sec									
	A_1 (°C)	A_2 (°C)			A_3 (°C)				T3 (sec)	
	all samples	all samples	ON - day	OFF - day	ON - night	OFF - night	ON - day	OFF - day	ON - night	OFF - night
					Mean values					
sap1	8.1619	1.8590	0.6043	0.7060	2.4148	2.2476	359.7753	597.0335	426.2301	525.0995
sap2	11.4666	2.2548	0.6344	0.8200	2.5468	2.2762	332.6534	674.5032	375.7670	598.7112
sap3	9.8276	1.7881	0.5918	0.6931	2.1276	2.0136	498.2336	596.3285	462.8862	589.7925
					Standard deviation					
sap1	0.2016	0.3006	0.7059	0.7792	0.1686	0.1336	72.9060	168.1608	27.4917	26.5894
sap2	0.3947	0.2840	0.7592	0.7962	0.2169	0.1630	53.9317	97.2802	38.9009	45.6109
sap3	0.2322	0.3970	0.6025	0.6296	0.1770	0.1361	76.3513	187.4831	38.1634	44.0477

2.4.2.5 Corrected sap flux densities

Once *ΔT* values were extrapolated and corrected according to equation [2.16], the original Granier calibration was applied. Sap flux densities thus corrected are presented in Table 2.3, together with the standard TDP data acquired the previous day in Step#2. Sap flux densities decreased substantially after implementation of the correction. The degree of reduction is however different in each species but consistent in the three TDP sensors installed per tree: *B. albitrunca* reduction was 65%, 58% and 64%, in sap1, sap2 and sap3 respectively; in *A. fleckii* 54%, 40% and 44%; in *A. luederitzii* 87%, 88% and 87%; and in *D. cinera* 89%, 85% and 92%. As expected, the percentage of reduction in TDP estimations after NTG correction is well correlated with the amplitude of the NTG themselves, *i.e.* large reduction for *A. luederitzii* and *D. cinera* which also showed the larger thermal gradients during unpowered mode (step#1).

Table 2.3 Mean sap flux densities before and after correction for NTG effect.

	mean sap flux densities $[cm^3/(cm^2/h)]$					
species	standard TDP - step#2			corrected values - step#3		
	s1	s2	s3	s1	s2	s3
Boscia albitrunca	7.840	5.250	5.990	2.770	2.191	2.184
Dichrostachys cinerea	1.440	0.478	2.564	0.160	0.070	0.210
Acacia fleckii	8.432	5.080	10.633	3.858	3.038	5.943
Acacia luederitzii	3.283	2.462	1.981	0.442	0.290	0.267

2.4.2.6. Verification of tree water consumption

The data set acquired during the verification experiment by the metering pump and the TDP sensors, was converted to rates of sap flow. TDP signal was corrected according to the proposed method and multiplied by sapwood area to be compared with the water consumed at a sampling interval (30min due to the

commutated signal). Table 2.4 shows the total consumption during the time of the verification experiment (~24h) in the four species tested. The same table presents for comparison the water consumption calculated with the method presented by Do and Rocheteau (2002). According to their formulations, S_f can be calculated from a cyclic ON&OFF signal as:

$$S_f = (11.3K_a/(1-K_a))^{0.707} \quad [l/(dm^2/h)] \qquad [2.17]$$

where $K_a = (\Delta T_{alternate-max} - \Delta T_{alternate})/ \Delta T_{alternate}$, $\Delta T_{alternate} = \Delta T_{ON} - \Delta T_{OFF}$ and $\Delta T_{alternate-max}$ is the maximum alternate signal obtained under zero flow conditions. The expression 'alternate signal' is linked to the calibration represented in equation [2.17] and it corresponds to the same commutated ON&OFF mode used in the proposed improvement.

Water consumption based on [2.17] resulted in considerably higher values (as presented in Table 2.4), indicating that the calibration presented by Do and Rocheteau (2002) to account for non-steady state conditions is not applicable in the species investigated here. Water uptake obtained from the corrected TDP signal based on the proposed method, corresponded to the volumetric verification within a 14% error in *A. fleckii* and 11% in *D. cinerea*; both inside the accepted error of S_f determination. In *A. luederitzii* the discrepancy was 19% and in *B. albitrunca* 32%. Water consumption during the verification experiment dropped significantly in the case of *B. albitrunca* and *A. fleckii* compared with the volumes measured previous to the cut in spite of continuous water availability in the cylinder. This decline is attributed to the reaction to stem injury and the differences in composition between the water provided to the tree during the experiment and water naturally obtained from soil. This difference possibly modifies tree transpiration patterns. Nevertheless, the comparison between the volumetric measurement of water uptake and the TDP measurements obtained from the experiment allows the evaluation of the corrected TDP signal although it does not provide realistic rates of transpiration for the species investigated.

Table 2.4 Total volume of water consumed during verification experiment. Volumetric measurement is compared with estimations based on Do and Rocheteau (2002) and the proposed method.

	water consumption [L]		
	metering pump	TDP-extrapolated commutated signal	TDP-alternate signal. D&R method
Dichrostachys cinerea	1.064	0.940	3.405
Boscia albitrunca	0.750	0.510	3.401
Acacia fleckii	1.675	1.435	6.408
Acacia luederitzii	4.340	5.175	23.320

2.5 Discussion

2.5.1 Extrapolated ΔT

The transfer of heat from TDP to tree wood and sap occurs under two possible scenarios. First, at nighttime transpiration is at a minimum and the amount of heat applied to the sapwood should be transferred principally by thermal conduction. In this case temperature at the measuring point will depend on K_w, δ_w and c_w of the materials involved with a defined and relatively stable thermal time constant T. Second, during daylight hours when transpiration takes place, the applied heat will not only flow by conduction but will also be transported by convection due to the upwards sap flow (a basic principle of TDP operation). In this case a combined process of conduction and convection occurs. To incorporate these two different scenarios in the model, T_1 and T_2 (corresponding to heater element and the aluminum tube respectively) were fixed in equations [2.14] and [2.15] and T_3 was included as a fitting parameter together with the thermal amplitudes A_1, A_2 and A_3.

From least square fitting $T_1 = 12sec$ and $T_2 = 80sec$ were obtained and the varying T_3 ranged between ~200sec and ~750sec. Careful observation of the fitting parameters variation presented in Figure 2.11 explains how the model describes the thermal processes taking place in the stem during day and night. The amplitude A_1 (corresponding to the heating filament) does not vary considerably between day and nighttime which is predictable due to more stable thermal properties of the materials involved, while the amplitude A_2 slightly decreases at the time of sap flow. The amplitude of the third term, A_3, drops heavily according to the transpiration activity as observed in Figure 2.11 and also showed more instability. To illustrate, for sap1, mean A_3 during daytime was 0.6043°C (STD 0.7059) and 0.7060°C (STD 0.7792) for ON and OFF cycles respectively, while during the night the same fitting parameter yielded 2.4148°C (STD 0.1686) and 2.2476°C (STD 0.1336) for ON and OFF cycles respectively. The variation of T_3 is similar; it not only differs between day and nighttime, showing more instability when transpiration occurs but is also lower for ON than for OFF cycles. The large T_3 values as compared with T_1 and T_2 are responsible for the impossibility of the system reaching steady state during the 15min sampling time.

2.5.2   Measured vs. Extrapolated ΔT

Comparison between *ΔT* at the end of each (ON&OFF) 15min interval and the corresponding extrapolated value show that the required time for the system to reach steady state is variable with a tendency to be larger during the night. To illustrate, the raw and extrapolated signal for the whole interval of measurements is plotted in Figure 2.12 (data from *B. albitrunca)*. The mean difference
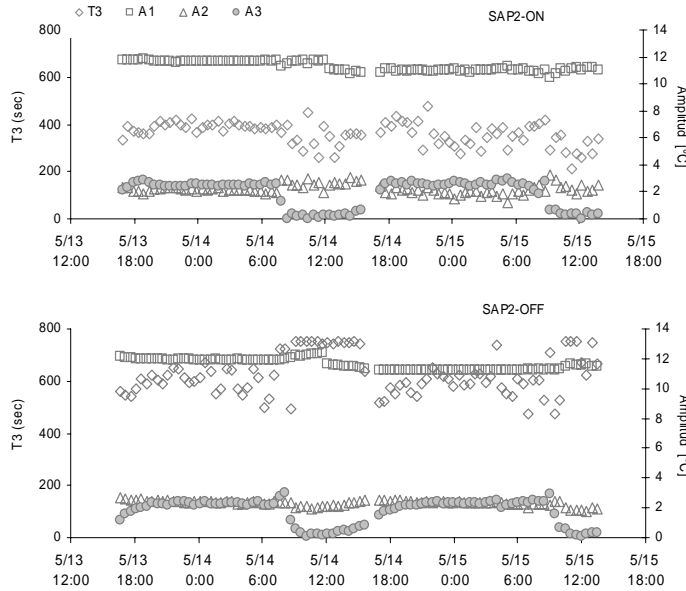
Figure 2.11. Diurnal variation of fitting parameters for multi-exponential extrapolation. Data from *B. albi-trunca*, sap2, step#3.

between measured and extrapolated *ΔT* is 0.18°C during the daylight hours and 0.37°C during nighttime. A similar reaction is observed in the other three species (data not presented). Figure 2.12 also reveals that nighttime thermal behavior of the system is extended beyond sunrise (~6h00 at the Serowe lati-tude) reaching ~8h00. Air temperature variations included in the same figure seem to be influential in the tree thermal schedule and consequently its effect can be variable according time of the year. From the power consumption point of view, analysis of the time interval required to reach steady state sheds light on how to design an optimal measuring scheme: for the ON cycles, on average 94% of the steady state *ΔT* was obtained after 5min and 95% after 10min during daytime. At night, 88% of the steady-state *ΔT* was obtained after 5min and 92% after 10min. These results show that possible adjustments in the cycle inter-val have to be considered independently for day and nighttime. The complete analysis of this issue is, however, out of the scope of this chapter.

2.5.3 Overall effect of NTG upon TDP signal

The continuous 3-steps of measurements are presented in Figure 2.13. Although each species shows a particular thermal dissipation pattern according to their own sap flow dynamic, this figure reveals common features that confirm the in-fluence of NTG in the Kalahari species: *i)* the diurnal variation of *ΔT* is highly
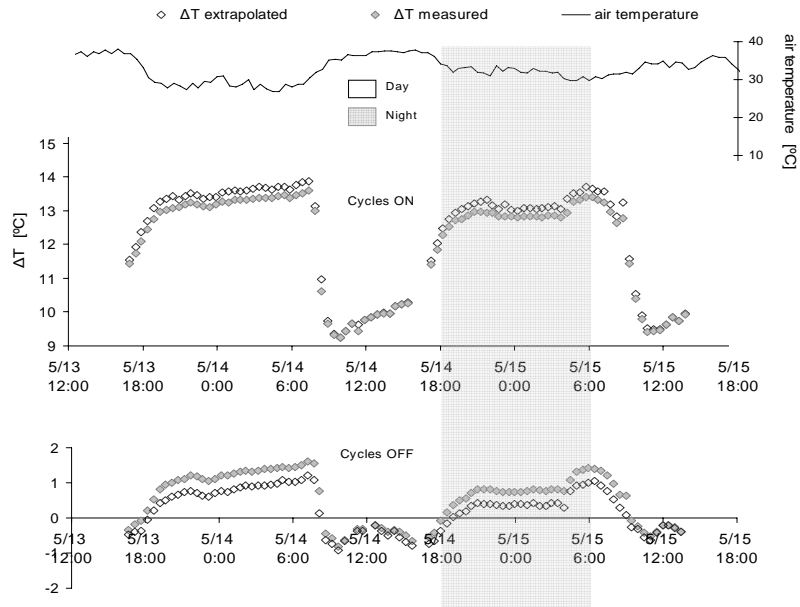
Figure 2.12. Measured ΔT vs. extrapolated ΔT emphasizing differences between day and night. Data from *B. albitrunca*
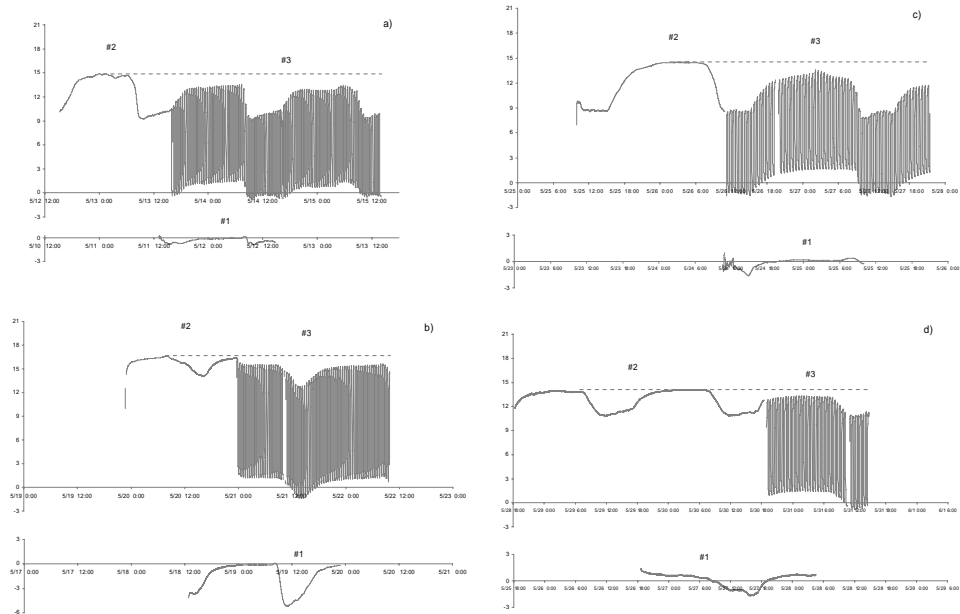
Figure 2.13. Raw TDP signal from steps#1-2-3 emphasizing ΔTmax decrease after the implementation of commutated signal. Data from a) *B. albitrunca*, b) *D. cinerea*, c) *A. fleckii* and d) *A. luederitzii*

influenced by the NTG pattern; this is specially evident in *D. cinerea* tree (Figure 2.13b) where the large negative gradient on the 19th of May at about noon (Figure 2.7) influences the course of TDP signal, both in continuous and commutated power mode (step#2 and step#3). *B. albitrunca* constitutes another example if one looks at the early morning rise (~8h00) in the ΔT curve which is reflected in the TDP raw signal of steps#2 and #3 as observed in Figure 2.13a. *ii)* The zero flow reference determined by ΔT_{max} is reduced when the commutated power mode is applied. This considerably influences the resulting sap flux densities calculated from equation [2.1] and [2.2].

The results obtained during the verification experiment (Table 2.4) showed that the method published by Do and Rocheteau (2002a) led to overestimations of water consumption in the species investigated in this study. Observations of the ΔT_{max} obtained after the implementation of equation [2.17] showed that such calibration did not compensate for the non-steady state conditions resulting from the commutated signal in the four Kalahari species studied. The conclusions presented above confirm the strong effect of NTG in Kalahari species and highlight once again the importance of removing their distorting effect in the TDP signal.

2.6 Conclusion

TDP method remains an efficient tool for the quantification of tree transpiration, provided that corrective measures are implemented to account for internal and climate-induced trunk thermal heterogeneities. The results of the 2005 campaign confirmed the misleading effect of NTG in TDP measurements conducted in open savannas. The proposed method based on the commutated ON&OFF signal allows the simulation of the continuous heating conditions, once extrapolated by a 3rd order exponential model, to be used with the standard Granier calibration. This characteristic of the method makes it species-independent although it has the disadvantage of increasing the complexity of the calculations and data logger memory requirements. However, with the increased use of flash memories *e.g.* as used in commercial digital photography, memory capacity is no longer a limitation. Furthermore with the current trends in micro-circuitry *i.e.* higher performance, lower consumption, lower costs, etc, it is likely that least square fitting of parameters will eventually be included in data acquisition modules. The method is considered adequate for measurements in semi-arid environments and open savanna type vegetation, where the effect of NTG is enhanced due to the combination of low sap flows, high solar radiation and sparsely distributed vegetation

References

Bauerle, W., T. Whitlow, C. Pollock and E. Frongillo 2002. A laser-diode-based system for measuring sap flow by the heat-pulse method. Agric For Meteorol. 110:275-284.

Burke, A. 2006. Savanna trees in Namibia - Factors controlling their distribution at the arid end of the spectrum. Flora. 201:189-201.

Canadell, J., R. Jackson, J. Ehleringer, H. Mooney, O. Sala and E. Schulze 1996. Maximum rooting depth of vegetation types at the global scale. Oecologia. 108:583-595.

Caylor, K. and H. Shugart 2006. Pattern and process in savanna ecosystems. *In* Dryland Ecohydrology Eds. P. D'Odorico and A. Porporato. Springer Netherlands, p. 231.

Caylor, K., H. Shugart, P. Dowty and T.M. Smith 2003. Tree spacing along the Kalahari transect in southern Africa. Journal of Arid Environment. 54:281-296.

Čermák, J., J. Kučera and N. Nadezhdina 2004. Sap flow measurements with some thermodynamic methods, flow integration within trees and scaling up from sample trees to entire forest stands. Trees. 18:529-546.

Childes, S.L. 1989. Phenology of nine common woody species in semi-arid, deciduous Kalahari Sand vegetation. Vegetatio. 79:151-163.

Clearwater, M.J., F.C. Meinzer, J.L. Andrade, G. Goldstein and N.M. Holbrook 1999. Potential errors in measurement of nonuniform sap flow using heat dissipation probes. Tree Physiol. 19:681-687.

Cole, M. and R. Brown 1976. The vegetation of the Ghanzi area of western Botswana. Journal of Biogeography. 3:169-196.

Curtis, B. and C. Mannheimer 2005. Tree Atlas of Namibia Ed. N.B.R. Institute, Windhoek. 674 p.

De Vries, J., E. Selaolo and H. Beekman 2000. Groundwater recharge in the Kalahari, with reference to paleo-hydrologic conditions. Journal of Hydrology. 238:110-123.

Demisse, G. 2006. Spatial distribution of savannah woody species biodiversity in Serowe, Botswana. Unpublished MSc thesis. International Institute for Geo-Information Science and Earth Observations, ITC. Esnchede, The Netherlands., Enschede.

Dennis, N., M. Knight and P. Joyce 1999. The Kalahari: Survival in a Thirstland Wilderness. New Holland Publishers.

Do, F. and A. Rocheteau 2002. Influence of natural temperature gradients on measurements of xylem sap flow with thermal dissipation probes. 1. Field observations and possible remedies. Tree Physiol. 22:641-648.

Dowty, P., K. Caylor, H. Shugart and W. Emanuel 2000. Approaches for the estimation of primary productivity and vegetation structure in the Kalahari region. *In* Towards Sustainable Natural Resource Management in the Kalahari Region Eds. S. Ringrose and R. Chanda. University of Botswana Press. .

Granier, A. 1985. Une nouvelle méthode pour la mesure du flux de sève brute dans le tronc des arbres Annales des Sciences Forestières 42:193-200

Granier, A., P. Biron, N. Breda, J.Y. Pontailler and B. Saugier 1996. Transpiration of trees and forest stands: short and long-term monitoring using sapflow methods. Global Change Biology. 2:265.

Granier, A., V. Bobay, J.H.C. Gash, J. Gelpe, B. Saugier and W.J. Shuttleworth 1990. Vapour flux density and transpiration rate comparisons in a stand of Maritime pine (*Pinus pinaster Ait.*) in Les Landes forest. Agric For Meteorol. 51:309-319.

Green, S. and B. Clothier 1988. Water use of kiwifruit vines and apple trees by heat-pulse technique. J Exp Bot. 39:115-123.

Hatton, T.J., S.J. Moore and P.H. Reece 1995. Estimating stand transpiration in a Eucalyptus populnea woodland with the heat pulse method: measurement errors and sampling strategies. Tree Physiol. 15:219-227.

Heritage, A. 2002. The Great World Atlas. Dorling Kindersley Publishing.

Köstner, B., A. Granier and J. Čermák 1998. Sapflow measurements in forest stands: methods and uncertainties. Annales des Sciences Forestières. 55:13-27.

Leistner, O. 1967. The Plant Ecology of the Southern Kalahari. *In* Memoirs of the Botanical Survey of South Africa. Department of Agricultural Technical Research, Pretoria. 172 p.

Lu, P., L. Urban and P. Zhao 2004. Granier's Thermal Dissipation Probe (TDP) Method for Measuring Sap Flow in Trees: Theory and Practice. Acta Bot Sin. 46:631-646.

Ludwig, F. 2001. Tree-grass Interactions on an East African Savanna: the effects of competition, facilitation and hydraulic lift. Wageningen University and Research Centre, sub-department of Nature Conservation, Wageningen.

Lundblad, M., F. Lagergren and A. Lindroth 2001. Evaluation of heat balance and heat dissipation methods for sapflow measurements in pine and spruce. Ann For Sci. 58:625-638.

Mapanda, W. 2003. Scaling-up tree transpiration of eastern Kalahari sandveld of Botswana using remote sensing and geographical information systems. MSc thesis. International Institute for Geoinformation Science and Earth Observations, ITC. Eschede, The Netherlands, p. 117.

Meinzer, F.C., S.A. James and G. Goldstein 2004. Dynamics of transpiration, sap flow and use of stored water in tropical forest canopy trees. Tree Physiol. 24:901-909.

Obakeng, O.T. 2007. Soil moisture dynamics and evapotranspiration at the fringe of the Botswana Kalahari. Vrije Universiteit, Amsterdam, NL.

Olbrich, B.W. 1991. The verification of the heat pulse velocity technique for estimating sap flow in *Eucalyptus grandis*. Can J For Res. 21:836-841.

Oren, R., N. Phillips, B.E. Ewers, D.E. Pataki and J.P. Megonigal 1999. Sap-flux-scaled transpiration responses to light, vapor pressure deficit, and leaf area reduction in a flooded *Taxodium distichum* forest. Tree Physiol. 19:337-347.

Otieno, D., M. Schmidt, J. Kinyamario and J. Tenhunen 2005. Responses of *Acacia tortillis* and *Acacia xanthophloea* to seasonal changes in soil water availability in the savanna region of Kenia. Journal of Arid Environments. 62:377-400.

Privette, J., Y. Tian, R. Roberts, R.J. Scholess, Y. Wang, K. Caylor, P. Frost and M. Mukelabai 2004. Vegetation structure characteristics and relationships of Kalahari woodlands and savannas. Global Change Biology. 10:281-291.

Ringrose, S., W. Matheson, P. Wolski and P. Huntsman-Mapila 2003. Vegetation cover trends along the Botswana Kalahari transect. Journal of Arid Environment. 54:297-317.

Roberts, J. 1977. The Use of Tree-cutting Techniques in the Study of the Water Relations of Mature *Pinus sylvestris L*. J Exp Bot. 28:751-767.

Roupsard, O., A. Ferhi, A. Granier, F. Pallo, D. Depommier, B. Mallet, H. Joly and E. Dreyer 1999. Reverse Phenology and Dry-Season Water Uptake by Faidherbia albida (Del.) A. Chev. in an Agroforestry Parkland of Sudanese West Africa Functional Ecology. 13:460-472.

Roupsard, O., A. Ferhi, A. Granier, F. Pallo, D. Depommier, B. Mallet, H.I. Joly and E. Dreyer 1998. Fonctionnement hydrique et profondeur de prélèvement de l'eau de Faidherbia albida dans un parc agroforestier soudanien. *In* In: L'Acacia au Sénégal. ORSTOM Editions, Paris, pp. 81-103.

Scholes, R., P. Dowty, K. Caylor, D. Parsons, P. Frost and H. Shugart 2002. Trends in savanna structure and composition along the aridity gradient in the Kalahari. Journal of Vegetation Sciences. 13:419-428.

Sekhwela, M. 2003. Woody vegetation resource changes around selected settlement along aridity gradient in the Kalahari, Botswana. Journal of Arid Environments. 54:469-482.

Seymour, C. and S. Milton 2003. A collation and overview of research information on Acacia erioloba (Camelthorn) and identification of relevant research gaps to inform protection of the species. Department of Water Affairs and Forestry, Pretoria, South Africa.

Smith, D.M. and S.J. Allen 1996. Measurement of sap flow in plant stems. J Exp Bot. 47:1833-1844.

Thomas, D.S.G. and P.A. Shaw 1991. Kalahari environment. Cambridge University Press, Cambridge etc. 284 p.

Vertessy, R.A., R.G. Benyon, S.K. O'Sullivan and P.R. Gribben 1995. Relationships between stem diameter, sapwood area, leaf area and transpiration in a young mountain ash forest. Tree Physiol. 15:559-567.

Vertessy, R.A., T.J. Hatton, P. Reece, S.K. O'Sullivan and R.G. Benyon 1997. Estimating stand water use of large mountain ash trees and validation of the sap flow measurement technique. Tree Physiol. 17:747-756.

Wullschleger, S.D., P.J. Hanson and D.E. Todd 2001. Transpiration from a multispecies deciduous forest as estimated by xylem sap flow techniques. For Ecol Manag. 143:205-213.

Wullschleger, S.D., F.C. Meinzer and R.A. Vertessy 1998. A review of whole-plant water use studies in trees. Tree Physiol. 18:499-512.

Wyk van, B. and P. Wyk van 1997. Field Guide to Trees of Southern Africa. Struik Publishers.

Conductive Sapwood Area

An overview of xylem functioning based on NMR

Abstract

The estimations of sap flow using thermal dissipation probes (TDP) in nine tree species of the Botswana Kalahari, highlighted the need to assess current methods of sapwood area evaluation. The extreme hardness of the stem wood in the species studied obviated the use of common methods in which wood cores are analyzed by chemical reagents or visual observation. Consequently, an approach termed *cut&dye* which has been previously used in studies of Kalahari species was implemented. Cut trees were submerged in a staining solution. Thin stem disks were then obtained from the cut tree and analyzed based on the colored section of the xylem. However, the stained pattern in most of the species did not reveal a clear delimitation of sapwood area. Moreover, in some species stained disks did not provide a comprehensive description of sapwood functionality. As a result, all the samples were imported to the Netherlands and exposed to X-ray computed tomography (CT). The results not only showed a different sapwood boundary compared to the wood staining method, but they also revealed sapwood sectoring, *i.e.* areas of contrasting composition inside the sapwood boundary in some species. CT proved to be a useful tool to discriminate areas of different density and water content inside the tree cross section but it cannot detect in which portion of the xylem sap flow takes place.

In a different approach, nuclear magnetic resonance (NMR) was used for the first time to investigate the relation between sapwood staining, CT scanning and the surface in which actual flowing occurs in a small tree. The results confirmed that only a relatively small percentage of the xylem is active and that high to slow speed channels exist in the functional annulus. Another important finding related to sapwood delimitation is that the active portion of the xylem varies with time and therefore the staining approach will reveal only the high speed

channels active at the moment of the dye implementation. A short review of the TDP method clarified that the potential sap conductive area, rather than the real-time flowing surface, should be combined with TDP measurements. The main conclusion is that wood staining is not an efficient approach for sapwood area determination as it can mislead the quantification of conductive tissue. Methods such as portable CT or visual observation of fresh wood cores or stem disks, can provide more reliable sapwood determination.

3.1 Introduction

Knowledge of processes related to plant water transport such as transpiration, photosynthesis and CO_2 uptake, has substantially increased during the last two decades, however some mechanisms involved are not yet completely understood. For example, scientists have been able to identify the microscopic conduits across which water circulates in plants but the general debate on how water can ascend to the apex of tall trees is still ongoing (Dixon and Joly 1895; Meinzer *et al.* 2001; Tyree 1997; Tyree 2003; Wei *et al.* 1999; Zimmermann et al. 2004; Zimmermann *et al.* 2002). Inside vascular plants, water withdrawn from moist soil flows through the narrow but thick-walled conduits of the xylem[5]. What occurs along this journey has numerous implications for plant transpiration and is therefore a subject of interest in different disciplines including plant physiology, forest hydrology, agriculture and micro-climatology.

Several methods have been used for measuring water transported by plants, for example lysimeters, potometers, ventilated chambers, chemical tracers, isotopes, energy balance, sap flow based methods, geophysical methods and recently, NMR (Nuclear Magnetic Resonance). Among them, thermal-based sap flow methods *e.g.* thermal dissipation probes (TDP) have been widely used. (For details on TDP operation the reader may refer to Granier 1987, Köstner *et al*, 1996 or Lu *et al* 2004, and Chapter 2 of this thesis). Despite its technical simplicity and good performance, TDP like other sap flow methods has two main disadvantages: *i)* They are invasive, as they normally require probes to be inserted into the xylem, and *ii)* they rely on precise determination of sapwood area. Traditional methods of sapwood area determination involve a considerable degree of uncertainty as they are based on macroscopic sample observation, in which the natural hydraulic mechanisms are disturbed. The dynamics of xylem hydraulic conduits are far more complex than in an artificial pressurized system. Moreover, their functionality and performance is time-variable, thereby complicating any method for determination of conductive sapwood area.

Among the possibilities for studying xylem tissue in detail, NMR flow imaging offers the most comprehensive description of the xylem transport processes (detailed explanation of NMR principles can be found in Callagham (1993) and Levitt (2001)). For the last two decades NMR and MRI (Magnetic Resonance Imaging) have been used for the characterization of the physical state of water in plant cell, tissue, phloem and xylem (Köckenberger *et al.* 1997; Mac Fall and Van As 1996; Peuke *et al.* 2006; Rokitta *et al.* 1999; Scheenen *et al.* 2002; Scheenen *et al.* 2007; Van As 2007; Van As *et al.* 1994; van der Toorn *et al.* 2000; Windt *et al.* 2006). An important advantage of the technique is that it is non-invasive and that it does not require tracers or markers: the MRI signal origi-

---

[5] In this study *sapwood* refers to the stem section through which sap flows, while the term *xylem* denotes the vascular tissue involved

nates from the protons of water that are already present in the plant. This characteristic makes MRI ideal for the study of xylem transport, which relies on fragile pressure gradients that are easily disrupted by invasive experimentation. However, MRI is not yet a common commercial tool for plant research as it requires dedicated hardware that allows the imaging of intact plants. Another disadvantage of MRI, besides the cost and complexity of the instrumentation is that it is not portable and therefore can not be used in field experiments.

Several difficulties were encountered in the determination of the sapwood area in the Kalahari species, from the technical and logistic problems consequent of the remoteness and harshness of the environment, to the erratic results offered by traditional methods. As a result, samples of *ca.* 180 trees from nine woody species were imported to the Netherlands where a detailed examination of the xylem tissue was carried out. Modern technology including computed X-ray tomography and MRI was used in an attempt to obtain a detailed understanding of plant xylem functioning.

In this chapter a short review on the methods for sapwood area determination is presented, followed by a discussion on the implications of xylem functioning in TDP sap flow estimations as learned from MRI.

3.2   *Methods for sapwood area determination*

Correct conductive sapwood area evaluation is critical for estimations of sap flow, however its determination in sap flow methods has been poorly discussed in scientific literature. The focus tends to be on the technical aspects of the sensors and the interpretation of the results, and little attention is given to the difficulties of measuring the sapwood area. A few published articles have addressed this specific topic e.g. Rust (1999) and Lu (2004), while others indirectly provide alternatives for sapwood area determination when presenting methods for studying internal structure of tree wood (Fromm *et al.* 2001; Homan *et al.* 2007; Steppe *et al.* 2004).

The most common method for delimiting a tree's conductive sapwood is the extraction of wood cores with an increment borer. In this method, wood cores can be visually analyzed, stained or measured for water content by gravimetric methods. Visual analysis methods are applicable if obvious changes in color and texture exist between sapwood and heartwood boundary (*e.g.* Norway spruces or some *Acacia spp*). However, one has to be cautious with this approach as contrast in color is not strictly related to the boundary between conductive and non-conductive wood (Lu *et al.* 2004). Another approach is the staining of wood cores which takes advantage of the difference in chemical composition between xylem and heartwood causing different coloration of the two tissues. Staining solutions

commonly used include benzidine and sodium nitrite, safranin astra and Eosin-B® (MERCK). Although successful in many studies, the staining method is not immune to uncertainties. In his comparative study of different methods for xylem determination, Rust (1999), found that in species such as *Pinus sylvestris* the existence of a non-functional xylem transitional zone would be detected as an active xylem since it is not chemically modified as the heartwood. This would lead to overestimations of xylem area and consequently of sap flow (15% in the case mentioned by Rust 1999). In the third approach, cores of wood that have been visually examined for the boundary between sapwood and heartwood, can be subject to water content evaluation by the gravimetric method. A sharp decrease in water content would define the edge of the sapwood (Kravka *et al.* 1999; Poyatos *et al.* 2005). An alternative approach, when wood cores cannot be easily obtained, is the resistance to penetration method (Rust 1999). Based on the difference in hardness between sapwood and heartwood, this method uses a specially designed rotating needle that is inserted into the wood. The power needed to penetrate at a certain rate is calibrated to detect the depth at which the change in tissue occurs. When the difference in wood hardness is not enough to be detectable with the system (which may happen), it can only be used under freezing temperatures when the frozen water present in the sapwood will make this tissue harder to penetrate than the heartwood. This method has provided good results, however it is mainly applicable in areas with certain frequency of frost.

If wood hardness does not allow core extraction or penetration, non-invasive methods such as portable compute tomography (CT) have proved to be a good option to scan wood anatomy (Fromm *et al.* 2001; Rust 1999; Steppe *et al.* 2004). The principle under which CT is used in this case, consists of the attenuation of the of beam radiation that the wood tissue experiments under increasing density and moisture. If differences in sapwood and heartwood density are too low to be detected by CT, the contrasting moisture between the two tissues will define the boundary between them. A disadvantage of this method, besides the high cost of the equipment, is the long time needed to acquire an image. For example, Rust (1999) reported a time between 30min. to 1 hour for a CT measurement in a 30cm diameter tree, compared with 5min. required for measurement using an increment borer. When the study justifies tree cutting, or when use of an increment borer or portable CT scanning is not feasible, thin stem disks can be obtained from the cut stem and analyzed in a laboratory. In some type of woods the boundary between sapwood and heartwood can be visually detected or it can be inferred from chemical analysis or stained with dyes. A cut tree can be fed with a staining solution which would delimitate the sapwood boundary. Some authors consider this approach the most accurate (Lu and Chacko 1998; Lu *et al.* 2004). However tree cutting is environmentally unfriendly and is not allowed or is very restricted in several countries, therefore this method is recommended only in conditions in which no other method is feasible.

Among the non-invasive methods, Nuclear Magnetic Resonance (NMR) can both determine the sapwood-heartwood boundary and provide a comprehensive description of the xylem functioning. For the last two decades, since the publication of the first NMR non-imaging method to measure xylem water transport (Van As and Schaafsma 1984), NMR and MRI have been used for the characterization of the physical state of water in plant cells, tissue, phloem and xylem. Moreover, NMR is currently used for the quantification of water transported within cells, over membranes, and in xylem and phloem (Köckenberger *et al.* 1997; Mac Fall and Van As 1996; Peuke *et al.* 2006; Rokitta *et al.* 1999; Scheenen *et al.* 2002; Scheenen *et al.* 2007; Van As 2007; Van As *et al.* 1994; van der Toorn *et al.* 2000; Windt *et al.* 2006). However, NMR is not yet a common commercial tool for plant water transport research as it requires dedicated hardware that allows the imaging of intact plants. An important advantage of the technique is that it is non-invasive and it does not require tracers or markers: the MRI signal originates from the protons of water that are already present in the plant. This characteristic makes MRI ideal for the study of the xylem and phloem transport, which rely on fragile pressure gradients that are easily disrupted by invasive experimentation. The disadvantage of MRI is the cost and complexity of the instrumentation and that its use is currently limited to laboratory experiments.

3.3   *Sapwood area determination in the Kalahari species*

The determination of sapwood area in the Kalahari species studied, encountered several difficulties. First, the implementation of the increment borer in the selected species was impractical due to wood hardness. Second, the remoteness of the study area and the number of measured trees (*ca.* 180) made the use of methods such us CT, either by portable device or laboratory-based instruments, unfeasible. After trials and consultations with local authorities, an approach termed here "cut&dye" was implemented. In this approach, trees from which sap flow measurements had been taken and biometric characteristics identified were felled and immediately immersed in a bucket filled with a staining solution (Eosin-B®). Trees placed in buckets were allowed to transpire for several hours and thin stem disks were then cut (Figure 3.1). According to the "cut&dye" method, the staining solution should have stained the conductive area red. Although the cut&dye method provided information about the sapwood-heartwood boundary in some species, it also raised concerns about the interpretation of the stained wood and xylem functioning in the context of sap flow estimations with TDP.

Direct observation of stained disks revealed a clear sapwood-heartwood boundary and uniform sapwood coloring in some species; e.g. *Dichrostachys cinerea*, *Terminalia sericea* and *Acacia erioloba*. However, in other species, the dye stained only certain sectors of the sapwood. This was inconsistent with what could be visually identified as sapwood, based on color contrast with the heartwood, e.g. *Acacia fleckii and Ochna pulchra* . The most intriguing case was *Boscia albi-*

trunca in which neither the staining solution nor direct observation of stem disks gave a clear indication of the sapwood-heartwood frontier, suggesting the non-existence of heartwood. An example of stained disks of each species is presented in Figure 3.2.

Figure 3.1 Cut&dye for the determination of conductive sapwood area. After sap flow measurements took place, every tree was cut and immersed in a staining solution. After hours of transpiration stem disks were obtained from which the area of conductive tissue was measured.
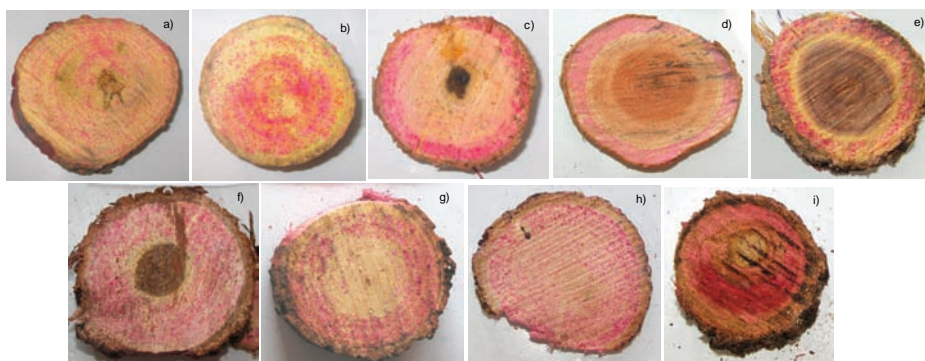
Figure 3.2 Stained stem disks of the species investigated. a) *Burkea Africana* ,b) *Lonchocarpus nelssi,* c) *Acacia fleckii* , d) *Ochna pulchra*, e) *Dichrostachys cinerea*, f) *Acacia erioloba*, g) *Acacia luederitzii*, h) *Boscia albitrunca* and i) *Terminalia sericea*

As these uncertainties would introduce serious misestimations of sap flow, further investigations were required. The tree disks were transported to the Netherlands where samples of five of the species studied were subjected to CT examination, with the collaboration of the Medisch Spectrum Twente in Enschede (CT scanning was performed by a SOMATOM PLUS x-ray, Siemens). The resulting images provided useful information on the characteristics of sapwood in the Kalahari species studied that are non-detectable by human eye. CT images confronted with the stained disks are presented in Figure 3.3. Sectoring of the xylem tissue was revealed in species such as *Acacia fleckii* (Figure 3.3a) in which the outer rings appear brighter in the CT, suggesting denser tissue in contrast with the inner rings that look darker in the image. A similar pattern was observed in *Burkea africana* (Figure 3.3c) in which the inner dark section of the sapwood region is not evident in the photograph of the stained disk. As observed from the Eosin staining, *Boscia albitrunca* (Figure 3.3b) has no well-defined heartwood and therefore staining occurred indiscriminately in the stem cross section, even at the center of the disk. On the other hand, in species such as *Dichrostachys cinerea* and *Acacia luederitzii* (Figure 3.3d and 3.3e), what appears to be the heartwood by direct observation is in agreement with the CT image; i.e. bright areas meaning very dense tissue compared with the dark central areas in the picture. However, the staining of *A. luederitzii* sapwood was non-uniform compared to what is observed in *D. cinerea*. A similar pattern was observed in most of the other 20 disks of the same species. The alternate bright and dark pattern inside sapwood represents earlywood - latewood differences in density within growing rings (Fromm *et al.* 2001).
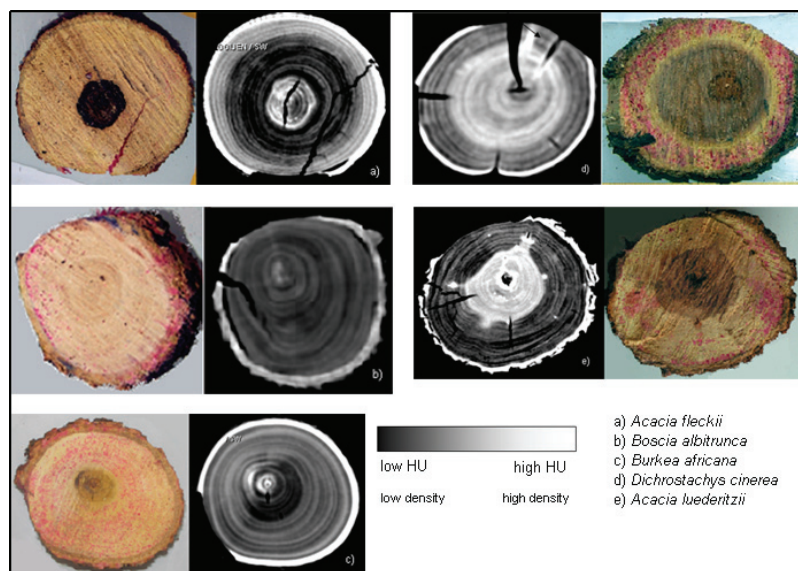
Figure 3.3 Disk stained with Eosin-B solution confronted with CT scanning in five species. The gray scale in the CT images represents the Hounsfield Units (HU) that are proportional to tissue density. Every image is scaled in a different range of HU to allow good resolution and therefore the scale presented is only indicative.

The methodology used above provides useful information on sapwood heterogeneities not revealed by the traditional methods of sapwood area determination. Although the CT images proved to be useful for an improved evaluation of conductive area to be combined with TDP measurements, they also introduced questions on xylem functioning and the possible implications for sap flow assessment from TDP measurements. The images presented in Figure 3.3 suggest that further investigation of the xylem anatomy in the Kalahari species is needed. It was not feasible to conduct additional studies in the framework of the Kalahari project. As such, another examination of sapwood functioning in the context of sap flow estimations was carried out using NMR technique on a local tree species in the Netherlands.

3.4   Xylem as seen by NMR

3.4.1   The experiment

For the study of the xylem in a live tree using NMR imaging, a young pot-grown *Ligustrum japonicum* tree was obtained from a local grower. The tree was 3.5m in height and 4.5cm DBH. The tree diameter selection was constrained by the inner diameter of the MRI gradient coil. The canopy of the tree was carefully wrapped in a plastic sheet to facilitate its introduction in the vertical free bore of the magnet. In order to undertake a volumetric measurement of water consumption for further comparison of sap flow estimation, the tree was separated from the roots at a low stem level before being placed in the MRI system. To avoid air entering into the xylem conduits, which can result in xylem embolism, a second cut was immediately performed under water, a few centimetres above the first. Next, and while still submerged, the tree was transferred to a plastic bag full of water and from there to a PVC cylinder. The water level in the PVC cylinder was fixed below the MRI imaging plane and maintained constant through the experiment (Figure 3.4). During the final hours of measurement, a solution of Eosin-B was added to the PVC cylinder to stain the sapwood of the transpiring tree. Simultaneous measurements with 3 TDP sensors were carried out in the same tree at different azimuths during *ca.* 20 hours and a volumetric measurement of water consumption implemented (the scheme of volumetric measurement closely followed the procedure presented in Chapter 2, section 2.2.6). The objective of the experiment was twofold: to compare xylem area determination by NMR with the cut&dye procedure and to analyze the effect of xylem area misestimations in sap flow estimations.

3.4.2 MRI setup

The experiment took place at the Wageningen NMR-centre in the Netherlands. The MRI system consists of an Avance console (Bruker, Karlsruhe, Germany) and a super conducting magnet with a 50cm vertical free bore (Magnex, Oxford, UK), generating a magnetic field of 3T (128 MHz proton frequency). A cylindrical gradient set with an inner diameter of 10cm was used. The gradient coil containing the radio frequency (RF) assembly and the tree were placed on top of a support system and inserted in the 50cm bore of the magnet as showed in Figure 3.4. Within the bore, the climate was controlled by a remote climate control unit. Before introducing the tree in the gradient, three tiny tubes filled with water were taped to the stem as a reference for non-flowing water.
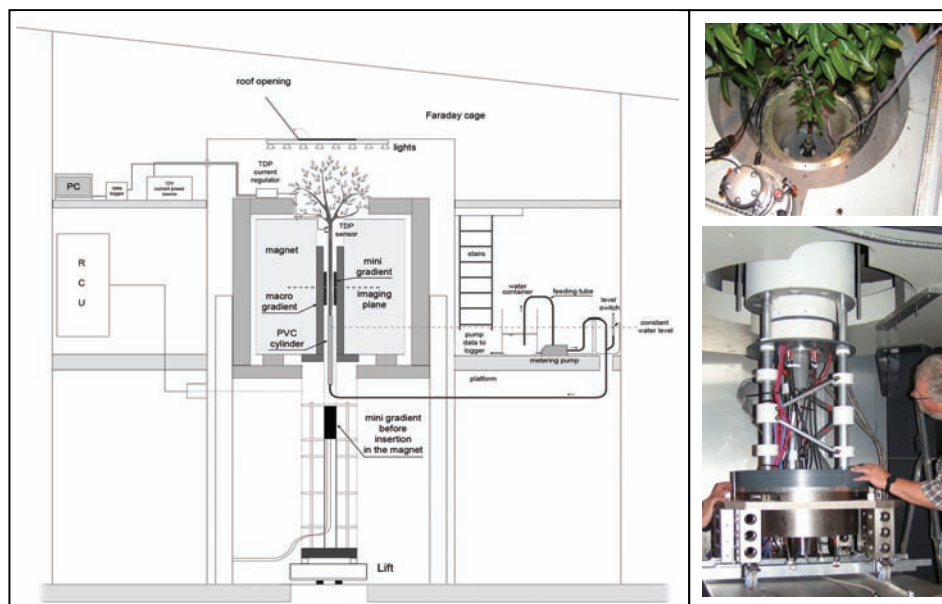
Figure 3.4 NMR experiment set-up at the Wageningen NMR center

3.4.3 MRI flow imaging

In this study, a PFG-MSE-TSE (pulsed field gradient - multi echo - turbo spin echo) sequence was used. From this sequence, tissue water content, density, average linear water velocity, the amount of flowing and stationary water, the flow conducting area and the volume of flow per pixel can be obtained. A Complete description of these sequences is available in Scheenen *et al* (2000a), Van As (2007) and Windt *et al* (2006). The imaging procedure can roughly be divided into three steps: excitation, flow encoding and image acquisition. MRI of

the investigated tree started simultaneously with sap flow measurements early on 08/06/05 and the imaging itself started at ~18h00 the same day. The resulting images (NMR flow maps) of the *L. japonicum* tree together with the stained cross section are presented in Figure 3.5. It should be noted that MRI images represent sap flow parameters at the time of the measurement and therefore are variable over time.
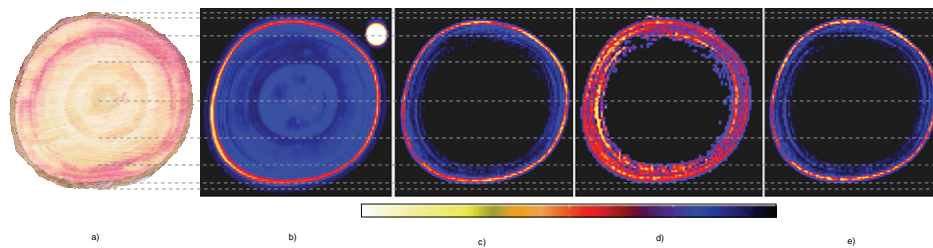
Figure 3.5 Tree cross section at the NMR imaging plane. a) photograph of the disk taken at the end of the experiment showing the stained sapwood. b) to e) MRI flow parameters maps: b) amplitude of the signal *i.e.* distribution of water in the stem both flowing and stationary, c) flowing water, d) average linear velocity and e) average flow per pixel. Every image is independently scaled for better resolution. The scale bar presented is indicative

The images presented in Figure 3.5 correspond to the moment of maximum flow which occurred shortly after the beginning of the experiment. Sap activity in the measured tree gradually declined, most likely as a reaction of stem severing

The MRI results show that although water (sap) is present in almost the totality of the cross section, represented by the signal amplitude shown in Figure 3.5b, only a fraction of it is in fact flowing (Figure 3.5c). Another important feature related to the water transport process observed by MRI is the localization of the flowing water; most of it takes place in the outer rings with its maximum in the North and North-West azimuth represented by the yellow pixels shown in Figure 3.5c.

Once the experiment concluded, a thin disk of the tree at the TDP level (above the NMR imaging plane as observed in Figure 3.4) was subject to CT scanning. The CT image revealed the position of the TDP needles in the sapwood. The tangential installation of the probes, different from the standard perpendicular-to-the-tree-axes, is necessary in trees with very thin stems as in the case of the tree used for this experiment. Figure 3.6 shows the CT image together with a normal photograph of the same disk at the TDP installation level. According to these images, what appears to be the sapwood area is discretised in sections of different bulk density. A low density ring represented in the image as a dark circular sector is located between two sections of higher density (bright gray in the CT), namely a very narrow ring in the most outer circumference and a wider area that gradually becomes lighter as it approaches the heartwood. The low density sapwood sector corresponded well with the area marked by MRI as a

flowing surface (scaled from blue to yellow in Figure 3.5c) in which high to low sap speed channels are asymmetrically distributed, with a concentration of the highest linear velocity (yellow pixels) in the SW azimuth (Figure 5d). The average MRI parameters per measurement during the *ca.* 20h of the experiment are presented in Table 3.1.
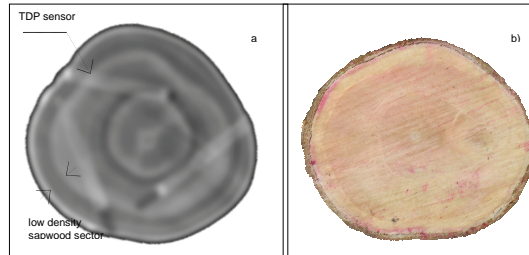
Figure 3.6 CT image, a) and normal photograph, b) of the tree cross section at the TDP insertion plane.

Table 3.1 MRI flow parameters during the first measurements (max. flow)

measurement # (starting 08/06/05 at 21h20)	interval minutes	vol. stationary	conducting area (mm2)	avg. velocity (mm/s)	volume flow (mg/s or ul/s)	volume flow (lit/h)	stationary area %	flowing area %
1	65	177.98	36.64	1.16	42.50	0.15	82.93	17.07
2	130	177.39	38.18	1.22	46.39	0.17	82.29	17.71
3	195	178.14	36.73	1.17	42.87	0.15	82.91	17.09
4	260	179.37	35.34	1.12	39.59	0.14	83.54	16.46

The staining pattern of the stem disk at the imaging plane (Figures 3.5a), does not show the highest conducting sapwood area in totality, however it should be noted that the stained wood is concentrated in the outer rings at some disk azimuths. Conversely, the staining of the disk at the TDP installation plane (Figure 3.6b) does not follow the same trend as the CT image of the same plane. However, the color contrast of the dry wood reveals the same two main sectors of the sapwood, *i.e.* conductive and less conductive areas. The main reason for the poor agreement between the stained disk and the other approaches is the addition of the Eosin solution during the last hours of measurement. At that time, the sap flow was much lower and some of the conductive vessels were less likely to be functioning at an optimal level.

Despite some degree of correspondence among the three approaches presented here, *i.e.* cut&dye, CT scanning and NMR, the lessons learnt by NMR imaging *e.g.* the variability of flowing surface with time and the sectoring of sapwood area, has implications for sap flow from TDP. Moreover, the staining pattern observed in the sapwood of the tree investigated triggers concerns about the validity of this approach for xylem area assessment in TDP sap flow estimations, as discussed in the next section

3.5 NMR vs. TDP. Possible problems related to sapwood area determination in TDP measurements

After the appropriate calibration of the different equipment and the necessary time for the MRI system flow encoding, simultaneous measurements of tree water consumption by TDP sensors, MRI and a metering pump ran for ~20 hours. In order to simulate the diurnal variations of light to which plants are exposed under natural conditions, the illumination of the site was turned off for ~4 h (and thereafter turned ON again) during the final period of measurements

In this experiment there are three different types of information available for the evaluation of sapwood area to be used in sap flow estimations. *i)* MRI surface flowing equal to $38.2mm^2$ at the moment of the maximum flow (Figure 3.5c). *ii)* CT scanning of the same disk at the TDP installation plane. The combination of the most conducting sap flow ring (dark area in CT) and the brighter wide annulus before approaching the heartwood (Figure 3.6a) yields a conductive area of $1025mm^2$, while the area of dark (less dense) outer ring alone is equal to $138mm^2$. Finally, *iii)* staining of the sapwood with the Eosin solution (Figure 3.5a) which indicated that only the less dense ring of the sapwood with an area of $138mm^2$ should be considered. Given the wide range of variation among the three types of results, a review of the principle of TDP method (presented in Chapter 2) is needed.

According to TDP theory, the sensing needle provides the integration of sap flow density along the probe. Consequently, TDP users do not require previous identification of the most active annulus of the xylem. TDPs were calibrated over the totality of the *potential* conductive area according to the definition of sap flux densities (Granier 1987). The concepts of *sap flux density* and *sapwood area,* used in the Granier method are not numerically related to any physical process; only the product of these two quantities, *i.e.* sap flow, is. Therefore, the flow conducting area provided by MRI does not represent the area of consideration for the TDP calculations; this should be the totality of the potential sapwood area. In this case, such area is equivalent to the totality of the sapwood observed in the CT image ($1025mm^2$) regardless of the evidence that a wide sector of it was not active at the moment of the measurements as observed by MRI. In trees with flow patterns similar to those observed in this experiment, TDP needles inserted perpendicular to the stem axes will always capture the sap high speed channels located in the outer rings. As the sensor approaches the center it will be in contact with sectors of the xylem in which reduced flow takes place and eventually will touch areas of zero flow. However as the method is calibrated to provide an integration of sap flow density along the probe, these flow heterogeneities are intrinsically considered.

According to TDP, maximum sap flow in the *Ligustrum* tree was recorded shortly after the beginning of the experiment and declined gradually as the measurements progressed. An expected rapid decrease of sap activity was observed after switching-OFF the lights at ~5h00 followed by a moderate recovery recorded immediately after the lights were switched-ON at ~9h30. Total water consumption of the tree during the measuring interval was 0.97 litres from the averaged results TDP sensors, 2.02 litres from MRI and 1.69 litres from the volumetric measurement. The temporal variability of water consumptions as recorded by each method is presented in Figure 3.7
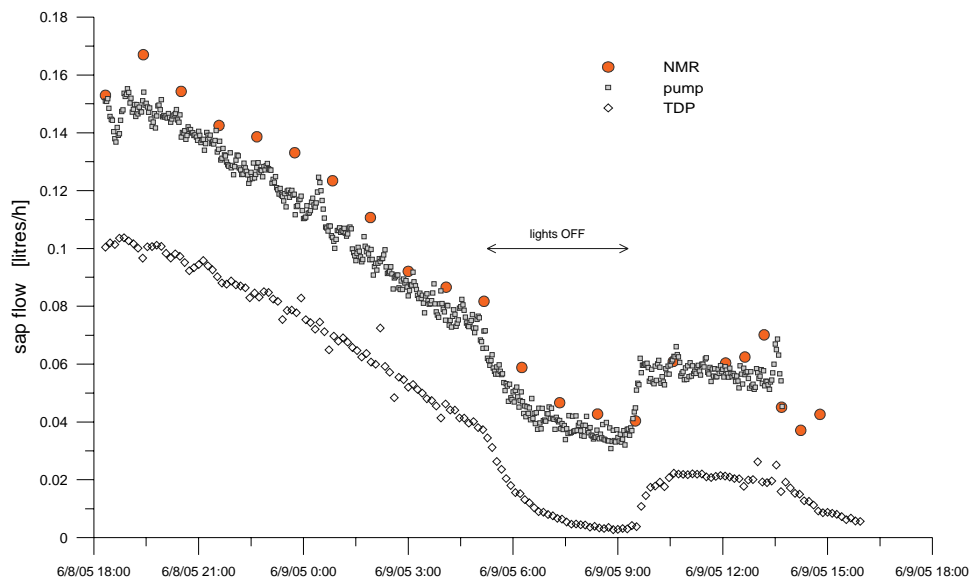
Figure 3.7 Comparison of sap flow from TDP sensors and MRI confronted with a volumetric measurement of tree water consumption with a metering pump in a *Ligustrum japonicum* tree

The results presented in Figure 3.7 show a clear underestimation of water consumption by the TDP sensors compared with MRI and the additional volumetric measurement. On the other hand, the same figure shows a good correspondence in the temporal variation of sap flow among the three methods. Scanning of the cross section with both CT and MRI show that $1025mm^2$ is the maximum value that can be assigned to the sapwood area, therefore underestimations of water consumption by TDP are not in this case due to incorrect sapwood area estimation. The remaining area of the complete cross section corresponds to the heartwood which is clearly shown as having a minimum amount of water (Figure 3.5b) and zero flowing sectors (Figure 3.5 b and c). The differences in sap flow in this case are attributed to the inconvenient positioning of the sensors. CT of the cut disk obtained after the experiment shows that the small diameter of the tree made sensor installation difficult and thus negatively impacted on the results. The

sensors were either mainly in the denser sector of the sapwood or touching what appears to be the heartwood (Figure 3.6a) resulting in insufficient exposure of the sensor to the cooling effect of sap flow and therefore underestimations of it. In practice, incorrect installation of standard TDP (2cm length) sensors in small trees is very likely to occur given the possible narrow xylem thickness (Lu *et al.* 2004). In trees with larger stem diameters, incorrect installation of TDPs is less frequent. Conventional probe installation, i.e. perpendicular to the main tree axes, increases the probability of capturing the xylem sector that is most active at the moment of the measurements

3.6   Conclusions

The experiment carried out with MRI confirmed that this method provides insight into the xylem functioning useful for sap flow estimations. It is known that sap transport in plants and trees takes place through the conduits of the xylem. It is less known however, that not all the xylem tissue operates in the same way. Wind *et al.* (2006), in comparing MRI and microscopy, showed that a percentage (ranging from 31% to 86%) of the potential conducting area of the xylem tissue is functional. However, the exact quantification of this functional portion of the xylem is not critical in the TDP method, provided that the total potential conductive area is properly determined. In this respect, a careful examination of the conductive tissue in wood cores or thin stem disks is essential. CT scanning (either *in-situ* or under laboratory conditions) is highly recommended for this type of study.

The sectoring of the tree xylem as shown by MRI and CT scanning in the *L. japonicum* tree, and by CT in the Kalahari species, unveiled another potential difficulty in TDP measurements not considered by the method. If the most conductive annulus of the xylem is located deeper than 2cm (the TDP needle length) from the stem surface, the sensor will fail to capture the high speed channels of the xylem, leading to underestimations of sap flow densities. This seems to be the case of Kalahari species such as *Acacia fleckii* and *Burkea Africana,* in which CT images presented in Figure 3.3 show a less dense sector of the xylem deep enough to be missed by the TDP sensor. If such a low density area (compared with the outer rings) represents the most conductive xylem area, the TDP needle would yield underestimated values of sap flow densities. Unfortunately, only by NMR imaging this possibility can be confirmed. However sapwood patterns such as in these two Kalahari species must be considered carefully in TDP results. Another scenario in which sectoring of the xylem might affect TDP measurements is exemplified by the experiment with the *L. japonicum* tree. When very thin trees are to be measured, shallow xylem depth might compel TDP sensors to be inserted diagonally, increasing the possibility that the most conductive sector of the xylem is not intercepted (Figure 3.6a). Underestimations of sap flow in this case

were confirmed by the concordance between MRI and volumetric measurement of water consumption.

The conclusions of this experiment suggest that the use of stains for sapwood determination is not always successful. Moreover, the colored pattern left by the staining can eventually mislead sapwood estimations, as it might indicate only the active flow channels at the time of the staining. Normally such staining, either in cores or in cut trees is implemented hours after TDP measurements when the tree may be less active. Considering the temporal variability of the flowing surface explained by MRI, the stained area does not necessarily fit into the sapwood concept of the TDP method. In the absence of CT and MRI instruments for field measurements, a careful observation of fresh wood cores or stem disks can provide the information needed for sapwood determination.

Acknowledgements

References

Callaghan, P. 1993. Principles of nuclear magnetic resonance microscopy. Ed. Oxford. Clarendon Press.

Dixon, H. and J. Joly 1895. On the ascent of sap. Philosophical Transactions of the Royal Society of London B. 186:563-576.

Fromm, J.H., I. Sautter, D. Matthies, J. Kremer, P. Schumacher and C. Ganter 2001. Xylem Water Content and Wood Density in Spruce and Oak Trees Detected by High-Resolution Computed Tomography. Plant Physiology. 127:416-425.

Granier, A. 1987. Evaluation of transpiration in a Douglas-fir stand by means of sap flow measurement. Tree Physiology. 3:309-320.

Homan, N., C. Windt, F. Vergeldt, E. Gerkema and H. Van As 2007. 0.7 and 3 T MRI and Sap Flow in Intact Trees: Xylem and Phloem in Action. Applied Magnetic Resonance. 32:157-170.

Köckenberger, W., J. Pope, J. Xia, K. Jeffrey, E. Komor and P. Callaghan 1997. A non-invasive measurement of phloem and xylem water flow in castor bean seedlings by nuclear magnetic resonance microimaging. Planta 201:53-63.

Köstner, B., P. Biron, R. Siegwolf and A. Granier 1996. Estimates of water vapor flux and canopy conductance of scots pine at the tree level utilizing different xylem sap flow methods. Theoretical and Applied Climatolog. 53:105-113.

Kravka, M., J. Krejzar and J. Čermák 1999. Water content in stem wood of large pine and spruce trees in natural forests in central Sweden. Agricultural and Forest Meteorology. 98-99:555-562.

Levitt, M. 2001. Spin Dynamics: Basics of Nuclear Magnetic Resonance. Wiley, Chichester.

Lu, P. and E.K. Chacko 1998. Evaluation of Granier's sap flow meter in mango (*Mangifera indica* L.) trees. Agronomie. 18:461-471.

Lu, P., L. Urban and P. Zhao 2004. Granier's Thermal Dissipation Probe (TDP) Method for Measuring Sap Flow in Trees: Theory and Practice. Acta Botanica Sinica 46:631-646.

Mac Fall, J. and H. Van As 1996. Magnetic resonance imaging of plants. *In* Nuclear magnetic resonance in plant biology Eds. Y. Shachar-Hill and P. Pfeffer. The American Society of Plant Physiologists, Rockville, pp. 33-76.

Meinzer, F., M. Clearwater and G. Goldstein 2001. Water transport in trees: current perspectives, new insights and some controversies. Environment and Experimental Botany. 45:239-262.

Peuke, A., C. Windt and H. Van As 2006. Effects of cold-girdling on flows in the transport phloem in Ricinus communis: is mass flow inhibited? Plant, Cell and Evironment. 29:15-25.

Poyatos, R., P. Llorens and F. Gallart 2005. Transpiration of montane *Pinus sylvestris* L. and *Quercus pubescens* Willd. forest stands measured with sap flow sensors in

NE Spain. Hydrology and Earth System Sciences Discussions 2:1011-1046.

Rokitta, M., A. Peuke, U. Zimmermann and A. Haase 1999. Dynamic studies of phloem and xylein flow in fully differentiated plants by fast nuclear-magnetic-resonance microimaging. Protoplasma. 209:126-131.

Rust, S. 1999. Comparison of three methods for determining the conductive xylem area of Scots pine (*Pinus syvestris*). Forestry. 72:103-108.

Scheenen, T., A. Heemskerk, P. de Jager, F. Vergeldt and H. Van As 2002. Functional Imaging of Plants: A Nuclear Magnetic Resonance Study of a Cucumber Plant. Biophysical Journal. 82:481-492.

Scheenen, T., D. van Dusschoten, P. de Jager and H. Van As 2000a. Microscopic displacement imaging with pulsed field gradient turbo spin-echo NMR. Journal of Magnetic Resonance. 142:207-215.

Scheenen, T., F. Vergeldt, A. Heemskerk and H. Van As 2007. Intact Plant Magnetic Resonance Imaging to Study Dynamics in Long-Distance Sap Flow and Flow-Conducting Surface Area. Plant Physiology. 144:1157-1165.

Steppe, K., V. Cnudde, C. Girard, R. Lemeur, J.P. Cnudde and P. Jacobs 2004. Use of X-ray computed microtomography for non-invasive determination of wood anatomical characteristics. Journal of Structural Biology. 148:11-21.

Tyree, M. 1997. The Cohesion-Tension theory of sap ascent: current controversies. journal of Experimental Botany. 48:1753-1765.

Tyree, M. 2003. Plant hydraulics: The ascent of water. Nature. 423:923.

Van As, H. 2007. Intact plant MRI for the study of cell water relations, membrane permeability, cell-to-cell and long distance water transport. Journal of Experimental Botany. 58:743-756.

Van As, H., J. Reinders, P. de Jager, P. van der Sanden and T. Schaafsma 1994. *In situ* plant water-balance studies using a portable NMR spectrometer. Journal of Experimental Botany. 45:61-67.

van der Toorn, A., H. Zemah, H. Van As, P. Bendel and R. Kamenetsky 2000. Developmental changes and water status in tulip bulbs during storage: visualization by NMR imaging. Journal of Experimental Botany. 51:1277-1287.

Wei, C., E. Steudle and M. Tyree 1999. Water ascent in plants: do ongoing controversies have a sound basis? Trends in Plant Science. Trends in Plant Science. 4:372–375.

Windt, C., F. Vergeldt, P. de Jager and H. Van As 2006. MRI of long-distance water transport: a comparison of the phloem and xylem flow characteristics and dynamics in poplar, castor bean, tomato and tobacco. Plant Cell and Environment. 29:1715-1729.

Zimmermann, U., H. Schneider, L. Wegner and A. Haase 2004. Water ascent in tall trees: does the evolution of land plants rely on a highly metastable state? New Phytologist. 162:575-615.

Zimmermann, U., H. Schneider, L. Wegner, H. Wagner, M. Szimtenins, A. Haase and F. Bentrup 2002. What are the driving forces for water lifting in the xylem conduit? Physiologia Plantarum. 114:327-335

Dry Season Sap Flow Patterns in the Botswana Kalahari

Abstract

A modified concept of hydraulic redistribution is introduced following observations based on sap flow patterns in nine woody species in the Kalahari dry season. In some cases, a bi-directional process is observed where an upward sap flow extending from ~9h00 to midnight is followed by a downward sap flow extended until ~3h after sunrise. In the case of deep rooted species this bi-directional process allows water tapped from deep soil layers to be brought upwards through the stem, branches and leaves for the transpiration process. Water non-transpired is allowed to go downwards (downwards sap flow, DSF) through the same channels to the roots located in the driest soil layers. Moreover, another process is recognized where air moisture is collected by tree foliage and twigs in a process termed air moisture harvesting (AMH). Moisture thus collected is channeled through the xylem (sapwood) conduits and flows downwards to the roots and adjacent soil. Sap flow measurements were performed by thermal dissipation probes (TDP) in which downward sap flow is identified by time-pattern matching. The species selected for this study, namely *Acacia fleckii , Acacia erioloba, Acacia luederitzii, Boscia albitrunca, Lonchorcarpus nelssi, Terminalia sericea, Burkea Africana, Ochna pulchra* and *Dichrostachys cinerea* are considered among the most abundant and representative of the Kalahari savanna. It is theorized that some observed habits of moisture acquisition aim to provide the necessary conditions for species own-development, while in other cases, they also act as facilitation mechanisms for understory vegetation survival. The DSF and bi-directional processes explained here are species-dependent and occur under specific environmental and tree physiological factors, not yet fully identified.

Keywords: air moisture harvesting, downward sap flow, dry-season, Kalahari savanna

4.1 Introduction

The term Kalahari is a derivation of the Setswana word *Kgalagadi* meaning "always dry" or "a waterless place". As the name implies, the Kalahari Desert has scarce permanent or episodic water courses. Nevertheless, the denomination of "desert" has been regarded as inappropriate given its ecological diversity and relatively well-developed vegetation. Furthermore, the term desert lacks a rigorous scientific meaning and it has been applied to a wide range of environments. Despite a dearth of water, the Kalahari is home to a rich mix of *Acacia* trees, *Acacia* scrub and grasslands. Therefore, in terms of vegetation the Kalahari is better described as a 'dry savanna', rather than as a desert. In these conditions, the survival of vegetation is ensured only if individual species or associations of species are able to implement mechanisms at a local scale to overcome regional or global scale constraints. Published research shows that regional water scarcity and global increases of CO_2 due to climate change, force vegetation to use water more efficiently (Alias and Milton 2003; Bond *et al.* 2003; Seymour 2006). In some vegetation species of the Kalahari, efficient water use strategies include extraordinary water extraction mechanisms. These mechanisms are complex and highly variable across space and time and therefore are not fully understood or even completely identified. In the fields of ecohydrology and ecophysiology, published research on vegetation water use in tropical and boreal environments is more abundant than research in African semi-arid savannas. Ironically, it is precisely in these more arid ecosystems where trees compete with humans for the precious water resources, that greater understanding of vegetation hydrological processes is required. The results presented in this chapter contribute to an understanding of the vegetation-water-climate relationship in the Kalahari.

Among the vast range of vegetation types, this study selected nine of the most abundant woody species in the area for investigation of water-use and transpiration habits. As earlier described in this thesis (Chapter 1), an approach based on sap flow estimations was implemented for the investigation of tree transpiration patters in the Kalahari. Chapters 2 and 3 discuss technical aspects of the sap flow measurements, including difficulties and uncertainties encountered in the studied species

This chapter focuses on the identification of vegetation water-use habits during the Kalahari dry season inferred from the results of the sap flow campaign. In the data set presented, species-dependent processes for the water exchange between soil and atmosphere are observed. These processes can be single-step or multi-step, unidirectional or bidirectional, and are dependent not only on tree physiological features but also on a combination of environmental factors. Careful analysis and interpretation of the observed patterns is essential before upscaling from tree to stand level for the mapping of transpiration.

4.2   Materials and Methods

4.2.1   Background

This study was executed in the framework of the KRP conducted in the Serowe area, Central District of Botswana (S 22°20', E 26°24') at the eastern fringe of the Kalahari basin (Figure 1.2). The area receives a mean annual precipitation (MAP) of 400mm; rainfall is seasonal with its highest intensity in summer (October-April) followed by a dry winter (June-September). The mean annual temperature is 20°C but summer temperatures can exceed 30°C during the day while in winter they can drop below 0°C at night. Surface water streams are ephemeral, making groundwater reserves the main source of water supply. Groundwater is mainly found in the Karoo rocks (sandstones, shales and basalts) below the mantle of Kalahari sands whose thickness increases from 0-5m close to the eastern fringe to 60-100m towards the centre (Obakeng 2007). The topography of the Serowe area is fairly flat and featureless, sloping gently to the west without prominent drainage lines. It is characterized by permeable sands with high infiltration rates and negligible surface runoff (Obakeng 2007). Figure 4.1 presents some climatic parameters of the Serowe area during the year 2004 when this study took place.
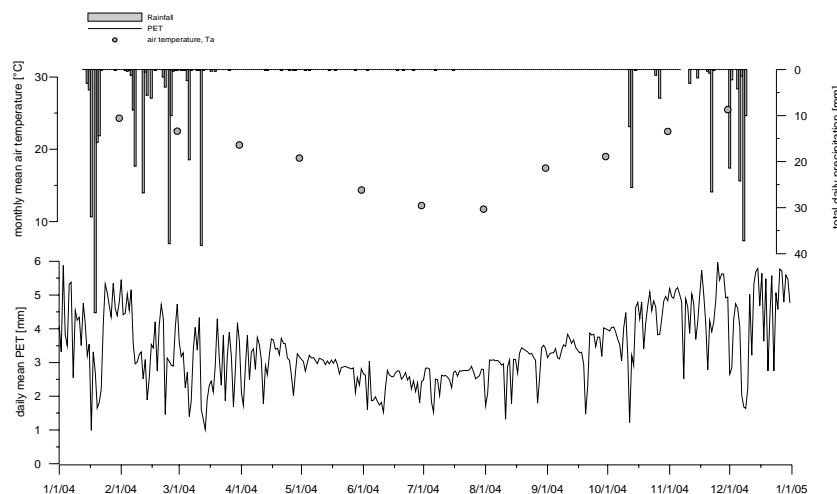
Figure 4.1. Daily precipitation, monthly air temperature and daily mean potential evapotranspiration in the Serowe area during 2004 (data from Obakeng, 2007).

The vegetation cover of the Serowe area was investigated during the KRP (Demisse 2006; Obakeng 2007) and the conclusions were in accordance with the findings reported by the Safari2000 project for the Kalahari precipitation gra-

dient. Woody species belonging mainly to the *Mimosaceae* family represented by the *Acacia* and *Dichrostachys* genera, correspond to a MAP of less than 400mm. Between 400 and 600mm MAP, species of the *Combretaceae* family, represented by the *Terminalia* genus are found. The vegetation cover of the Serowe area is accordingly a mosaic of savanna grassland and low thorny trees, most of them with a marked seasonal variation in leaf cover. Among the most abundant species in the area, nine were selected for this study on the basis of their frequency of occurrence and phenological distinctiveness, namely: *Acacia fleckii, Acacia erioloba, Acacia luederitzii, Boscia albitrunca, Lonchorcarpus nelssi, Terminalia sericea, Burkea Africana, Ochna pulchra* and *Dichrostachys cinerea*. One of the remarkable characteristics of some of these Kalahari species is their ability to tap groundwater during the dry season when surface moisture is unavailable. This attribute is connected with rooting system morphology and physiology, aspects that been investigated in previous studies in the Kalahari (Cole and Brown 1976; Seymour and Milton 2003). Such studies have revealed significant differences in the rooting habits between trees species but have also confirmed fidelity of habits in individual species occupying contrasting habitats (Cole and Brown 1976). Some species mainly belonging to the *Acacia* genus have been portrayed as having both large tap roots and well developed lateral rooting systems, which enable them to make full use of available soil moisture (Burke 2006; Canadell *et al.* 1996; Cole and Brown 1976; Leistner 1967; Ludwig 2001; Otieno *et al.* 2005; Roupsard *et al.* 1999; Sekhwela 2003; Seymour and Milton 2003). Obakeng (2007) explored rooting depths of the Serowe trees during the KRP by putting lithium chloride (LiCl) as a tracer in deep boreholes located near well developed trees. Subsequently, young leaves of the trees were analyzed during consecutive days to monitor the uptake of the tracer. Although the concentration of LiCl revealed a complex moisture movement in the neighbourhood of the roots, it was evident that some species were able to absorb the tracer within a few days at considerable depths. Traces of LiCl were found in *Boscia albitrunca* leaves one day after insertion in a borehole at 40m depth and in *Acacia erioloba* leaves three days after injection at 70m depth. The findings confirmed the deep-rooted character of these two species previously reported in other studies (Alias and Milton 2003; Seymour 2006; Seymour and Milton 2003; Wand *et al.* 1999). Table 4.1 presents general information of the rooting system for the nine species investigated, obtained from published literature. Root description is related to the morphological classification of root systems for the Kalahari species presented by Leistner (1967).

Another important feature related to the water-use habits of the Kalahari species, is their phenology during the vegetative year. Observations during the KRP and information from published literature has shown that the schedule of phenophases in the Kalahari species is variable, and that moisture availability and air temperature variations are the main environmental cues (Childes 1989). Table 4.2 presents an approximate phenological schedule of the studied species combined with the two main environmental influencing parameters: precipitation and air temperature. Table 4.2 indicates periods of flowering, defoliation, moderate

Table 4.1 Morphological description of root system in the Kalahari species

species	root type (from Leistner, 1967)	comment	references
Acacia fleckii	primary roots / bipartite system	Both tap and secondary roots well developed, most secondaries at shallow levels. Common in Xerophytes, typical dry-habit system	Cole and Brown 1976, Burke 2006; Leistner, 1967
Acacia erioloba	primary roots / bipartite system	25cm individual can have roots of 320cm. Mature individuals with tap roots as deep as 60m	Canadell et al. 1996, Seymour 2006; Leistner 1967, Seymour and Milton 2003
Boscia albitrunca	primary roots / tap root system	Primary root well developed. Secondary roots small or absent, lack lateral roots	Cole and Brown 1976, Alias and Milton 2003; Curtis and Mannheimer 2005, Burke 2006
Acacia luederitzii	primary roots / generalized system ?	No clear information on rooting patterns but it is possible that has no deep roots given its high rate of mortality during droughts	Sekhwela and Yates 2007
Terminalia sericea	adventituous roots / intensive centralized system	roots attached to a small stem area forming dense network; roots extending outwards in all directions from a central rockstock; in some cases develop robust lateral roots	Leistner, 1967; Cole and Brown 1976, Childes 1989; Hipondoka et al, 2003
Lonchocarpus nelsii	adventituous roots / intensive centralized system	roots attached to a small stem area forming dense network; roots extending outwards in all directions from a central rockstock	Leistner, 1967; Cole and Brown 1976
Burkea africana	primary roots / generalized system	shallow 15-60cm depth roots	Burke 2006, Childes 1989.
Ochna pulchra	primary roots / generalized system	both primary and secondary roots well developed. secondary roots not concentrated at any level	Leistner, 1967; Childes 1989.
Dichrostachys cinerea	mixed primary and adventituous roots / unintensive descentralized system	widely and deeply extending system with tap roots, strong secondaries and rhizomes	Leistner, 1967; Cole and Brown 1976

Root system classification
according to Cannon, 1949 and Walter,1960 as presented by Leistner, 1967

A. primary roots * :
- generalized system
- tap root system
- bipartite system

* after Leistner, 1967

B. adventituous roots *
- intensive centralized system
- intensive descentralized system

C. mixed primary and adventituos roots *
- unintensive decentralized system

leafiness and full leafiness, as they can be clearly correlated with tree water-use which is the focus of this study. Table 4.2 also indicates the period in which each species was measured with regard to sap flow.

The information presented in Table 4.1 and Table 4.2, together with observations during the KRP suggest that deep-rooting species in the Kalahari flower and come into leaf before the rains, as early as July or August. This indicates independence of available moisture in the upper soil layers and marked response to the rise in temperature (Childes 1989; Curtis and Mannheimer 2005; van Wijk and Rodriguez-Iturbe 2002; Wyk van and Wyk van 1997). After the rains, these species maintain their leaves during part or all of the dry season and start defoliating as temperatures drop according to their degree of resistance to frost e.g. sclerophyllous trees. On the other hand, species with a shallow root system begin vegetative growth only after the onset of the rainy season. As stated earlier in this chapter, the information presented in Tables 4.1 and 4.2 was obtained from available literature; it represents vegetation trends and therefore there may be individual trees that do not follow that trend

4.2.2 Micrometeorological measurements from KRP

The microclimatic monitoring network established in 2001 by the KRP (Obakeng 2007), consisted of eleven Automatic Data Acquisition Systems (ADAS) stations, conceived to measure parameters for evapotranspiration assessment, precipitation and soil moisture characterization. Measurements were acquired continuously from 2001 to the beginning of 2005. Ten of the ADAS stations were installed at fixed locations in the Serowe area, and the remaining one, a mobile station, was used for sap flow measurements. The mobile ADAS station also collected solar radiation, air temperature, relative humidity and wind speed data at each sap flow-measurement site.

4.2.3 Sap flow campaign

Sap flow density (sap flow per conductive sapwood area per unit of time) measurements of the nine selected species were collected during the dry season (July to September) of 2004 using thermal dissipation probes (TDP) (UP Gmbh, Germany) method (Granier 1985; Granier 1987). Sap flow, conductive sapwood area and biometric parameters were simultaneously measured in groups of 18 to 24 trees of each species. Continuous records of sap flow collected every 30min during 3 or 4 days at each site were stored in multi channel data loggers (DataHog2, Skye instruments Ltd, UK). Sap sensors were installed ensuring that the measuring spot on the stem experience minimal sun exposure by proper azimuth selection and adequate sun shielding. Details about the sap flow measurements sites are presented in Table 4.3.

Table 4.2 Phenological schedule of nine tree species in the Serowe area, compared with mean monthly air temperature and total precipitation.
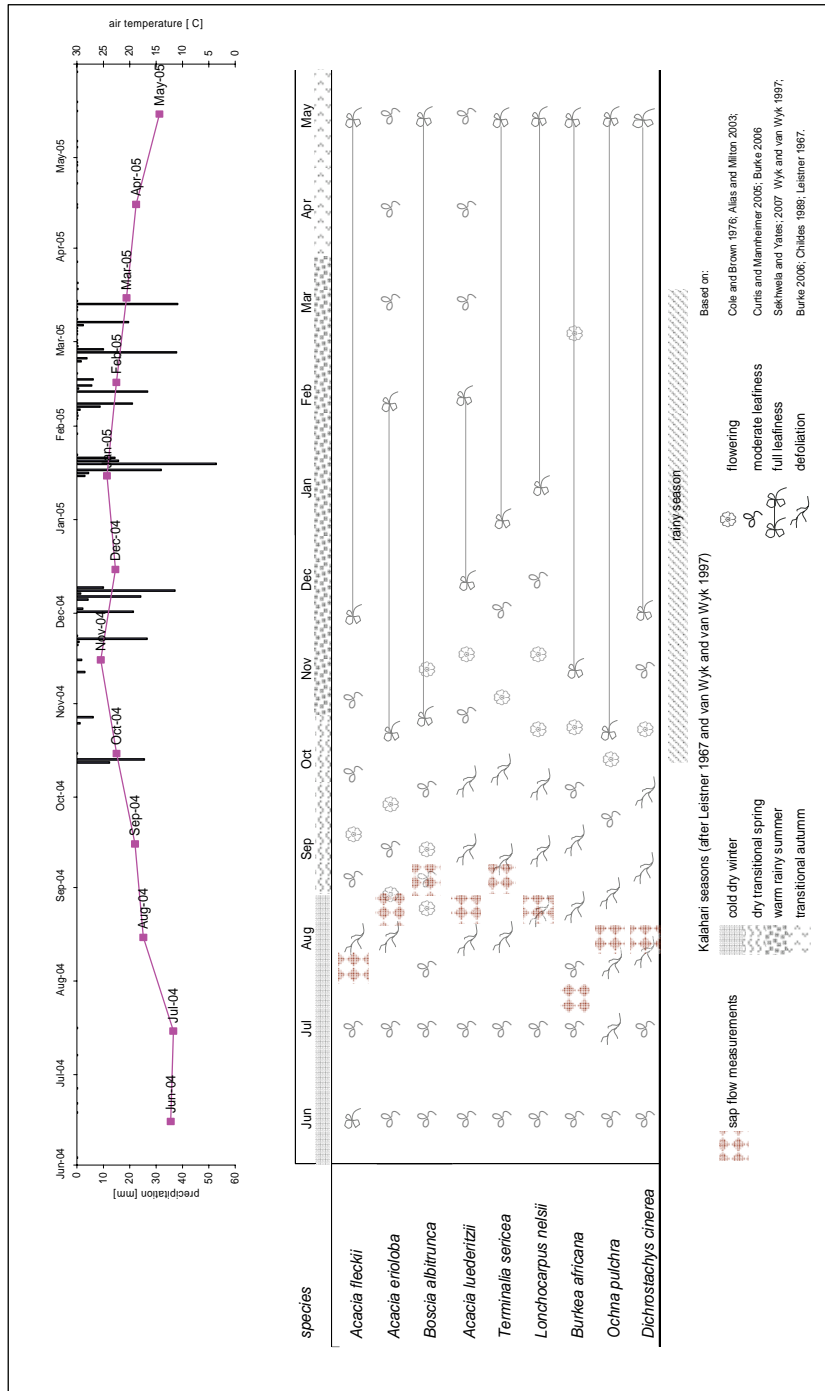
Table 4.3 Sap flow measurements and meteorological parameters acquired during the 2004 dry season campaign.

species	location		period	No. trees	additional measurements
Burkea africana	22°22'19" S	26°22'03 E	30 Jul 04 -2 Aug 04	18	no data
Lonchocarpus nelsii *	22°22'26" S	26°22'09 E	2 Aug 04 - 8 Aug 04	24	WS, SR, RH, Ta
Acacia fleckii	22°23'17" S	26°23'09 E	8 Aug 04 - 11 Aug 04	24	WS, SR, RH, Ta
Ochna pulchra	22°22'26" S	26°22'11 E	12 Aug 04 - 16 Aug 04	24	WS, SR, RH, Ta
Dichrostachys cinerea	22°22'26" S	26°22'13 E	16 Aug 04 - 20 Aug 04	24	WS, SR, RH, Ta
Acacia erioloba	22°22'27" S	26°22'15 E	21 Aug 04 - 26 Aug 04	24	WS, SR, RH, Ta
Lonchorarpus nelsii	22°22'26" S	26°22'09 E	26 Aug 04 - 29 Aug 04	18	WS, SR, RH, Ta
Acacia luederitzii	22°16'33" S	26°15'15 E	29 Aug 04 - 1 Sep 04	21	WS, SR, RH, Ta
Boscia albitrunca	22°16'52" S	26°15'23 E	2 Sep 04 - 6 Sep 04	24	WS, SR, RH, Ta
Terminalia sericea	22°24'21" S	26°24'27 E	7 Sep 04 - 9 Sep 04	18	WS, SR, RH, Ta

WS = wind speed
SR = solar radiation
RH = relative humidity
Ta = air temperature

* aborted campaign. Data not used due to animal disturbances.

4.3   Results

Continuous records of sap flow for the nine species selected are presented in Figures 4.2a to 4.2i. Differences in magnitude and diurnal patterns reflect species-specific sap flow behaviour, assuming soil homogeneity among the sites and generally similar climate conditions during the 44 days or measurements. The singularity of sap flow patterns inherent in species of the same genus is corroborated by the observation of differences in sap flow patterns among the three *Acacia* species investigated. *Acacia luederitzii* (Figure 4.2e) showed small sap flux densities reaching barely 5cm^3/(cm^{2}xh) around mid-day, which is expected during this time of intense defoliation. Variation in peak sap flow among specimens is well correlated with the variation in leafiness. Among the 21 *Acacia luederitzii* trees measured, at least half showed sensitivity to the sun azimuthal position. In general however, there is not much shielding from other neighbouring trees because of the large size of this type of trees. Although displaying a comparable state of defoliation to *Acacia luederitzii*, *Acacia fleckii* (Figure 4.2f) results show slightly higher sap flows with peaks ranging from 5cm^3/(cm^{2}xsec) to 10cm^3/(cm^{2}xsec) for the most leafy trees. Specimens in leaf at this time of the year, have leaves localized mainly on the tree upper branches. *Acacia erioloba* (Figure 4.2g), despite being almost leafless, proves to deserve its reputation as a dry-resistant species (Seymour and Milton 2003) by showing high sap flow activity at the end of the dry season with midday flux densities up to 22cm^3/(cm^{2}xsec)

Sap flow patterns show high sensitivity to the tree crown's position with respect to the sun azimuthal angle. This is reflected in the big range of peak-time occurrence during the daylight hours in the 24 trees measured. The morphology of the acacia tree canopies in general, makes the sap flow pattern more susceptible to sun orientation as compared to the more rounded canopies of other Kalahari species e.g. *Lonchocarpus nelsii*, in which peak sap flows are much more synchro-

nous (Figure 4.2b). The diurnal sap flow pattern of *Lonchocarpus nelsii* reflects sun intensity fluctuations, for example the ones recorded by a pyranometer on the 27th and 28th of August. In order to establish correlations between sap flow and some micro-climatic parameters, Figures 4.3a to 4.3d present representative sap flow curves of four species with contrasting transpiration dynamics. Figure 4.3a illustrates how the two short cloudy events on the afternoon of the 27th of August result in temporary drops of sap flow. The synchronous variations of the pyranometer and TDP records show the rapid reaction of this species to solar radiation oscillations (Figure 4.2b indicates the same behaviour in nearly all the trees of this species measured). *Lonchocarpus nelsii* and *Burkea africana* were at an early stage of defoliation at the time of the measurements and therefore there were no specimens of these two species completely leafless. The presence of matured leaves at the beginning of the annual decline (end of July) seems to be an indicator of delayed transpiration cessation during the dry season.

The five species described above present standard daylight hours transpiration, *i.e.* moisture absorbed from soil by tree roots moved upwards through the stem and branches' xylem and evaporated into the atmosphere at the leaf surface. This process is driven by solar radiation and therefore takes place during daylight hours and declines as solar radiation reduces. Several authors however, report other types of water transfer by trees that result in non-standard transpiration. These processes are identified as hydraulic redistribution (HR), hydraulic lift (HL), hydraulic descend (HD), etc (Amenu and Kumar 2007; Burgess *et al.* 1998; Espeleta *et al.* 2004; Hultine *et al.* 2004; Hultine *et al.* 2003; Moreira *et al.* 2003; Schulze *et al.* 1998; Smith *et al.* 2004). Most of the reported cases involve roots but at least two publications refer to cases involving tree stems, either assumed (Burgess and Bleby 2006) or measured (Hultine *et al.* 2004). In the research presented here, we observed cases of downward sap flow in at least four species namely *Boscia albitrunca*, *Terminalia sericea*, *Dichrostachys cinerea* and *Ochna pulchra*, although standard upwards transpiration was observed in some specimens of the same species.

As TDP sap sensors are insensitive to phloem flow (normally downwards), because the phloem layer is too thin and too near the bark to significantly influence the TDP signal, we conclude that such downward flow must be within the xylem. Moreover, in the case of *Boscia albitrunca* several, though not all, of the specimens present upward sap flow during part of the day. In such cases of bidirectional xylem sap flow, the xylem channels are time-shared *e.g. Boscia albitrunca* where upward sap flow takes place from ~9h00 to ~2h00 on the following
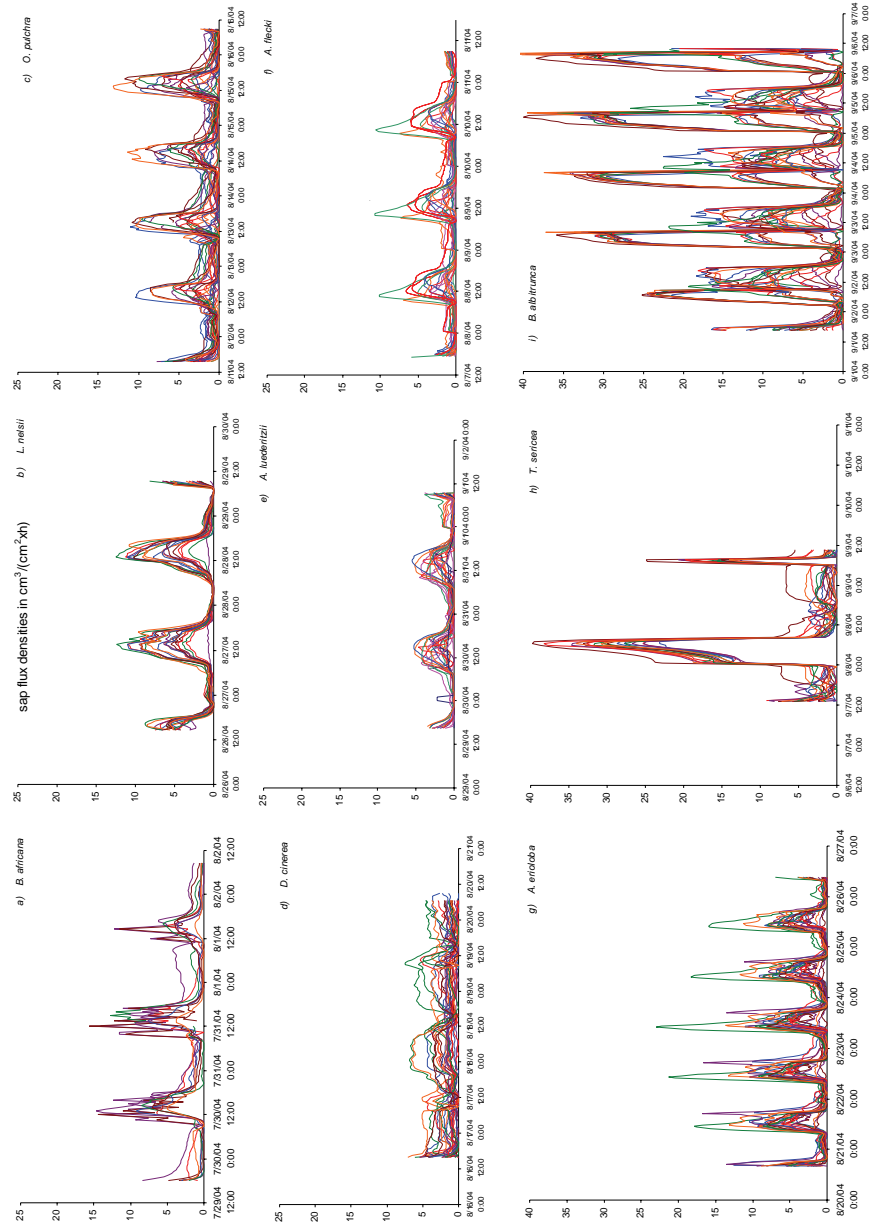
Figure 4.2 sap flux densities (real and apparent) of nine species of the Botswana Kalahari during the dry season of 2004

day, while downward flow occurs from ~02h00 to ~9h00, for the period when this species was investigated (Figure 4.2i). Between these two sap flow 'shifts', there is an interval of nearly zero sap flow between midnight and ~2h00. The transition from downward to upward flow at ~9h00 is, however, quasi instantaneous so that the zero crossing of the sap flux density curve can easily be missed with a 30min TDP sampling scheme (Figure 4.3d). TDP sensors are not intrinsically sap direction sensitive. The procedure implemented to detect upward and downward flow is described below with reference to Figures 4.2 and 4.3.
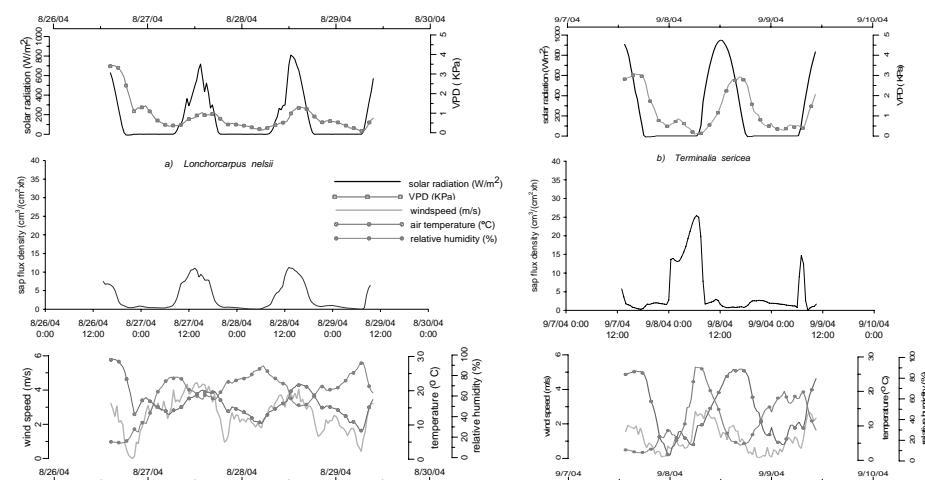
Figure 4.3a and 4.3b. Sap flux densities (real and apparent) of a) *Lonchorcarpus nelsii* and *b) Terminalia sericea*, combined with meteorological parameters: solar radiation (W/m²), vapour pressure deficit, VPD (KPa), air temperature (°C), relative humidity (%) and wind speed (m/sec)

Figures 4.2i and 4.3d are used to illustrate the case of bidirectional xylem flow in *Boscia albitrunca*. At ~9h00 each day (*i.e.* about 2.5 hours after sunrise on 2nd to 6th of September 2004) standard upward sap flow begins and each specimen reaches its maximum sap flow anytime between 10h00 and 17h30. The sap flow peak-time depends on a combination of factors including foliage access to changing sun position, air temperature, soil and air moisture content, wind etc. By the time that sun irradiance has dropped to ~20% of its maximum value at ~17h30, the tree enters a different phase. It is theorized that from that moment, the upward sap flow, instead of being driven directly by the sun-induced photosynthesis, is consuming the accumulated chemical energy and undergoes an exponential time-decay, until it asymptotically approaches zero sap flux density at ~midnight (for this specific site and time of the year). At a given time, which varies between midnight and ~2h00 for this group of trees, sap flow re-started abruptly and reached its maximum value at ~8h00 with an apparent sap flux density roughly twice as high as the day-time upward flow. When this process starts (~2h00) there are no sources of energy for upward sap flow, however the

energy requirements would be larger than during daylight time because of the double apparent 'velocity' (sap flux density). On the other hand, in a downward flow the apparent sap flux density is overestimated by the TDP sensor. When downwards flow occurs, the heated sap flows toward the reference sensor, producing a lower ΔT reading, compared with the signal in normal upward flow. As a result, a higher-than-real apparent sap flux density is recorded (details about TDP principle are presented in Chapter 2). Under this hypothesis, this flow pattern indicates that some specimens of this species have the potential for downward sap flow in the xylem under a specific combination of conditions, not yet fully identified. It is then concluded that among the 24 *Boscia albitrunca* trees simultaneously investigated, 12 *i.e.* 50% present downward sap flow (DSF) with peaks approximately twice as high as the ones occurring during daylight hours. In the other 12 specimens, peak DSF is slightly higher or at least equivalent to the daylight time peaks. At sunrise, DSF starts decreasing in most of the trees but in a few specimens (probably with foliage oriented less directly to sun position) continues rising for a very short time. About 2.5 hours after sunrise all DSF abruptly ceases and upward sap flow re-starts following a sap flux density zero crossing (Figure 4.3d). If the nocturnal sap flow is related to nighttime transpiration, there would be no such 'velocity' zero crossing but rather a smooth transition between night and day sap flux density. Daylight time upward sap flow in *Boscia albitrunca* reaches flux densities as high as $24cm^3/(cm^2xsec)$ during the dry season, the highest among the measured species, a feature that appears consistent with its evergreen character. However at the time of the measurements *i.e.* towards the end of the dry season, leaves of *Boscia albitrunca* are not as abundant and vigorous as in other seasons.
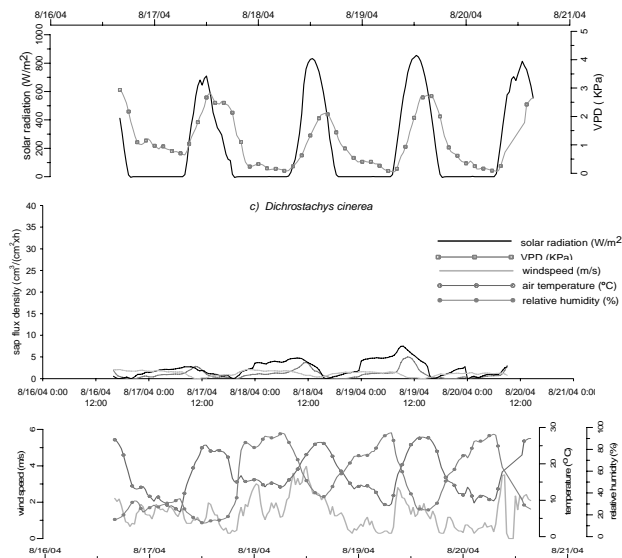
Figure 4.3c Sap flux densities (real and apparent) of *Dichrostachys cinerea* combined with meteorological parameters: solar radiation (W/m²), vapour pressure deficit, VPD (KPa), air temperature (°C), relative humidity (%) and wind speed (m/sec
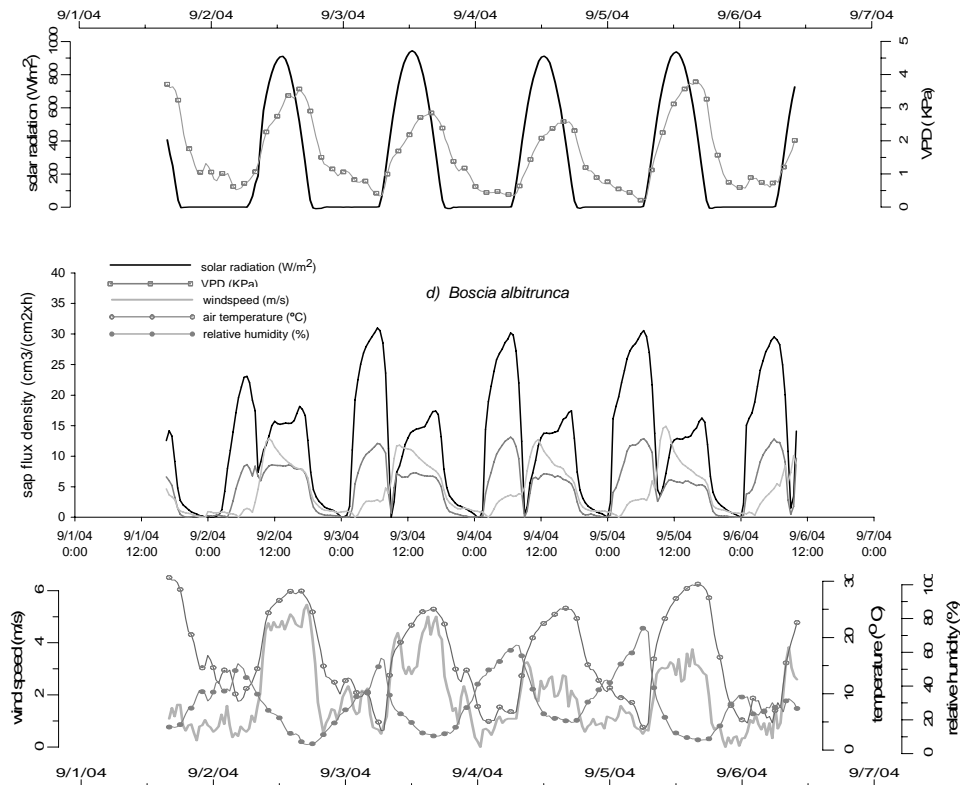
Figure 4.3d Sap flux densities (real and apparent) of *Boscia albitrunca* combined with meteorological parameters: solar radiation (W/m²), vapour pressure deficit, VPD (KPa), air temperature (°C), relative humidity (%) and wind speed (m/sec

Nighttime flow pattern of *Terminalia sericea* (Figures 4.2h and 4.3b) is theorized to be DSF, based on analogy with the *Boscia albitrunca* pattern, namely: *i)* apparent sap flux density twice as high as normal upward daylight hours flow at this time of the year (Obakeng 2007), but no source of energy available for upward sap flow at this time of the day, *ii)* abrupt 'start' and 'stop' flow transition in all measured trees, *iii)* synchrony of the 'stop' transition at ~9h00 *i.e.* 2.5h after sunrise among all the specimens. However, the timing of enhanced DSF is more irregular than for *Boscia albitrunca*. In *Terminalia sericea* it is also observed that there is minimum daylight hours' upwards sap flow at the time of the measurements. Consequently, it is hypothesized that the sapwood is not time-shared between upward and downward sap flow for this species during the period of measurements.

Sap flow observed in *Dichrostachys cinerea* is unidirectional within any given specimen (Figure 4.2d). DSF on this species is much lower than for *Boscia albi-*

trunca or *Terminalia sericea* but slightly more than half of the specimens showed DSF, while the remaining ones had upward sap flow (Figure 4.3c). The identification of flow direction is based on the observation that trees with DSF reached their daily minimum during daylight hours while at a similar time of the day specimens with upward sap flow reached their maximum flow. *Dichrostachys cinerea* had no leaves at the time of the measurements and in general this species has a low xylem/hardwood area ratio compared with *Boscia albitrunca* (details about sapwood area of the nine species investigated are presented in Chapter 3); low sap flux densities and shallow sapwood contribute to low levels of sap flow.

In the case of *Ochna pulchra* (Figure 4.2c), only two trees show clear DSF pattern (with a minimum during daylight hours) although possibly a mixed type of flow occurred in other trees. This species sheds its leaves earlier than the other species, and consequently was leafless at mid-August when sap flow measurements took place.

4.4 Discussion and Conclusions

The ability of Kalahari species to survive xeric conditions has been the subject of several studies (Bond *et al.* 2003; Childes 1989; Hipondoka *et al.* 2003; Scanlon *et al.* 2007; Sekhwela and Yates 2007; Seymour 2006; Sole 2007). Such studies show that vegetation exhibits remarkable capabilities to cope with moisture deficiency, either through the presence of special root morphology and habits that enable them to obtain moisture or by adjustments on the phenological schedule that might reduce periods of transpiration. These capabilities are frequently presented as adaptation strategies developed by the plant to survive harsh conditions. We have identified some of these capabilities in the species investigated in the Serowe area, referred to as tree adaptation mechanisms hereafter. "Adaptation" in this context is understood to be a convenient characteristic favoured by natural selection, *i.*e. a change that allows an organism to live successfully in a certain environment. In other words, adaptation refers to a special attribute of that organism which is well fitted to the eventual stress and pressure of its environment. From this perspective, the Kalahari vegetation is well adapted (suited) to its environment by physicochemical long term fine-tuning. Such adaptations aim to overcome the primary limiting factor of vegetation survival *i.*e. water availability. Therefore they *i)* facilitate water and nutrient acquisition to sustain photosynthetic activity during dry periods or *ii)* they set the vegetative clock to maximize nutrient availability and minimize the risk of dehydration by shifting phenological events. Both strategies are reflected in the transpiration activity of vegetation and consequently in their sap flow patterns.

Trees are structured for upward sap flow. They extract water and soluted minerals by deep tapping or shallow lateral roots (depending on the soil moisture content) and lift it through the tree's sapwood to its upper branches. This process is driven by various interacting forces linked by biochemical, biophysical and structural factors. Among these factors, sun-induced photosynthesis and vapour pressure deficit (VPD), are probably the ultimate driving mechanisms. When these mechanisms are inactive (normally at night), trees in general have mechanisms to maintain the non-transpired water in the sapwood channels in a "one-way valve" fashion, *i.e.* water is not sent back to the roots and soil by gravity but rather stored in the tree stem, branches and twigs. However, under a combination of environmental and tree-physiological factors not yet fully identified, trees can implement a downward sap flow (DSF) in which water is apparently sent back to the soil in the vicinity of the roots. This phenomenon has been observed in this study in four out of the nine species investigated: *Boscia albitrunca, Terminalia sericea, Ochna pulchra and Dichrostachys cinerea* as reported in the previous section,

Conceptually, two sources of moisture can be considered in the DSF process. First, moisture not used during the daily transpiration activity and stored in the xylem channels (stem and branches). This precious reserve can however be lost if subsequent days are poor in transpiration driving forces. In this case, moisture will travel downwards during the night and the xylem channels will dry-out until new upward flow replenishes them. For a well fitted Kalahari tree this might happen under a combination of conditions thus insuring tree survival. A second source of moisture is water harvested from air moisture. This appears to be a quite safe and easily available water source for DSF. Zimmerman *et al,* (2004) (Zimmermann *et al.* 2004)states that according to published reports, moisture can be captured by the aerial parts of trees (leaves, twigs and even bark) by a process termed reverse transpiration and later redistributed within the tree. In this case intracellular and xylem mucilage may be involved in this water uptake from the atmosphere. The same authors found that the morphology of small leaves is ideal for reverse transpiration as they may adopt a funnel-like configuration after rainfall that can easily collect water. This might be the case of some species of *Acacias* and other Kalahari species also with small leaves, but further research is required to fully understand the mechanisms involved at the tree-leaf level. Air moisture harvesting (AMH) may occur during nights with relatively high air relative humidity. Moisture thus obtained can flow downwards to shallow or deep soils according to the differential water potential.

The complete identification of environmental and physiological factors triggering DSF requires further investigation. Among possible parameters are: air moisture content (relative humidity); air temperature; wind speed and direction; leafs and branch morphology and physiology and canopy orientation with respect to other air moisture collectors. Consequently the definite identification of species that

perform DSF and the conditions under which it occurs requires a investigation of the above listed parameter in addition to sap flow patterns.

Based on the observations made in this study, we conclude that in the Kalahari the extraction of moisture and nutrients is not limited to deep-rooted species. Some shallow rooted species (Table 4.1) may utilize a range of mechanisms to survive the dry season *e.g.* preventing or reducing transpiration by rapid defoliation, or by capturing moisture from the air at night by AMH. *Lonchocarpus nelsii* for example gradually reduces its transpiration activity and enters a state of dormancy by shedding its leaves as the dry season progresses. Thereby it decreases sap rates by defoliation. Evidence of this behaviour is found in the results of the 2004 sap flow campaign. The first set of measurements was collected from the 2nd to the 7th of August. During this period, peak sap flux densities recorded at ~10h00 reached 20 $cm^3/(cm^2 xh)$. These measurements had to be repeated due to animal disturbances of the identification tags attached to the stems. The same group of trees were measured again from the 26th to the 29th of August when a pronounced reduction in sap flow magnitudes was recorded: peak sap flux densities recorded at ~10h30 reached only a maximum of 12 $cm^3/(cm^2 xh)$. The increased air temperature (see Table 4.2) might be the environmental cue for leaf loss and consequently for sap flow reduction. This conclusion support the theory that transpiration decreases drastically during leaf shedding as a protection against plant dehydration (Roupsard *et al.* 1999; Smith *et al.* 2004). Likewise, *Burkea Africana* drops its leaves and only upward daytime sap flow of low magnitude was recorded compared to its sap rates during other seasons (Obakeng 2007).

A completely different behaviour was observed in *Terminalia sericea,* whose sap flow signature indicates intense activity during night-time (Figure 4.2h and Figure 4.3b). This sap flow pattern is identified as DSF during a state of intense defoliation (see Table 4.2) and is not related to following-day transpiration (anti-correlation with VPD is observed in Figure 4.3b). Evidence of DSF during the dormant season when no transpiration takes place, has been previously identified in warm-desert phreatophytes (Hultine *et al.* 2004). DSF provides the necessary moisture to growing roots that later will act as tap roots. This could be the case in *Terminalia sericea* which does not develop a deep rooting system, developing instead robust lateral roots that can reach ~9m in length. DSF can provide the moisture needed for root growth during the dry season by AMH or by reverse transpiration through branches and twigs (the relative humidity peak was higher the first night of measurement compared with the second as was sap flow; see Figure 4.3b). Moisture collected by *Terminalia sericea* at night sustains its sub-surface growth, despite competition from grasses for water and nutrients (Hipodonka *et al*, 2003 stated that in the upper soil layers of the Kalahari, grasses are better competitors for water than trees forcing the latter to develop deep roots). In addition, moisture could also be available to be used by associated vegetation. We consider this possibility for two reasons: firstly, the previously

identified habit of this species to grow in associations (Strohbach *et al.* 2004) in the Kalahari and secondly, the presence of green shrubs in an otherwise brown grass environment observed in the proximity to the *Terminalia sericea* trees investigated in this study. Recent studies have shown that water re-circulation by trees (*e.g.* DSF from AMH) is a strategy that not only allows the trees to compete for scarce moisture with other species, but also facilitates the survival of other associated vegetation e.g. shrub or grasses (Ludwig 2001; Scanlon *et al.* 2007; Sole 2007; Zou *et al.* 2005). In the same studies it is theorized that self-organized communities of plants specialized for dry environments, create facilitation mechanisms at a local scale to minimize the overall effect of water scarcity. Roots of *Terminalia sericea* appear to grow interconnected with roots of associated vegetation. It is therefore possible that the moisture collected during the night through AMH provides its understory vegetation with the water and nutrients necessary to either compete or collaborate with the near-surface high moisture consumers: grasses (Hipondoka *et al.* 2003) or shrubs (this study). Further research of *Terminalia sericea* should focus on how AMH linked with nocturnal DSF at the time of defoliation, benefits its own growth and facilitates survival of understory vegetation, and how this facilitation mechanism acts in different seasons.

Among the deep-rooted species, *Boscia albitrunca* presents the most complex sap flow pattern of the group of species investigated. The 24-hour activity of this species, recorded at the end of the dry season, must be the result of a combination of conditions defined by both the environment and the physiology of the tree itself. The fact that *Boscia albitrunca,* in spite of loosing part of its foliage, remains in leaf throughout the dry season is the consequence of two physiological characteristics reported in other studies in the Kalahari, *i.e.* its sclerophyllous leaves resistant to extremely dry (during the day) and freezing (during the night) conditions (Wand *et al.* 1999), and the presence of tap roots which contribute to the moisture and nutrient supply from deep groundwater (Alias and Milton 2003; Cole and Brown 1976). The evergreen character of this species has made it a symbol of endurance in the Kalahari, however this species is vulnerable to dehydration because of permanent transpiration activity (Wand *et al.* 1999). This situation is not faced by species that enter a dormancy phase during the dry season. The nocturnal activity of *Boscia albitrunca* at the zenith of the dry season is identified in this study as DSF. This may originate from water not transpired during the day and acquired at a high energy expense (root water uptake), or by a much lower-cost energy process such as AMH. In this scheme, the surplus of moisture thus obtained, is sent by shallow roots to the upper soil assumed here to be the driest soil layer *i.e.* .having the lowest water potential to be used the following day by normal transpiration. Monitoring of sap flow in roots at the same time of the year, using a scheme sensitive to flow-direction should be implemented in order to corroborate the interpretation of stem sap flow patterns presented in this study.

The DSF connected to moisture obtained from deep soil via tree stem, commonly termed hydraulic redistribution (HR), as identified in *Boscia albitrunca,* has been reported in other studies following rainfall or irrigation events when the surface soil is wet. These reports have shown downward sap rates as high or higher than daylight time upward sap flows in roots (Burgess and Bleby 2006). The apparent magnitude of DSF in *Boscia albitrunca* at the time where measurements took place also surpassed daylight time upward flow but these results show for the first time that nocturnal DSF using the stem as a pathway might occur during the dry season. In this case, the wide sapwood area, as observed in Figure 4.4 may facilitate the inversion of flow direction. Additional measurements of sap flow at different stem heights and azimuths would provide more information of the water pathways when this process occurs.

In the group of nine tree species investigated in this study (four of them showing DSF), it must be emphasized that the measuring period, i.e. 2 to 6 days or 0.5 – 1.5% of a complete year, is very short and insufficient to define whether the species not showing DSF do or do not have the capability to do it. Additional measurements of sap flow combined with a comprehensive investigation of the soil moisture at different depths and investigations of the leaf stomata conductance variation must be done at different time of the year for a better identification and understanding of the underlying processes in the Kalahari trees. However the results presented here prove that monitoring of sap flow provides valuable information about tree internal functioning (as it reproduces the schedule of activity or stillness), without going into the complexity of soil moisture dynamics which is highly influenced by the scale of consideration and that can be difficult to investigate during the dry season due to the almost negligible moisture in the upper soil layers.

References

Alias, D. and S. Milton 2003. A collation and overview of research information on *Boscia albitrunca* (Shepherd's tree) and identification of relevant research gaps to inform protection of the species. Department of Water Affairs and Forestry, South Africa, Pretoria.

Amenu, G. and P. Kumar 2007. A model for hydraulic redistribution incorporating coupled soil-root moisture transport. Hydrology and Earth System Sciences Discussions. 4:3719-3769.

Bond, W., F. Woodward and G. Midgley 2003. Does elevated CO2 concentration play a role in bush encroachment? *In* Forest and Woodlands, Knysna, SA.

Burgess, S., M. Adams, N. Turner and C. Ong 1998. The redistribution of soil water by tree root systems. Oecologia. 115:306-311.

Burgess, S. and T. Bleby 2006. Redistribution of soil water by lateral roots mediated by stem tissues. Journal of Experimental Botany. 57:3283-3291.

Burke, A. 2006. Savanna trees in Namibia - Factors controlling their distribution at the arid end of the spectrum. Flora. 201:189-201.

Canadell, J., R. Jackson, J. Ehleringer, H. Mooney, O. Sala and E. Schulze 1996. Maximum rooting depth of vegetation types at the global scale. Oecologia. 108:583-595.

Childes, S.L. 1989. Phenology of nine common woody species in semi-arid, deciduous Kalahari Sand vegetation. Vegetatio. 79:151-163.

Cole, M. and R. Brown 1976. The vegetation of the Ghanzi area of western Botswana. Journal of Biogeography. 3:169-196.

Curtis, B. and C. Mannheimer 2005. Tree Atlas of Namibia Ed. N.B.R. Institute, Windhoek. 674 p.

Demisse, G. 2006. Spatial distribution of savannah woody species biodiversity in Serowe, Botswana. Unpublished MSc thesis. International Institute for Geo-Information Science and Earth Observations, ITC. Esnchede, The Netherlands., Enschede.

Espeleta, J., J. West and L. Donovan 2004. Species-specific patterns of hydraulic lift in co-ocurring adult trees and grasses in a sandhill community. Oecologia. 138:341-349.

Granier, A. 1985. Une nouvelle méthode pour la mesure du flux de sève brute dans le tronc des arbres Annales des Sciences Forestières 42:193-200

Granier, A. 1987. Evaluation of transpiration in a Douglas-fir stand by means of sap flow measurement. Tree Physiology. 3:309-320.

Hipondoka, M., J. Aranibar, C. Chirara, L. M. and S. Macko 2003. Vertical distribution of grass and tree roots in arid ecosystems of Southern Africa: niche differentiation or competition? Journal of Arid Environments. 54:319-325.

Hultine, K., R. Scott, W. Cable, D. Goodrich and D. Williams 2004. Hydraulic redistribution by dominant, warm-desert phreatophyte: seasonal patterns and response to precipitation pulses. Functional Ecology. 2004:530-538.

Hultine, K., D. Williams, S. Burgess and T. Keefer 2003. Contrasting patterns of hydraulic redistribution in three desert phreatophytes. Oecologia. 135:167-175.

Leistner, O. 1967. The Plant Ecology of the Southern Kalahari. *In* Memoirs of the Botanical Survey of South Africa. Department of Agricultural Technical Research, Pretoria. 172 p.

Ludwig, F. 2001. Tree-grass Interactions on an East African Savanna: the effects of competition, facilitation and hydraulic lift. Wageningen University and Research Centre, sub-department of Nature Conservation, Wageningen.

Moreira, M., F. Scholz, S. Bucci, L. Sternberg, G. Goldstein, F. Meinzer and A. Franco 2003. Hydraulic lift in a neotropical savanna. Functional Ecology. 17:573-581.

Obakeng, O.T. 2007. Soil moisture dynamics and evapotranspiration at the fringe of the Botswana Kalahari. Vrije Universiteit, Amsterdam, NL.

Otieno, D., M. Schmidt, J. Kinyamario and J. Tenhunen 2005. Responses of *Acacia tortillis* and *Acacia xanthophloea* to seasonal changes in soil water availability in the savanna region of Kenia. Journal of Arid Environments. 62:377-400.

Roupsard, O., A. Ferhi, A. Granier, F. Pallo, D. Depommier, B. Mallet, H. Joly and E. Dreyer 1999. Reverse Phenology and Dry-Season Water Uptake by Faidherbia albida (Del.) A. Chev. in an Agroforestry Parkland of Sudanese West Africa Functional Ecology. 13:460-472.

Scanlon, T., K. Caylor, S. Levin and I. Rodriguez-Iturbe 2007. Positive feedbacks promote power-law clustering of Kalahari vegetation. Nature. 449:209-212.

Schulze, E., M. Caldwell, J. Canadell, H. Mooney, R. Jackson, D. Parson, R. Scholes, O. Sala and P. Trimborn 1998. Downward flux of water through roots (i.e. inverse hydraulic lift) in dry Kalahari sands. Oecologia. 115:460-462.

Sekhwela, M. 2003. Woody vegetation resource changes around selected settlement along aridity gradient in the Kalahari, Botswana. Journal of Arid Environments. 54:469-482.

Sekhwela, M. and D. Yates 2007. A phenological study of dominant acacia tree species in areas with different rainfall regimenes in the Kalahari Botswana. Journal of Arid Environments. 70:1-17.

Seymour, C. 2006. Slowly does it: *Acacia erioloba* growing large in southern Kalahari savannas. *In* Arid Zone Ecology Forum, Kamieskroon, SA.

Seymour, C. and S. Milton 2003. A collation and overview of research information on Acacia erioloba (Camelthorn) and identification of relevant research gaps to inform protection of the species. Department of Water Affairs and Forestry, Pretoria, South Africa.

Smith, M., S. Burgess, D. Suprayogo, B. Lusiana and Widianto 2004. Uptake, partitioning and redistribution of water by roots in mixed-species agroecosystems. *In* Below-ground interactions in tropical agroecosys-

tems: concepts and models with multiple plant components Eds. M. Noordwijk van, G. Cadisch and C. Ong. CAB International, p. 464.

Sole, R. 2007. Scaling laws in the drier. Nature. 449:151-153.

Strohbach, B., M. Strohbach, J. Kutuahuripa and H. Mouton 2004. A Reconnaissance Survey of the Landscape, Soils and Vegetation of the Eastern Communal Areas (Otjiozondjupa and Omaheke Regions), Namibia Ed. N.B.R.I.a.A.-E.S. Programme. Ministry of Agriculture, Water and Rural Development, Namibia, Windhoek, p. 118.

van Wijk , M. and I. Rodriguez-Iturbe 2002. Tree-grass competition is space and time: Insights from a simple cellular automata model based on ecohydrological dynamics. Water Resources Research. 2002:18.1-18.15.

Wand, S., K. Esler, P. Rundel and H. Sherwin 1999. A preliminary study of the responsiveness to seasonal atmospheric and rainfall patterns of wash woodland species in the arid Richterveld. Plant Ecology. 142:149-160.

Wyk van, B. and P. Wyk van 1997. Field Guide to Trees of Southern Africa. Struik Publishers.

Zimmermann, U., H. Schneider, L. Wegner and A. Haase 2004. Water ascent in tall trees: does the evolution of land plants rely on a highly metastable state? New Phytologist. 162:575-615.

Zou, C., P. Barnes, S. Archer and M.M. C. 2005. Soil moisture redistribution as a mechanism of facilitation in savanna tree-shrub clusters. Oecologia. 145:32-40.

Object Oriented Classification of High Resolution Imagery in the Botswana Kalahari

Abstract

High spatial resolution airborne images (G, R and NIR) and satellite IKONOS imagery were used to map vegetation as a complementary step for transpiration mapping in the tree-bush of the Botswana Kalahari. Airborne images were acquired with digital TETRACAM camera mounted on a small aircraft to collect data in 30cm, 60cm and 1m spatial resolution. The classified airborne images were compared with the classification of the1m pansharpened IKONOS image using eCognition®, an object-oriented classification tool. In environments such as the Kalahari, eCognition® proved to be more suitable for species differentiation than the previously applied pixel based methods. The spectral characteristics of the airborne images were similar to the IKONOS image, while the spatial pattern of tree canopies was clearer in the airborne images. This was reflected in substantial differences in the accuracy levels between the airborne and satellite data of the same resolution, both quantitatively e.g. Kappa coefficient values and number of species identified, and qualitatively *i.e.* canopy delineation. The low accuracy of the classified IKONOS images can be partly attributed to the pansharpening process and the time of the image acquisition. The results suggest that due to the clustered and mixed composition of the Kalahari savanna, very high resolution images are needed to succeed in individual canopy delineation. This characteristic of the savannah vegetation must be considered when applying sap flow upscaling functions as species with significant differences in hydrological behavior might have similar spectral response. In general this study demonstrated that the higher the spatial resolution, the higher the number of tree species properly

identified hence the higher the accuracy. The more well-defined individual tree crowns are, the better the distinction among their spectral signatures, especially where tree species shed and regain their leaves with season, thus affecting the stable green color associated with their spectral reflectance.

5.1   Introduction

Spatial information of individual tree canopies extracted from remotely sensed classified images can be a very useful tool for forest management and other related applications. Examples of these applications include forest cover mapping, species spatial distribution analysis, forest monitoring, monitoring of forest fragmentation, forest fire management, wildlife habitat assessment, planning of forest road networks, etc (Gougeon and Leckie 2006; Hajek 2006; Laliberte *et al.* 2004; Leckie *et al.* 2003).

From the Ecohydrological perspective, forest classification and automatic tree canopy delineation are essential for the mapping of transpiration fluxes based on ground measurements of sap flow. Transpiration thus quantified requires a detailed characterization of sap flow patterns and evaluation of net sap flow per species. Mean net sap flow can be correlated with biometric measurements of the trees such as canopy area, steam area or sapwood area for the determination of upscaling functions used for transpiration mapping. Given the particular sap flow dynamics of tree species, a detailed sap flow characterization based on ground observations will only be justified if it is to be combined with reliably classified images. Previous attempts at transpiration assessment from upscaled sap flow in the Kalahari have shown that standard pixel-based classification techniques are not suitable for species differentiation even when applied to high resolution imagery (Mapanda 2003).

As a key step in the transpiration mapping based on the combination of ground and remote sensing data, this chapter analyses the applicability of an object-oriented classification approach for species separation in high resolution images. In an attempt to define the optimal platform and spatial resolution for savannah transpiration assessment, a comparison is made between satellite and airborne data. Furthermore, a comparison is made among three spatial resolutions of airborne images *i.e.* 30cm, 60cm and 1m.

5.2   Methods

5.2.1 Study area

The study area is located west of the Serowe in the Central District of Botswana. The study area is located in a gently undulating sand plateau sloping towards the west without prominent drainage lines. More detailed description of the Serowe area is presented in Chapter 1.

The vegetation of the study area was investigated during the KRP (Demisse 2006; Obakeng 2007) and the conclusions were in agreement with the findings reported by the Safari2000 project. Areas of less than 400mm MAP are characterised by woody species belonging mainly to the *Mimosaceae* family represented by the *Acacia* and *Dichrostachys* genera, while areas with MAP ranging from 400 to 600mm are characterized by woody species of the *Combretaceae* family, represented by the *Terminalia* genus. The vegetation cover of the study area is accordingly a mosaic of open savanna grassland and low thorny trees, between 3m and 5m in height, most of them with a marked seasonal variation in leaf cover. All the trees occur predominantly in clusters and are normally accompanied by a variety of grass and shrubs species e.g. *Grewia retinervis, Aristida* and *Eragrostis*. The most common tree species reported in the above mentioned studies and during field observations are: *Acacia fleckii, Acacia erioloba, Acacia luederitzii, Boscia albitrunca, Lonchorcarpus nelssi, Terminalia sericea, Burkea Africana, Ochna pulchra, Dichrostachys cinerea* and *Peltophorum africanum.*

Observations during the KRP and information from published literature as reported in Chapter 4, have shown that the schedule of pheno-phases in the Kalahari species is variable, and that moisture availability and air temperature variations are the main environmental cues (Childes 1989). As the presence of foliage is necessary to obtain spectral information of the tree canopies, the classification procedure was carried out using images from the end of summer to the beginning of autumn (Feb-May) when the trees are still in leaf. Once species are discriminated in the study area, upscaling functions derived from the dry-season sap flow campaign can be applied for the mapping of the dry-season transpiration, which is the final goal of this study.

5.2.2   Remote Sensing Data

An IKONOS image of the 2nd of February 2002 was used for this study. The IKONOS satellite, launched on 24th September 1999 provides global, accurate and high-resolution images. The panchromatic sensor with 82cm ground sample distance (GSD) at nadir provides high resolution imagery. Simultaneously, the multi-spectral sensor collects blue (445–516nm), green (506–595nm), red (632–698nm), and near-infrared (NIR) (757–853nm) spectral bands with 3.28m nadir resolution, providing natural-color imagery for visual interpretation and color-infrared imagery for remote sensing applications.

Although the IKONOS resolution (4m pixel size) is suitable for other forestry applications, it is inadequate for the small canopy sizes of the Kalahari species. For this reason, a pansharpening process was carried out *i.e.*, the fusion of high resolution panchromatic images with lower resolution multi-spectral images as explained in the next section. The area covered by the IKONOS image was considered representative of the study area and therefore was used as the baseline

for the geo-referencing of the airborne data and for providing subsets to be classified as a part of the methodology for transpiration mapping in the Kalahari.

The airborne campaign was carried out in the framework of the Kalahari Research Project (KRP) from the 6th to the 11th of May of 2004, using a multi-spectral digital camera Tetracam ADC (Agricultural Digital Camera). The camera collected data on green (520–600nm), red (620–750nm), and near infra-red (750–950nm) spectral bands. For the airborne data collection, the camera was mounted on a Cessna 210 aircraft provided by the Botswana Geological Survey which flew over the study area, fully imaging the polygon covered by the IKONOS image. From this overpass a set of images at 1m spatial resolution was obtained. All the airborne images have rectangular frames of 1280 by 1024 pixels with 20% front and side overlap. The images were saved by the camera in Digital Compressed Archive (DCA) format, which can be decompressed and transferred into a bitmap format accepted by most types of image processing software. Two additional flights took place over 5 sub-areas (approx. 100m by 100m plots) inside the IKONOS polygon, from which images at 60cm and 30cm spatial resolution were obtained. In selecting the 5 subareas, care was taken that the most abundant species present in the IKONOS polygon were covered (the same species investigated with regard to sap flow, as presented in Chapter 4), and that there were baseline features e.g. road junctions, road curves or unmistakable particular trees that helped in the identification of the plots on the ground. Figure 5.1 presents the IKONOS image and the location of the 5 sub-areas used for the classification, and the appendix shows some scenes of the air campaign.

5.2.3 IKONOS Image Pansharpening

The fusion of high resolution panchromatic and lower resolution multispectral or SAR images has been previously used for forest classification (Dai and Khorram 1998; Kosaka *et al.* 2005; Pugh *et al.* 2004; Susaki and Shibasaki 2000), and several fusion techniques and software have been developed. Perhaps the most common and successful techniques are the IHS (Intensity, Hue, Saturation), PCA (Principal Component Analysis), arithmetic combination based fusion, and wavelet based fusion (Pohl and Van Genderen 1998; Zhang 2002). In the absence of high resolution SAR images of the area, which would add the roughness effect desirable for classification purposes, the ratio-image technique (in the category of arithmetic combinations) was selected for this study. The Brovey ratio algorithm using three bands: NIR, Red and Green was applied to the IKONOS image resulting in a new image with a spatial resolution of 1 m. One advantage of this algorithm is that it preserves the spectral information of the visible and NIR bands adding textural information from the panchromatic imagery (Kosaka *et al.* 2005).
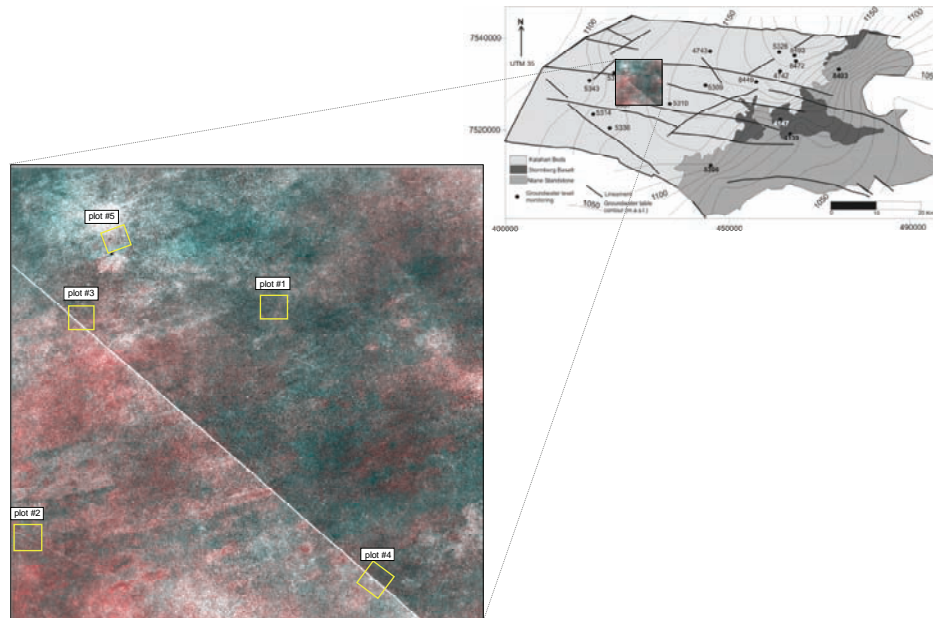
Fig 5.1 localization of the IKONOS image and the 5 plots used for classification

5.2.4 Classification Technique and Software

If pixel based classification is to be applied, high resolution satellite imagery such as IKONOS can have classification problems due to the large spectral variation within a particular class and also the existence of a high degree of shadow (Laliberte *et al*. 2004). Conversely, an object-oriented classification approach based on fuzzy logic, allows the integration of a number of different object features, including spectral values, shape and texture. It incorporates contextual and semantic information and not only uses image object attributes, but also the relationship among the different image objects. In object-oriented classification, pixels are aggregated into image objects by segmentation, the basic processing unit. By means of segmentation techniques a hierarchical network of image objects is constructed in which small objects are sub-objects of larger ones. The hierarchical structure represents the information of the image data in different resolutions simultaneously. Each object knows its context, its neighborhood and its sub/super-objects. Thus, it is possible to define relations between objects (Benz *et al*. 2004). The suitability of the object oriented approach for vegetation classification with high resolution images has been demonstrated in published literature (Gougeon and Leckie 2006; Hajek 2006; Laliberte *et al*. 2004; Leckie *et al*. 2003).

In this study, image classification was carried out using eCognition® (Definiens), the first object-oriented image analysis software in the market. Although based on objects identification, eCognition® also recognizes pixel information but adds significant value to this information by creating a cognition association and a semantic network, through a series of iterative standard segmentation and classification steps. This feature enhances the value of intelligence and information extracted from the image. To emulate the human mind, eCognition uses the color, shape, texture, size, smoothness and compactness of objects as well as their context and relationships, to draw similar conclusions and inferences that an experienced analyst would draw. It uses advanced machine learning concepts to train the system and render this knowledge in a production environment (Definiens 2007; Hajek 2006).

5.2.5 Vegetation sampling

For each plot, about 100 trees of different species were recorded. The number of trees per plot was controlled by the identification and linking of individual trees both on the image and on the ground, as exemplified in Figure 5.2 The spatial distribution pattern of the trees in the image was considered through the sampling, in such a way that all the species present in each plot were considered. This means that the selection of the sample plots was made through purposive sampling. The total number of trees entered in the field for each plot was divided into two categories; firstly, approximately two-thirds were used as a training sample after which the images were classified. The remaining third was used as a validation sample for the classification (Benz et al. 2004; Walter 2004).

5.2.6 Classification accuracy assessment

Accuracy assessment is an important step in the image classification process. In this context, the term accuracy is normally used to explain or express the degree of correctness of the classification i.e. the degree by which the derived image classification agrees with the reality or conforms to the truth (Foody 2002).

The most common way of representing classification accuracy is by an error (confusion) matrix, which is a square array of numbers in rows and columns that describes the pattern of class allocation relative to the reference data. Different measures of classification accuracy may be derived from an error matrix depending on the user's concerns about predicted/actual agreement. When the focus is on the accuracy of individual classes rather than on the overall accuracy of the classification, the percentage of cases correctly allocated can be derived from the error matrix. This percentage per each class can be related to the total number of cases of that class, giving rise to the terms *user's* and *producer's* accuracy.
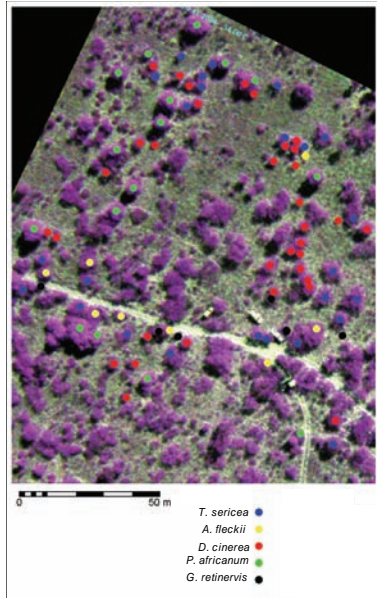
Figure 5.2 Scheme of vegetation sampling

In the context of object oriented classification, *user's accuracy* is the probability that an object classified on the image actually represents that category on the ground; it informs the user how well the image represents what is on the ground. The result is a measure of commission error *i.e.* the proportion of observed features on the ground that are not classified on the image. Conceptually, user's accuracy (%) = 100% − error of commission (%), and numerically it is computed as:

$$\text{User's accuracy} = \frac{n_{kk}}{n_{k+}}$$
[5.1]

Where n_{kk} is the number of objects classified in certain category (row k and column k) in the error matrix, which actually belong to that category, and n_{k+} is the marginal total of the same row.

On the other hand, the *producer's accuracy* measures how well a certain area has been classified. It includes the error of omission which refers to the proportion of observed features on the ground that are not classified in the image. The more errors of omission that exist, the lower the producer's accuracy. (Banko 1998; Congalton 1991). Producer's accuracy (%) = 100% − error of omission (%), and it is computed as:

Producer's accuracy $= \dfrac{n_{kk}}{n_{+k}}$ [5.2]

Where n_{+k} is the marginal total of the same column.

Given the purpose of the classification presented in this chapter, i.e., assigning to every object a species-specific upscaling function for transpiration quantification, the User's accuracy becomes more important than the Producer's accuracy.

Although the indicators obtained from equations [5.1] and [5.2] provide useful information about the classified image, they do not contemplate the effect of chance agreement; hence the introduction of the Cohen's Kappa coefficient (Foody 2002; Skidmore 1999) and is calculated as:

$$Kappa\ \ coefficient = \dfrac{n\sum\limits_{k=1}^{q} n_{kk} - \sum\limits_{k=1}^{q} n_{k+} + n_{+k}}{n^2 - \sum\limits_{k=1}^{q} n_{k+} + n_{+k}}$$ [5.3]

Where q is the number of rows (classes) and n is the total number of observations

The Kappa coefficient evaluates the classification as a whole rather than providing information per class. It can have both positive and negative values. When agreement obtained is greater than that by chance, it leads to positive values; when obtained agreement equals chance agreement, K is zero (0), and when the agreement by chance outweighs the actual agreement, the kappa coefficient assumes negative values. The upper value of K, however, is 1 (100%) when there is perfect agreement between the measured and the observed (Cohen 1960).

The accuracy analysis of the image classification presented in this chapter pursues two main objectives. Firstly, to determine the most suitable spatial resolution of the airborne images compared with the IKONOS image for species differentiation in mixed forest such as the Kalahari. This analysis is done by comparing the Kappa coefficient obtained for each plot at different spatial resolution, *e.g.* 30cm, 60cm, 1m of the airborne images, and 1m in both airborne and IKONOS images. Secondly, to investigate the separability of the classified species in the five locations inside the reference IKONOS polygon. For this, the user's accuracy of each species is analyzed under the hypothesis that the spatial resolution that

yields the best Kappa indicator will also provide the best species separability as measured by the user's accuracy

5.3   Results

The five selected plots were classified using eCognition in the three available resolutions of the airborne images and in the IKONOS image. Table 5.1 presents a summary of the accuracy assessment of the classifications based on the Kappa coefficient and Figure 5.3 shows plot#2 at the 3 spatial resolutions as an example of the classification comparison. Detailed description of the results including the corresponding error matrixes can be found in Kimani 2005.

Table 5.1 Kappa coefficient of agreement for airborne images of 5 plots at 30cm, 60cm, and 1m spatial resolution inside the IKONOS polygon

	Kappa coefficient airborne images		
	30cm	60cm	1m
	0.89	0.89	0.82
	0.86	0.79	0.86
	0.94	0.93	0.91
	0.84	0.86	0.90
	0.93	0.83	0.84
Mean	0.89	0.86	0.87
Std	0.04	0.05	0.03

According to the categorization presented by (Congalton 1996), the resulting Kappa coefficient indicates strong agreement (values greater than 0.80) in most of the plots and for the 3 spatial resolutions. A one-way-ANOVA indicated a very low value (close to zero) of standard deviation among the Kappa values in each plot, and hence no significant difference among the classification accuracy of the 3-resolution images. However, classification of 30cm resolution images not only provided slightly higher accuracy but also resulted in a higher number of species classified (Kimani et al. 2007). Figures 5.4 and 5.5 shows the 5 plots at 30cm resolution and their corresponding classification.

The comparison between airborne and satellite images at 1m resolution was carried out in plots #2 and #4 yielding the Kappa coefficients shown in Table 5.2. Both airborne and satellite Images and their classification for the two plots are presented in Figure 5.6. There was a significant difference between the airborne and satellite data of the same resolution both in quantitative (e.g. their Kappa coefficient values and the number of tree species correctly identified) and qualitative (i.e. mapping quality of different features appear in classified maps) manner. The airborne data was superior in both qualitative and quantitative measurements mainly because of its higher spatial resolution and image quality.
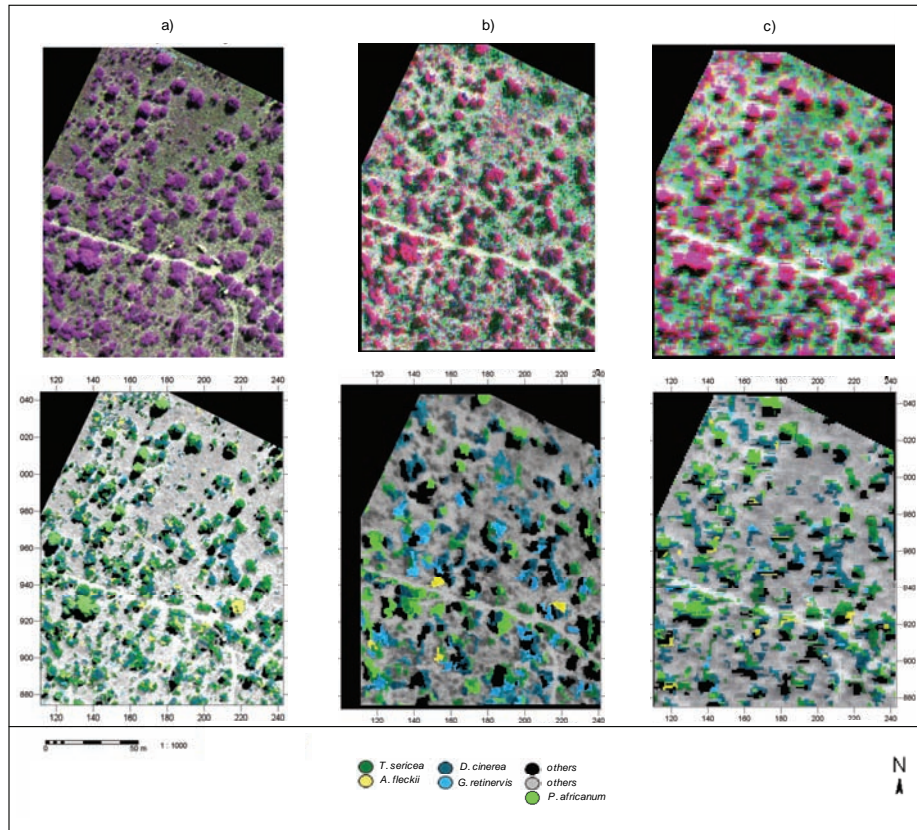
Figure 5.3 Classification of plot#2 at 3 spatial resolutions. a) 30cm, b) 60cm and c) 1m

Table 5.2. Classification accuracy comparison between airborne images at 1m resolution and pansharperned IKONOS images of plots 2 and 4

| | Airborne image | | IKONOS image | |
plot	Kappa coeff.	# species	Kappa coeff.	# species
2	0.86	5	0.56	3
4	0.90	4	0.51	3

A total of 6 species were identified in the 5 plots. In some cases the classification of 60cm and 1m resolution images was not able to discriminate certain species identified at 30cm, which appears to be logical. In other cases the number of identified individuals per species decreased dramatically from 30cm to 60cm resolution. The contrasting capability of the software to delineate individual tree
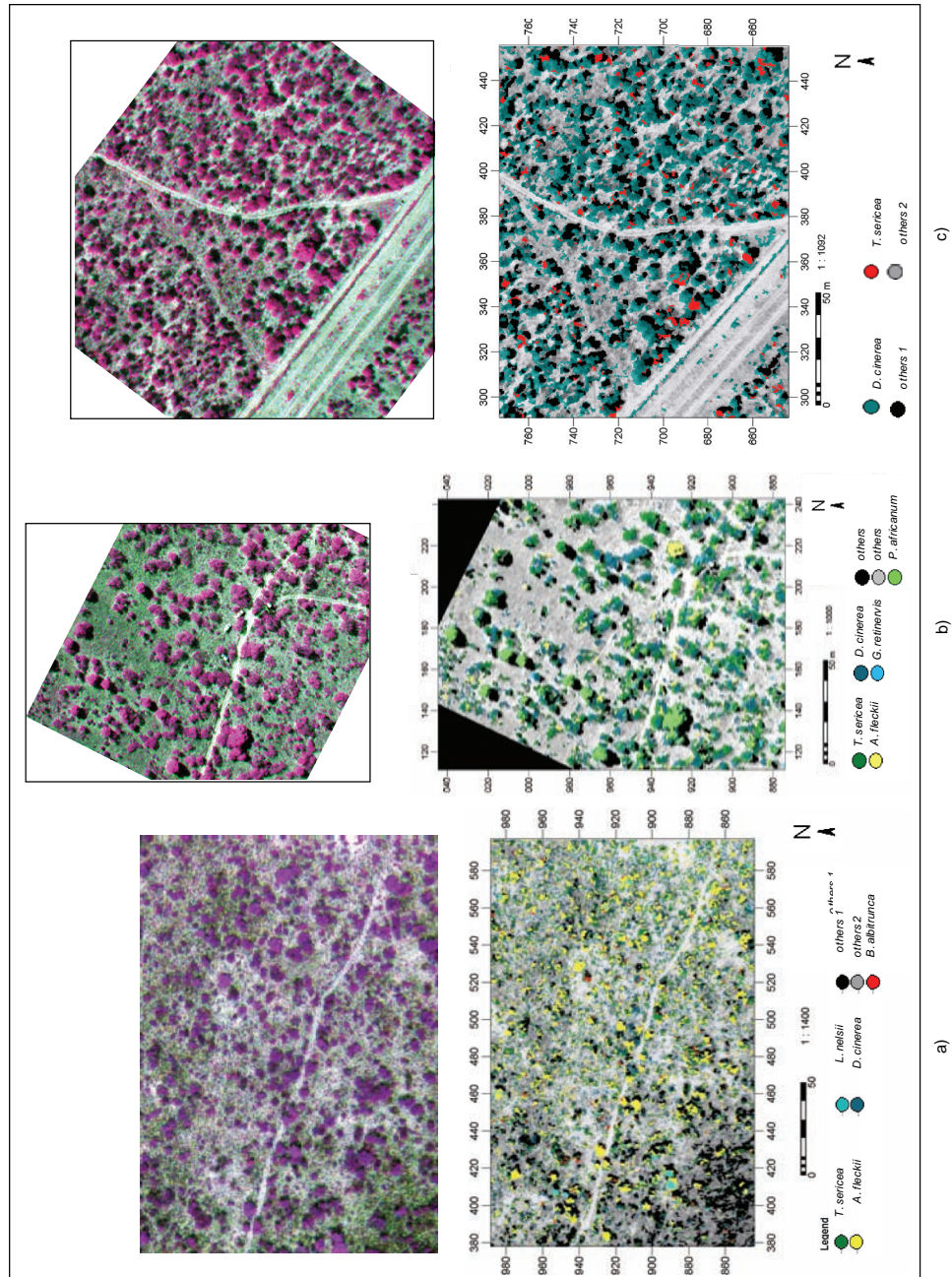
Figure 5.4 Classification of a) plot#1, b) plot#2 and c) plot#3 at 30cm spatial resolution

crowns in the 3 resolution images is clearly observed in Figure 5.3. After grouping the results per species in the 5 classified plots, a preliminary analysis of the separability of each species was done based on the user's accuracy as presented in Table 5.3.
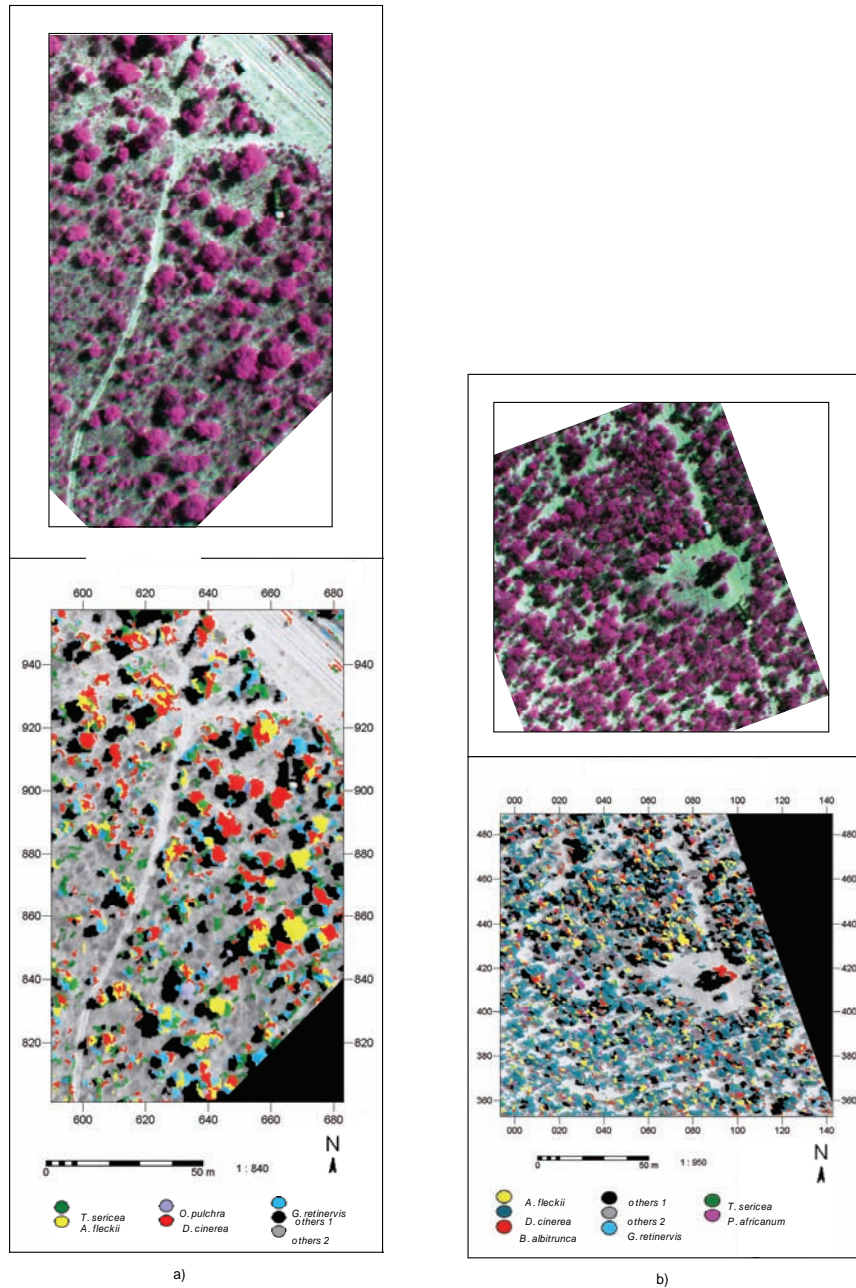
Figure 5.5 Classification of a) plot#4, and b) plot#5 at 30cm spatial resolution
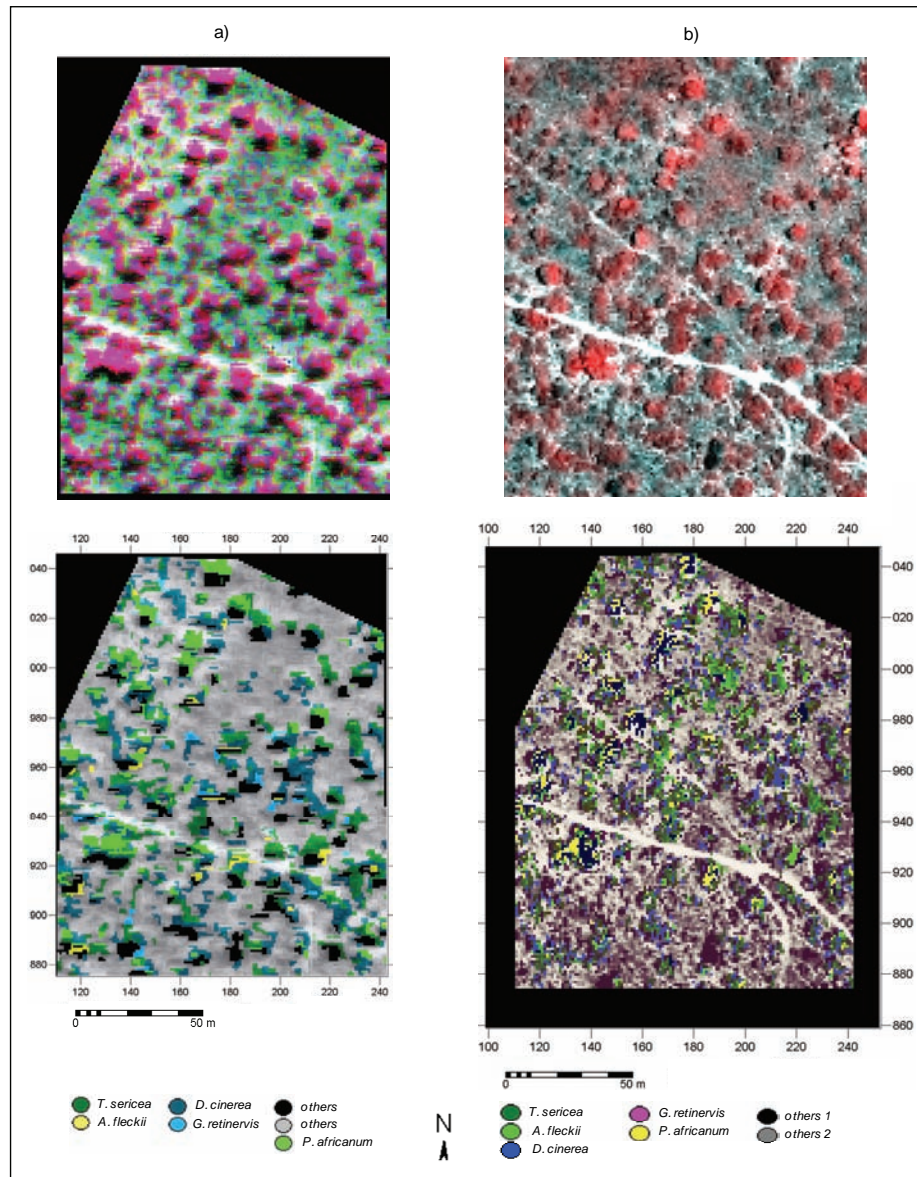
Figure 5.6 Comparison between classified a) airborne image at 1m spatial resolution and b)pansharpened IKONOS image of plot#2. Upper row original images, lower row classified images.

Table 5.3 User's accuracy per species. Mean values from the 5 plots classified

	user's accuracy		
	30cm	60cm	1m
Terminalia sericea	0.82	0.75	0.73
Lonchocarpus nelsii	1.00		1.00
Acacia fleckii	0.75	0.60	0.85
Boscia albitrunca	0.95	1.00	1.00
Dichrostachys cinerea	0.83	0.85	0.82
Ochna pulchra	0.69	0.41	

Taking the images at 30cm resolution as the most suitable for species differentiation based on the results presented in Table 5.1, a preliminary assessment of the separability of the species can be obtained. In this way, following the criterion presented by Congalton, 1991 for the Kappa coefficient, *L. nelsii* and *B. albitrunca* with user's accuracy of 100%and 95% can be categorized as highly separable while *T. sericea, A. fleckii, D. cinerea* and *O. pulchra* would be defined as moderately separable (accuracy between 80% and 40%). Among the several factors influencing the spectral signature of the canopies, foliage morphology can be related the separability of the species. At this respect, it is worth noting that based on 'easy-to-observe' vegetative features in their field guide to trees of southern Africa, Wyk van and Wyk van (1997) classified *B. albitrunca and L. nelsii* in the same group of species with simple leaves. On the contrary, species such as *A. fleckii, D. cinerea* and *O. pulchra* are classified as species with leaves *bipinnately* compound (twice divided). It is possible that this characteristic, present in most of the *Acacia* species and other southern African trees, makes difficult their separability by GIS/RS techniques. This conclusion however needs further verification and it falls outside the scope of this thesis.

5.4 Discussion and Conclusion

The capabilities and constraints of the object-oriented approach for the classification of high resolution airborne and satellite images of a typical African savanna, are presented in this chapter. Although such classification is mainly done for forest inventories or biodiversity studies, in this case it constitutes a key step in the methodology for transpiration mapping from sap flow measurements, which is the main topic of this research. The results are therefore discussed from this perspective. However, the general conclusions presented in this chapter can be used as a reference for other types of applications where species differentiation in high resolution images is needed.

In savanna vegetation, a large proportion of tree species occur in clusters, adding a degree of difficulty to individual canopies separation compared with other

environments. This study shows how high spatial resolution *i.e.* 30 cm images, improve the detection of narrow boundaries or spaces between individual crowns of clustered tree species e.g., *D. cinerea or T. sericea* which contribute to the tree crown closure in the segmentation step. This characteristic of the 30cm images resulted in not only better accuracy level but also in successful classification of more species. As the spatial resolution is reduced from 30cm to 1m, boundaries between the cluster members became undetectable and the whole cluster, especially in 1m resolution was recognized as one tree crown (Figure 5.3). This did not only lead to mixing of tree species but also to the reduction of both training and test samples because only a small number of trees could be recognized as individuals from the clusters.

Accuracy level, according to the results, was also influenced by the number of tree species existing in each plot. This was demonstrated in plot 3 where only 2 tree species were to be classified and the highest Kappa coefficient value (0.94 as presented in Table 5.1) was obtained. In comparison, plot 2 with lower Kappa coefficient value (0.86) had 5 tree species to be classified. When the number of species (classes) to be classified is increased the classifier has to separate more signatures of classes. In this respect, the conclusion is that is it important to consider the number of species identified and not only the Kappa coefficient if one wants to compare the accuracy of certain classification process between different locations or different spatial resolutions.

The relatively poor classification obtained from the IKONOS image compared to the same resolution airborne image classification was caused by a number of factors. Firstly, the quality of the image is highly dependent on the season in which it was acquired. The airborne data was collected during May 2004, which is the peak of the growing season, while the IKONOS was acquired during February 2002, when trees had not yet regained the stable green color of their leaves. The spectral signatures, which depend on the leafy component of a plant, constitute an integral part of segmentation process and therefore play a major role in the object-oriented classification. In the study area, most of the tree species shed their leaves during the dry winter season (June to September) and gradually regain them after the first rains (October or November). There is generally a time lag between the peak of the growing season (April) and the time that trees fully acquire the green color of their leaves (May). Therefore in the IKONOS image (acquired in February), the spectral signatures of most of the species were poorly represented and this led to difficulties in the classification, resulting in low accuracy. Further attempts to compare airborne and satellite images of the same resolution should be done with scenes of the same season. Unfortunately this could not be done in this study with the available resources.

Secondly, although care was taken to select a pansharpening algorithm suitable for vegetation classification, the fusion of two images will inevitably affect the spectral signature of the foliage, especially at the edge of individual canopies.

Therefore it is understandable that the 1m airborne image yielded much better results. As possible solution, it is recommended that newly developed spectral-preserving models are applied in the pansharpening process, in order to keep the color and grey value variances as close as possible to the ones in the original image (Zhang 2002).

The results of this study like those of previous attempts to classify the Kalahari savanna, show that object-oriented classification is superior to pixel based classifiers. When airborne data are not available for this type of application, satellite high resolution data can be used provided special attention is given to the pansharpening techniques and the adequate image date. The results presented here demonstrate that the higher the spatial resolution, the higher the number of tree species successfully identified hence the higher the accuracy. The more fully-formed the crowns of individual tree species, the better the distinction among their spectral signatures. This is especially true where tree species seasonally shed and regain their leaves thus emphasizing the stable green color associated with their spectral reflectance, leading to unique segmentation of the individual crowns as objects. The degree of differentiability of the species identified during the classification process, led to concerns on the sap flow upscaling process. The important differences in the hydrological behavior of the investigated species (Chapter 4) might register similarly in terms of spectral signature, texture, shape and smoothness and can thereby lead to critical misestimation of plot transpiration fluxes. When more resources are available for the classification of mixed forest such as the Kalahari savanna, high resolution images together with intensive field sampling and an appropriate classification algorithm have to be used. The example presented in this chapter, though unveiling the limitations of the available data, provides a milestone for the vegetation mapping of the Kalahari.

References

Banko, G. 1998. A Review of Assessing the Accuracy of Classifications of Remotely Sensed Data and of Methods Including Remote Sensing Data in Forest Inventory. *In* Interim Reports Ed. S. Nilsson. International Institute for Applied Systems Analysis, IIASA, Laxenburg, Austria.

Benz, U., P. Hofmann, G. Willhauck, I. Lingenfelder and M. Heynen 2004. Multi-resolution, object-oriented fuzzy analysis of remote sensing data for GIS-ready information. ISPRS Journal of Photogrammetry and Remote Sensing. 58:239-258.

Childes, S.L. 1989. Phenology of nine common woody species in semi-arid, deciduous Kalahari Sand vegetation. Vegetatio. 79:151-163.

Cohen, J. 1960. A coefficient of agreement for nominal scales. Educational and Psychological Measurement. 20:37-46.

Congalton, R. 1991. A Review of Assessing the Accuracy of Classifications of Remotely Sensed Data. Remote Sensing of Environment. 37:35-46.

Congalton, R. 1996. Accuracy assessment: A critical component of land cover mapping. IN: Gap Analysis: A Landscape Approach to Biodiversity Planning. *In* ASPRS/GAP Symposium, Charlotte, NC, pp. 119-131.

Dai, X. and S. Khorram 1998. A hierarchical data fusion framework for vegetation classificationfrom multisource remotely sensed imagery. *In* Geoscience and Remote Sensing Symposium. IGARSS '98. 1998 IEEE International. IEEE Xplore, Seattle, WA, USA.

Definiens 2007. Definiens eCognition Server. Available at http://www.definiens.com/, p. Web page.

Demisse, G. 2006. Spatial distribution of savannah woody species biodiversity in Serowe, Botswana. Unpublished MSc thesis. International Institute for Geo-Information Science and Earth Observations, ITC. Esnchede, The Netherlands., Enschede.

Foody, G. 2002. Status of land cover classification accuracy assessment. Remote Sensing of Environment. 80:185-201.

Gougeon, F. and D. Leckie 2006. The Individual Tree Crown Approach Applied to Ikonos Images of a Coniferous Plantation Area. Photogrammetric Engineering and Remote Sensing. 72:1287-1297.

Hajek, F. 2006. Object-oriented classification of Ikonos satellite data for the identification of tree species composition. Journal of Forest Science 52:181-187.

Hernandez-Riquene, A. 2002. Mapping of woody vegetation in arid zones: a multi-sensor analysis. International Institute for Geo-information Sciences and Earth Observation, ITC. Unpublished MSc thesis.

Kimani, J. 2005. Mapping of Dry Savannah Tree Species Using Object Oriented Classification and High Resolution Imagery in Serowe, Botswana. Unpublished MSc. Thesis. International Institute for Geo-Information Science and Earth Observations, ITC. Esnchede, The Netherlands.

Kimani, J., Y. Hussin, M. Lubczynski, D. Chavarro-Rincon and O.T. Obakeng 2007. Mapping Savannah Trees in Kalahari Using High Resolution Re-

mote Sensing Images and Object-Oriented Classification. International Journal of Geoinformatics. 3:29-39.

Kosaka, N., T. Akiyama, T. Bien and T. Kojima 2005. Forest type classification using data fusion of multispectral and panchromatic high-resolution satellite imageries. *In* Geoscience and Remote Sensing Symposium, 2005. IGARSS '05. Proceedings. 2005 IEEE International, pp. 2980-2983.

Laliberte, A., I. Rangoa, K. Havstada, J. Parisb, R. Beckc, R. McNeelyc and A. Gonzalez 2004. Object-oriented image analysis for mapping shrub encroachment from 1937 to 2003 in southern New Mexico. Remote Sensing of Environment. 93:198-210.

Leckie, D., F. Gougeon, N. Walsworth and D. Paradine 2003. Stand delineation and composition estimation using semi-automated individual tree crown analysis. Remote Sensing of Environment. 85:355-369.

Mapanda, W. 2003. Scaling-up tree transpiration of eastern Kalahari sandveld of Botswana using remote sensing and geographical information systems. Unpublished MSc thesis. International Institute for Geoinformation Science and Earth Observations, ITC. Eschede, The Netherlands

Obakeng, O.T. 2007. Soil moisture dynamics and evapotranspiration at the fringe of the Botswana Kalahari. Vrije Universiteit, Amsterdam, NL.

Pohl, C. and J. Van Genderen 1998. Multisensor image fusion in remote sensing: concepts, methods and applications. International Journal of Remote Sensing. 19:823-854.

Pugh, M., A. Waxman, M. Duggin and J. Hassett 2004. Neural image fusion of remotely sensed electro-optical and synthetic aperture radar data for forest classification. *In* Geoscience and Remote Sensing Symposium, 2004. IGARSS '04. Proceedings. 2004 IEEE International Ed. I. Xplore.

Skidmore, A. 1999. Accuracy assessment of spatial information. *In* Spatial Statistics for Remote Sensing Eds. A. Stein, F. Van der Meer and B. Gorte. Kluwer Academic Publishers, Dordrecht, The Netherlands.

Susaki, J. and R. Shibasaki 2000. Fusion of AVHRR and TM data for vegetation classification based onunmixing technique. *In* Geoscience and Remote Sensing Symposium, 2000. Proceedings. IGARSS 2000. IEEE 2000 International. IEEE Xplore, Honolulu, HI, USA.

Walter, V. 2004. Object-based classification of remote sensing data for change detection. ISPRS Journal of Photogrammetry and Remote Sensing 58:225-238.

Wyk van, B. and P. Wyk van 1997. Field Guide to Trees of Southern Africa. Struik Publishers.

Zhang, Y. 2002. Problems in the fusion of commercial high-resolution satellite as well as Landsat 7 images and initial solutions. International Archives of Photogrammetry and Remote Sensing IASPRS). 34

Chapter 6

Transpiration Mapping from Up-scaled Sap Flow

Abstract

A transpiration mapping approach that combines sap flow measurements of nine woody species in the Botswana Kalahari, with high resolution classified airborne images is presented. After analysis of sap flow patterns, mean sap flow was correlated with biometric measurements of the same trees for the development of species-specific upscaling functions. Given the capability of GIS/RS techniques for canopy area (CA) determination in the classified images, the upscaling functions used CA as a main scalar. Simple GIS operations were applied to 5 classified images of the Kalahari Research Project (KRP) experimental site to obtain maps of transpiration. The results confirmed that among the nine measured species: *Acacia fleckii, Acacia erioloba, Acacia luederitzii, Boscia albitrunca, Lonchocarpus nelsii, Burkea africana, Ochna pulchra* and *Dichrostachys cinerea*, the presence of the evergreen *B. albitrunca* defines areas of high water extraction. The total transpiration flux in the five images ranged from 0.021mm/day for the image with predominant presence of *Dichrostachys cinerea* and *Terminalia sericea,* to 0.165mm/day for the image where *Boscia albitrunca* was abundant. Transpiration fluxes obtained from the RS-based upscaling approach yielded more realistic values than energy balance methods previously applied in the same area.

Keywords: *canopy area, GIS, sap flow, transpiration flux, upscaling.*

6.1 Introduction

Water extracted by trees is regarded as either a required mechanisms for CO_2 intake (forest and ecological perspective), or as a negative component of water or groundwater balances (hydrological perspective). Reliable quantification of tree water uptake has become fundamental to forest hydrology. From the individual tree water-use perspective, both disciplines benefit from transpiration fluxes quantification. For example agro-foresters use such quantification to ensure that water demands can be met, while ecohydrologists can motivate limiting the proliferation of certain species as a groundwater level control. In semi-arid open savannas such as the Kalahari, concerns about groundwater supply sustainability have led to the investigation of vegetation's groundwater-use and the identification of high water-consuming species (the importance of the quantification of tree water-use in the Kalahari has been discussed in the fist chapters of this thesis).

The importance of mapping transpiration fluxes has increased with the rapid propagation of spatially-distributed hydrological models. For such models, transpiration maps have been obtained by the implementation of algorithms based on the energy balance equation using RS images and in some cases also micro-meteorological data (Baldocchi and Vogel 1996; Bastiaanssen and Bandara 2001; Meijerink *et al.* 2005; Timmermans and Meijerink 1999). Energy balance based methods can quantify water lost by evapotranspiration and its spatial variation, but they cannot discriminate between soil evaporation and tree transpiration and therefore do not provide insight into species' hydrological functioning. Additionally, some energy balance based methods require measurements above the tree canopy level with the consequent logistical complications.

Another approach is the upscaling of sap flow from tree to stand or plot level (Granier 1987; Hatton *et al.* 1995; Vertessy *et al.* 1995; Vertessy *et al.* 1997; Wullschleger *et al.* 2001). In this case sap flow measurements are collected and upscaled using an easily measured parameter *e.g.* stem diameter, stem area or sapwood area. In some cases leaf area index (LAI) has been successfully used as a scalar. This approach takes the advantage of the common correlativeness between biometric parameters and sap flow but has the disadvantage that it requires an inventory of all the trees in the stand or plot and measurements of the scalar in each of them.

This chapter presents an alternative approach which combines the capabilities of GIS/RS techniques for vegetation classification and tree canopy delineation with the local and specific information provided by sap flow measurements. As presented before in this thesis, technical and tree physiological issues related to sap flow measurements were initially considered (Chapters 2 to 4). Thereafter, high resolution images were classified and tree canopies delineated (Chapter 5) to

be combined with species-specific upscaling functions resulting in transpiration maps. This study aims to provide a practical and affordable tool for hydrological studies, especially in those emerging countries where water availability is a main issue

6.2 Materials and Methods

6.2.1   Study area

This study was executed within the framework of the KRP conducted in the Serowe area, Central District of Botswana (S 22°20', E 26°24') at the eastern fringe of the Kalahari basin. The area receives a MAP of 400mm; rainfall is seasonal with its highest intensity in summer (October-April) followed by a dry winter (June-September). The mean annual temperature is 20°C but summer temperatures can exceed 30°C during the day while in winter they can drop below 0°C at night. Surface water streams are ephemeral making groundwater reserves the main source of water supply. Groundwater is mainly found in the Karoo rocks (sandstones, shales and basalts) below the mantle of Kalahari sands. The thickness of this sand mantle increases from 0-5 m close to the eastern fringe to 60-100m towards the centre (Obakeng 2007). The topography of the Serowe area is fairly flat and featureless, sloping gently to the west without prominent drainage lines. The area is characterized by permeable sands with high infiltration rates and negligible surface runoff.

6.2.2   Sap flow campaign

Sap flux density (sap flow per conductive sapwood area per unit of time) measurements of nine woody species were collected during the dry season (July to September) of 2004 using the thermal dissipation probes (TDP) method (Granier 1985; Granier 1987). The measured species, namely *Acacia fleckii, Acacia erioloba, Acacia luederitzii, Boscia albitrunca, Lonchorcarpus nelsii, Terminalia sericea, Burkea Africana, Ochna pulchra* and *Dichrostachys cinerea,* were selected based on frequency of occurrence in the study area. Groups of trees ranging from 18 to 24 individuals of each species were simultaneously measured with regards to sap flow, conductive sapwood area and biometric parameters. Details about the sap flow campaign are presented in Chapter 2 of this thesis and a discussion about the sap flow patterns observed during the campaign and their implications in transpiration quantification can be found in Chapter 4.

As presented in the mentioned chapters, some of the measured species showed nighttime sap flow activity. Based on the conclusions drawn in Chapter 4, the

quantification of mean net sap flow to be used in transpiration assessment has to disregard nighttime sap flux densities (S_d). The author theorizes that sap flow observed during periods of no solar radiation can be related to hydraulic redistribution using mechanisms such as reverse flow and air moisture harvesting. These theories require further verification, but the exclusion of nightime sap flow in the quantification of transpiration is considered essential independently of the process linked with it.

Once nocturnal records of sap densities were removed, mean daily values were combined with sapwood measurements to obtain mean sap flow for each measured tree (key aspects related to the determination and interpretation of sapwood area are presented in Chapter 3 of this thesis). A statistical analysis of sap flow, sap flux densities and the allometric parameters collected during the campaign was carried out using the R-project for statistical computing and visualisation (http://www.r-project.org)

6.2.3   Sapwood area from stem diameter

The quantification of sapwood area in the trees investigated was made from direct measurements of cut stems as described in Chapter 3. The available data however, allows the development of correlations between the measured parameters e.g. stem diameter, stem area or canopy area and sapwood area per species. Such correlations can be used in further studies of the same species to avoid the use of invasive or destructive methods for sapwood area determination.

6.2.4   Upscaling functions

The upscaling of sap flow for transpiration mapping based on GIS/RS techniques must use a scalar that can be easily retrieved in RS images. Earlier in this thesis, Chapter 5 describes how object-oriented GIS packages are able to delineate and classify tree canopies. In this way, e'Cognition software was used to indentify and classify tree canopies in 5 sub-areas inside the KRP experimental Serowe area. Consequently, any upscaling approach used in this study uses tree canopies as a main scalar.

In order to obtain the optimal upscaling function with the available data, four approaches were investigated based on the following parameters: sap flow (SF), canopy area (CA), stem diameter (SD), stem area (SA) and sapwood area (SW). The first approach explored the possibility of obtaining SF in one step directly from CA (identified as approach I hereafter). In the other three approaches (II, III and IV), CA is used first to retrieve another possible scalar e.g. SA, SW or SD to be later correlated with SF. Before fitting a regression between

parameters, the degree of correlation between variables was checked using the Pearson's product-moment correlation coefficient (PMCC). PMCC ranges from -1 to 1 for a perfect negative or positive correlation respectively. PMCC equal to 0 indicates no relationship between the two variables. Although PMCC was used as an indicator of proportionality between variables, statistical analysis was applied to possible regressions in the four upscaling approaches. Comparison of statistical indicators such as residual standard error (RSE), the coefficient of determination R^2 and PMCC led to the selection of the best upscaling function for each species.

Taking into account the evidence that many of the Kalahari woody species are self-organized in clusters (Caylor *et al.* 2003; Privette *et al.* 2004; Scholes *et al.* 2002), when developing the upscaling functions trees were considered not only individually but in their natural spatial arrangement. Therefore, a cluster of any number of trees is considered as a single larger tree with biometric characteristics (CA, SA, SW, and SD) and sap flow (SF), equal to the sum of the same parameters of its members. Statistical analysis of SF with the allometric parameters thus includes SF for individual trees and for clusters.

6.2.5 Transpiration mapping

The final step of the methodology for transpiration mapping is the application of upscaling functions in classified RS images. For that purpose, the five sub-areas of the reference IKONOS image, in which tree canopies were delineated and classified, were subject to simple GIS operations (details of the sub-areas location and classification procedure are presented in Chapter 5). The applied GIS procedure in every sub-area can be summarize in four main steps: *i)* calculation of ground-projected tree CA irrespectively of the tree species, *ii)* determination of the selected intermediary scalar SA, SW or SD, from species-dependent functions based on CA, (only for approaches II, III, and IV), *iii)* calculation of sap flow (SF) per tree from species-dependent functions and *iv)* determination of transpiration fluxes per tree canopy and per 25mx25m plot.

6.3 Results

6.3.1 Summary of the measured parameters

Figures 6.1 to 6.6 present a statistical description of the allometric and sap flow measurements collected during the dry-season 2004 campaign. As an indicator of the order of magnitude of every parameter and its distribution in the data set, a histogram of frequency is presented. The results are presented for the

complete set of measurements and discriminated per category (species in this case). Finally box-plots depicting the smallest observation, lower quartile (Q1), median (Q2), upper quartile (Q3), the largest observation and the possible outliers are presented. In the case of species in which night-time sap flux densities were removed, the statistical analyses include also the original 24h records for comparison.

Key for Figures 6.1-6.6:
AER = *Acacia erioloba,*
AFL = *Acacia fleckii,*
ALU = *Acacia luederitzii,*
BAF = *Burkea Africana,*
BAL = *Boscia albitrunca,*
BAL_D = *Boscia albitrunca* daytime values,
DCI = *Dichrostachys cinerea,*
DCI_D = *Dichrostachys cinerea* daytime values,
LNE = *Lonchorcarpus nelsii,*
OPU =*Ochna pulchra,*
TSE =*Terminalia sericea,*
TSE_D = *Terminalia sericea* daytime values

Fig 6.1 Statistical summary of sap flow density measurements.

canopy area, CA (m^2)

Min. 1st Qu. Median Mean 3rd Qu.   Max.
1.10   4.55   8.30 11.00 13.38 64.00

summary per category

canopies$CATEGORY: AER
 Min. 1st Qu. Median   Mean 3rd Qu.   Max.
 1.700 2.600 3.800 3.719 4.800 6.400

canopies$CATEGORY: AFL
 Min. 1st Qu. Median   Mean 3rd Qu.   Max.
 1.80   7.90 10.05 10.39 12.87 18.50

canopies$CATEGORY: AFL_C
 Min. 1st Qu. Median   Mean 3rd Qu.   Max.
 1.80 10.20 13.40 17.29 21.55 52.20

canopies$CATEGORY: ALU
 Min. 1st Qu. Median   Mean 3rd Qu.   Max.
 4.90 10.60 21.60 23.72 29.70 64.00

canopies$CATEGORY: BAF
 Min. 1st Qu. Median   Mean 3rd Qu.   Max.
 1.700 3.800 5.100 5.093 6.050 8.600

canopies$CATEGORY: BAL
 Min. 1st Qu. Median   Mean 3rd Qu.   Max.
 1.100 2.250 3.800 3.771 4.750 7.500

canopies$CATEGORY: BAL_C
 Min. 1st Qu. Median   Mean 3rd Qu.   Max.
  2.3   7.3   9.2 10.1 13.2 20.4

canopies$CATEGORY: DCI
 Min. 1st Qu. Median   Mean 3rd Qu.   Max.
 2.80   8.90 11.60 15.22 18.90 42.90

canopies$CATEGORY: LNE
 Min. 1st Qu. Median   Mean 3rd Qu.   Max.
 6.00   9.70 11.95 12.39 14.30 20.80

canopies$CATEGORY: OPU
 Min. 1st Qu. Median   Mean 3rd Qu.   Max.
 1.300 2.400 3.000 3.854 5.500 8.000

canopies$CATEGORY: TSE
 Min. 1st Qu. Median   Mean 3rd Qu.   Max.
 7.500 8.475 11.300 11.730 13.200 20.500

canopies$CATEGORY: TSE_C
 Min. 1st Qu. Median   Mean 3rd Qu.   Max.
 8.30   8.75 17.60 19.17 25.95 40.00

variance per category

canopies$CATEGORY: AER
[1] 1.724619

canopies$CATEGORY: AFL
[1] 18.02563

canopies$CATEGORY: AFL_C
[1] 160.1355

canopies$CATEGORY: ALU
[1] 280.7965

canopies$CATEGORY: BAF
[1] 3.946381

canopies$CATEGORY: BAL
[1] 3.116069

canopies$CATEGORY: BAL_C
[1] 30.645

canopies$CATEGORY: DCI
[1] 88.38178

canopies$CATEGORY: LNE
[1] 19.34901

canopies$CATEGORY: OPU
[1] 4.354359

canopies$CATEGORY: TSE
[1] 15.00565

canopies$CATEGORY: TSE_C
[1] 126.7322

Fig 6.2 Statistical summary of tree canopy area measurements.

stem area, SA (cm^2)

Min. 1st Qu. Median   Mean 3rd Qu.   Max.
14.50 45.18 73.10 92.07 108.30 546.60

summary per category

stems$CATEGORY: AER
 Min. 1st Qu. Median   Mean 3rd Qu.   Max.
 14.50 27.90 38.50 60.01 99.20 172.60

stems$CATEGORY: AFL
 Min. 1st Qu. Median   Mean 3rd Qu.   Max.
 32.50 66.95 102.20 98.95 121.60 208.80

stems$CATEGORY: AFL_C
 Min. 1st Qu. Median   Mean 3rd Qu.   Max.
 32.5   69.7 110.3 160.8 218.1 546.6

stems$CATEGORY: ALU
 Min. 1st Qu. Median   Mean 3rd Qu.   Max.
 32.30 47.25 181.10 151.80 233.80 291.80

stems$CATEGORY: BAF
 Min. 1st Qu. Median   Mean 3rd Qu.   Max.
 40.00 53.35 67.60 81.31 84.60 259.00

stems$CATEGORY: BAL
 Min. 1st Qu. Median   Mean 3rd Qu.   Max.
 30.90 50.08 62.20 63.98 75.40 98.90

stems$CATEGORY: BAL_C
 Min. 1st Qu. Median   Mean 3rd Qu.   Max.
 58.8   73.1 187.0 170.6 234.2 304.2

stems$CATEGORY: DCI
 Min. 1st Qu. Median   Mean 3rd Qu.   Max.
 16.80 36.95 49.10 52.47 67.65 108.20

stems$CATEGORY: LNE
 Min. 1st Qu. Median   Mean 3rd Qu.   Max.
 44.50 89.45 96.70 103.70 111.40 194.90

stems$CATEGORY: OPU
 Min. 1st Qu. Median   Mean 3rd Qu.   Max.
 15.30 35.00 64.80 65.24 98.00 114.20

stems$CATEGORY: TSE
 Min. 1st Qu. Median   Mean 3rd Qu.   Max.
 27.90 40.85 50.15 69.18 78.35 197.80

stems$CATEGORY: TSE_C
 Min. 1st Qu. Median   Mean 3rd Qu.   Max.
 38.3   45.8   85.8 113.2 164.4 241.2

variance per category

stems$CATEGORY: AER
[1] 2393.974

stems$CATEGORY: AFL
[1] 1742.638

stems$CATEGORY: AFL_C
[1] 18145.43

stems$CATEGORY: ALU
[1] 9744.39

stems$CATEGORY: BAF
[1] 2856.844

stems$CATEGORY: BAL
[1] 388.3901

stems$CATEGORY: BAL_C
[1] 7472.174

stems$CATEGORY: DCI
[1] 549.066

stems$CATEGORY: LNE
[1] 1204.854

stems$CATEGORY: OPU
[1] 1120.289

stems$CATEGORY: TSE
[1] 2178.812

stems$CATEGORY: TSE_C
[1] 5287.001
 >

Fig 6.3 Statistical summary of stem area measurements

stem diameter , SD

Min.	1st Qu.	Median	Mean	3rd Qu.	Max.
4.30	7.60	9.65	11.30	11.78	58.20

summary per category

diameter$CATEGORY: AER
Min. 1st Qu. Median Mean 3rd Qu. Max.
4.300 6.000 7.000 8.105 11.200 14.800
diameter$CATEGORY: AFL
Min. 1st Qu. Median Mean 3rd Qu. Max.
6.40 9.35 11.35 10.96 12.23 16.70
diameter$CATEGORY: AFL_C
Min. 1st Qu. Median Mean 3rd Qu. Max.
6.40 9.40 11.80 18.07 23.35 58.20
diameter$CATEGORY: ALU
Min. 1st Qu. Median Mean 3rd Qu. Max.
6.40 8.40 16.70 14.39 17.90 25.00
diameter$CATEGORY: BAF
Min. 1st Qu. Median Mean 3rd Qu. Max.
7.10 8.25 9.30 9.84 10.35 18.20
diameter$CATEGORY: BAL
Min. 1st Qu. Median Mean 3rd Qu. Max.
6.300 8.000 8.900 8.917 9.750 11.200
diameter$CATEGORY: BAL_C
Min. 1st Qu. Median Mean 3rd Qu. Max.
8.70 9.60 26.40 23.78 34.40 39.10
diameter$CATEGORY: DCI
Min. 1st Qu. Median Mean 3rd Qu. Max.
4.600 6.850 7.900 7.965 9.300 11.700
diameter$CATEGORY: LNE
Min. 1st Qu. Median Mean 3rd Qu. Max.
7.50 10.65 11.10 11.36 11.95 15.80
diameter$CATEGORY: OPU
Min. 1st Qu. Median Mean 3rd Qu. Max.
4.400 6.700 9.100 8.777 11.200 12.100
diameter$CATEGORY: TSE
Min. 1st Qu. Median Mean 3rd Qu. Max.
6.000 7.175 8.000 9.006 10.000 15.900
diameter$CATEGORY: TSE_C
Min. 1st Qu. Median Mean 3rd Qu. Max.
7.00 7.65 10.50 14.72 21.60 27.70

variance per category

diameter$CATEGORY: AER
[1] 11.24248
diameter$CATEGORY: AFL
[1] 5.770043
diameter$CATEGORY: AFL_C
[1] 186.6595
diameter$CATEGORY: ALU
[1] 36.44485
diameter$CATEGORY: BAF
[1] 7.318286
diameter$CATEGORY: BAL
[1] 1.924058
diameter$CATEGORY: BAL_C
[1] 139.0244
diameter$CATEGORY: DCI
[1] 3.381462
diameter$CATEGORY: LNE
[1] 3.533242
diameter$CATEGORY: OPU
[1] 6.59859
diameter$CATEGORY: TSE
[1] 7.560556
diameter$CATEGORY: TSE_C
[1] 67.55564

Frequency histogram of stem diamter

stem diameter (cm)
Counts shown above bar, actual values shown with rug plot

stem diameter classified by tree species

Fig 6.4 Statistical summary of stem diameter measurements.

sapwood area, SW

Min.	1st Qu.	Median	Mean	3rd Qu.	Max.
6.40	27.05	46.25	62.52	75.83	395.20

summary per category

sapwood$CATEGORY: AER
Min. 1st Qu. Median Mean 3rd Qu. Max.
9.70 20.80 25.30 37.93 63.40 113.00
sapwood$CATEGORY: AFL
Min. 1st Qu. Median Mean 3rd Qu. Max.
26.20 44.85 58.95 66.91 80.85 160.70
sapwood$CATEGORY: AFL_C
Min. 1st Qu. Median Mean 3rd Qu. Max.
26.2 48.2 70.2 111.2 152.9 395.2
sapwood$CATEGORY: ALU
Min. 1st Qu. Median Mean 3rd Qu. Max.
20.3 35.5 127.0 118.1 150.1 296.1
sapwood$CATEGORY: BAF
Min. 1st Qu. Median Mean 3rd Qu. Max.
30.6 38.5 53.5 61.2 63.0 198.1
sapwood$CATEGORY: BAL
Min. 1st Qu. Median Mean 3rd Qu. Max.
24.40 35.78 44.00 46.58 60.00 78.80
sapwood$CATEGORY: BAL_C
Min. 1st Qu. Median Mean 3rd Qu. Max.
40.3 59.1 145.0 124.2 146.9 219.0
sapwood$CATEGORY: DCI
Min. 1st Qu. Median Mean 3rd Qu. Max.
6.40 13.85 19.70 20.61 27.05 43.30
sapwood$CATEGORY: LNE
Min. 1st Qu. Median Mean 3rd Qu. Max.
32.20 68.75 75.65 81.59 88.92 158.90
sapwood$CATEGORY: OPU
Min. 1st Qu. Median Mean 3rd Qu. Max.
11.40 26.10 37.90 42.83 65.00 77.50
sapwood$CATEGORY: TSE
Min. 1st Qu. Median Mean 3rd Qu. Max.
16.30 22.45 28.90 37.73 39.82 99.10
sapwood$CATEGORY: TSE_C
Min. 1st Qu. Median Mean 3rd Qu. Max.
21.80 26.25 50.10 61.73 90.15 128.20

variance per category

sapwood$CATEGORY: AER
[1] 821.3053
sapwood$CATEGORY: AFL
[1] 1041.718
sapwood$CATEGORY: AFL_C
[1] 9425.928
sapwood$CATEGORY: ALU
[1] 7515.282
sapwood$CATEGORY: BAF
[1] 1699.633
sapwood$CATEGORY: BAL
[1] 257.6548
sapwood$CATEGORY: BAL_C
[1] 3717.405
sapwood$CATEGORY: DCI
[1] 87.05992
sapwood$CATEGORY: LNE
[1] 864.3223
sapwood$CATEGORY: OPU
[1] 491.9456
sapwood$CATEGORY: TSE
[1] 551.4762
sapwood$CATEGORY: TSE_C
[1] 1472.598

Frequency histogram of sapwood area

sapwood area (cm2)
Counts shown above bar, actual values shown with rug plot

sapwood area classified by tree species

Fig 6.5 Statistical summary of sapwood measurements.

sap flow , SF (liters*h^{-1})

Min. 1st Qu. Median   Mean 3rd Qu.   Max.
0.0030 0.0390 0.0825 0.1564 0.2085 1.0750

summary per category

sapflow$CATEGORY: AER
  Min. 1st Qu. Median   Mean 3rd Qu.   Max.
0.00800 0.02600 0.03900 0.08119 0.09600 0.26200
----
sapflow$CATEGORY: AFL
  Min. 1st Qu. Median   Mean 3rd Qu.   Max.
0.01400 0.02625 0.04450 0.08159 0.12800 0.26700
----
sapflow$CATEGORY: AFL_C
  Min. 1st Qu. Median   Mean 3rd Qu.   Max.
 0.0140 0.0400 0.0650 0.1623 0.2180 0.7990
----
sapflow$CATEGORY: ALU
  Min. 1st Qu. Median   Mean 3rd Qu.   Max.
 0.0150 0.0330 0.0630 0.1322 0.1970 0.4580
----
sapflow$CATEGORY: BAF
  Min. 1st Qu. Median   Mean 3rd Qu.   Max.
 0.0360 0.0685 0.0820 0.0942 0.1090 0.2090
----
sapflow$CATEGORY: BAL
  Min. 1st Qu. Median   Mean 3rd Qu.   Max.
 0.0480 0.2243 0.3570 0.3584 0.4872 0.7340
----
sapflow$CATEGORY: BAL_C
  Min. 1st Qu. Median   Mean 3rd Qu.   Max.
 0.1420 0.2680 0.7040 0.6134 0.8530 1.0750
----
sapflow$CATEGORY: BAL_D
  Min. 1st Qu. Median   Mean 3rd Qu.   Max.
 0.0290 0.1450 0.2215 0.2300 0.2853 0.5080
----
sapflow$CATEGORY: DCI
  Min. 1st Qu. Median   Mean 3rd Qu.   Max.
0.00300 0.01000 0.01600 0.02126 0.02200 0.07800
----
sapflow$CATEGORY: DCI_D
  Min. 1st Qu. Median   Mean 3rd Qu.   Max.
0.00500 0.01650 0.02050 0.02780 0.03275 0.07800
----
sapflow$CATEGORY: LNE
  Min. 1st Qu. Median   Mean 3rd Qu.   Max.
 0.0410 0.1113 0.1645 0.1676 0.1747 0.4340
----
sapflow$CATEGORY: OPU
  Min. 1st Qu. Median   Mean 3rd Qu.   Max.
0.00900 0.03000 0.05100 0.06431 0.07800 0.16100
----
sapflow$CATEGORY: TSE
  Min. 1st Qu. Median   Mean 3rd Qu.   Max.
 0.0720 0.1212 0.1630 0.1875 0.1992 0.5270
----
sapflow$CATEGORY: TSE_C
  Min. 1st Qu. Median   Mean 3rd Qu.   Max.
 0.0490 0.0760 0.0800 0.1435 0.1930 0.3950
----
sapflow$CATEGORY: TSE_D
  Min. 1st Qu. Median   Mean 3rd Qu.   Max.
0.03400 0.05150 0.07300 0.08772 0.07800 0.33600

variance per category

sapflow$CATEGORY: AER   sapflow$CATEGORY: BAL_D
[1] 0.006468262   [1] 0.01649456
-------------------------------- --------------------------------
sapflow$CATEGORY: AFL   sapflow$CATEGORY: DCI
[1] 0.005564158   [1] 0.0003004743
-------------------------------- --------------------------------
sapflow$CATEGORY: AFL_C   sapflow$CATEGORY: DCI_D
[1] 0.04272552   [1] 0.0004341778
-------------------------------- --------------------------------
sapflow$CATEGORY: ALU   sapflow$CATEGORY: LNE
[1] 0.01934040   [1] 0.009076247
-------------------------------- --------------------------------
sapflow$CATEGORY: BAF   sapflow$CATEGORY: OPU
[1] 0.002081886   [1] 0.002469897
-------------------------------- --------------------------------
sapflow$CATEGORY: BAL   sapflow$CATEGORY: TSE
[1] 0.03272164   [1] 0.01436721
-------------------------------- --------------------------------
sapflow$CATEGORY: BAL_C   sapflow$CATEGORY: TSE_C
[1] 0.1271098   [1] 0.01101807
-------------------------------- --------------------------------
                               sapflow$CATEGORY: TSE_D
                               [1] 0.005472565

Frequency histogram of sap flow

sap flow (l/h)
Counts shown above bar, actual values shown with rug plot

Sap flow classified by tree species

Fig 6.6 Statistical summary of sap flow estimations.

6.3.2. Stem diameter vs. Sapwood area

Considering SD as the most direct allometric measurement in trees, and the good correlations between SD and SW, the regressions suggested for determination of sapwood in further studies are based on SD. Figure 6.7 presents the regressions thus obtained per species
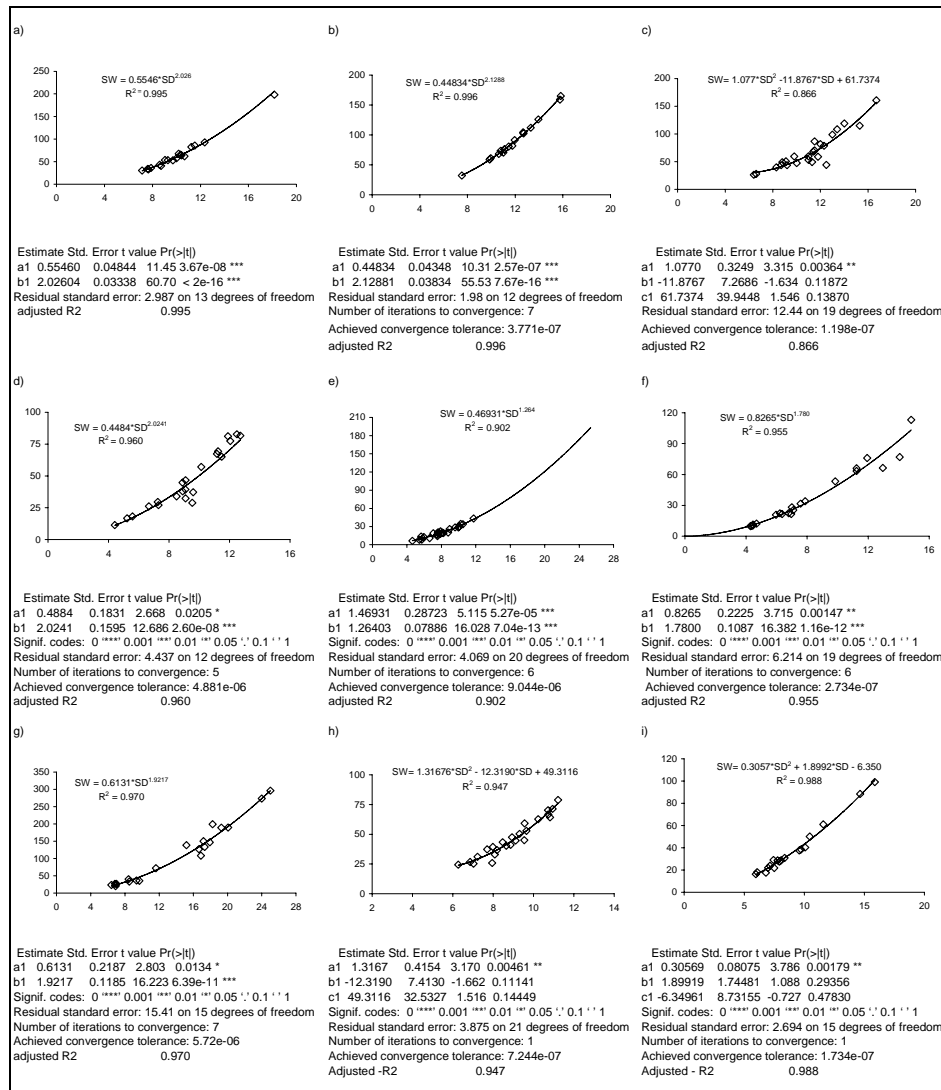
Figure 6.7 Correlations between stem diameter, SD, and sapwood area, SW, for the nine species investigated. a) *Burkea Africana,* b) *Lonchorcarpus nelsii,* c) *Acacia fleckii,* d) *Ochna pulchra,* e) *Dichrostachys cinerea,* f) *Acacia erioloba,* g) *Acacia luederitzii,* h) *Boscia albitrunca* and i) *Terminalia sericea.* For species growing in clusters, the correlations were developed based on measurements of individual specimens.

6.3.3 Upscaling functions

Table 6.1 presents PMCC and R^2 obtained for the four upscaling approaches. In approaches II to IV, PMCC was obtained as an average of the two set of measurements involved.

Table 6.1. Pearson Momentum-Correlation Coefficient (PMCC), and R^2 for the four upscaling approaches and the nine species studied. Where applicable, trees were analyzed both as individuals and as clusters. CA=canopy area, SD=stem diameter, SA= stem area, SW= sapwood area and SF = sap flow.

species	upscaling approach										
	CA vs SF		CA vs SA		SA vs SF	CA vs SW		SW vs SF	CA vs SD		SD vs SF
	PMCC	R^2	R^2	PMCC	R^2	R^2	PMCC	R^2	R^2	PMCC	R^2
B. africana	0.525	0.404	0.572	0.701	0.674	0.578	0.649	0.655	**0.721**	**0.720**	**0.697**
L. nelssi	0.587	0.463	0.641	0.822	0.902	0.608	0.793	0.898	**0.821**	**0.812**	**0.889**
A. fleckii	0.264	-	-	0.339	-	-	0.438	-	-	0.350	-
A. fleckii - clusters	0.801	0.643	0.593	0.880	0.656	**0.707**	**0.890**	**0.758**	0.620	0.888	0.665
O. pulchra	0.762	0.396	0.809	0.801	-	0.814	0.818	-	**0.841**	**0.776**	**0.603**
D. cinerea - clusters	**0.887**	**0.927**	0.773	0.781	0.845	0.795	0.830	0.850	0.604	0.864	0.910
A erioloba	**0.823**	**0.775**	0.534	0.741	0.620	0.542	0.766	0.686	-	0.758	0.624
A. luederitzii	0.673	0.514	0.768	0.697	0.781	0.792	0.837	0.617	**0.878**	**0.806**	**0.850**
B. albitrunca-ind.	0.446	-	0.720	0.623	-	0.675	0.606	-	0.658	0.623	0.353
B. albitrunca-clusters	0.729	0.708	0.884	0.864	0.756	0.901	0.872	0.758	**0.868**	**0.893**	**0.858**
T. sericea-ind	0.315	0.450	0.627	0.703	0.925	0.635	0.703	0.900	0.498	0.697	0.894
T. sericea-clusters	0.689	0.683	**0.859**	**0.867**	**0.925**	0.848	0.862	0.915	0.878	0.850	0.629

The data set used for fitting regression lines was prepared taking into account the following criterion: *i)* SF samples resulting from faulty measurements *i.e.* improper probe-wood contact or sensor malfunctioning were disregarded, and *ii)* outliers of the data set as presented in figures 6.1 to 6. 6 were not excluded when they correspond to a tree much bigger or smaller than the average size of other trees in the same site.

The final correlations used in the upscaling process are presented in Figures 6.8 to 6.10. As showed by the PMCC indicator, in most of the species (except *for D. cinerea* and *A. erioloba)* the lowest proportionality between the two variables was for the first approach (CA vs. SF), suggesting the necessity for an intermediary scalar *e.g.* SA, SW and SD. Giving the convenience of SD as a scaling parameter, approach IV was preferred even in cases where PMCC was slightly lower than in other approaches such as in the case of *L. nelsii*.

6.3.4 Transpiration maps

The application of the upscaling functions presented in Figures 6.8 to 6.10 resulted in transpiration maps of the five sub-areas previously classified. Figures 6.11 to 6.15 illustrate in four steps the upscaling process per sub-area: a) original multi-spectral (NIR,R,G) airborne image at 30cm spatial resolution, b) classified image from object-oriented method in which tree canopies are delineated,

Burkea africana

Parameters:
  Estimate Std. Error t value Pr(>|t|)
a1 -0.06745 0.06560 -1.028 0.324141
b1 2.19441 0.43286 5.070 0.000275 ***
Signif. codes: 0 '***' 0.001 '**' 0.01 '*' 0.05 '.' 0.1 ' ' 1
Residual standard error: 2.107 on 12 degrees of freedom
Achieved convergence tolerance: 3.87e-08
Adjusted-R2   [1] 0.7210275

Parameters:
  Estimate Std. Error t value Pr(>|t|)
a1 0.0001821 0.0002106 0.865 0.4040
b1 0.0079311 0.0026074 3.042 0.0102 *
Signif. codes: 0 '***' 0.001 '**' 0.01 '*' 0.05 '.' 0.1 ' ' 1
Residual standard error: 0.02979 on 12 degrees of freedom
Achieved convergence tolerance: 2.972e-08
Adjusted-R2   [1] 0.6981829

Lonchocarpus nelsii

Parameters:
  Estimate Std. Error t value Pr(>|t|)
a1 -0.040634 0.007383 -5.504 0.000101 ***
b1 1.471070 0.116541 12.623 1.14e-08 ***
Signif. codes: 0 '***' 0.001 '**' 0.01 '*' 0.05 '.' 0.1 ' ' 1
Residual standard error: 1.555 on 13 degrees of freedom
Achieved convergence tolerance: 8.498e-08

Adjusted-R2   [1] 0.8112014

Parameters:
  Estimate Std. Error t value Pr(>|t|)
a1 0.0027244 0.0004235 6.433 2.23e-05 ***
b1 -0.0170314 0.0051226 -3.325 0.00548 **
Signif. codes: 0 '***' 0.001 '**' 0.01 '*' 0.05 '.' 0.1 ' ' 1
Residual standard error: 0.03466 on 13 degrees of freedom
Achieved convergence tolerance: 4.451e-09

Adjusted-R2   [1] 0.8917435

Acacia Fleckii

  Estimate Std. Error t value Pr(>|t|)
a1 0.08269 0.06813 1.214 0.2425
b1 4.28730 1.52946 2.803 0.0128 *
Signif. codes: 0 '***' 0.001 '**' 0.01 '*' 0.05 '.' 0.1 ' ' 1
Residual standard error: 33.36 on 16 degrees of freedom
Achieved convergence tolerance: 1.108e-07
Adjusted-R2   [1] 0.7073321

  Estimate Std. Error t value Pr(>|t|)
a1 -1.163e-06 1.105e-06 -1.053 0.308
b1 1.145e-03 2.029e-04 5.646 3.64e-05 ***
Signif. codes: 0 '***' 0.001 '**' 0.01 '*' 0.05 '.' 0.1 ' ' 1
Residual standard error: 0.03297 on 16 degrees of freedom
Achieved convergence tolerance: 5.376e-09
Adjusted-R2   [1] 0.7584892

Figure 6.8 Upscaling functions for *Burkea Africana, Lonchorcarpus nelsii* and *Acacia fleckii*

Ochna pulchra

SD = -0.2807xCA² + 3.6349xCA
R² = 0.880

SF = 0.0011xSD² - 0.0026xSD
R² = 0.6056

Estimate Std. Error t value Pr(>|t|)
a1 -0.28068 0.04114 -6.822 1.84e-05 ***
b1 3.63491 0.25055 14.508 5.69e-09 ***
Signif. codes: 0 '***' 0.001 '**' 0.01 '*' 0.05 '.' 0.1 ' ' 1
Residual standard error: 1.227 on 12 degrees of freedom
Achieved convergence tolerance: 1.171e-07
Adjust. R-squared: [1] 0.8800998

Estimate Std. Error t value Pr(>|t|)
a1 0.0010457 0.0005263 1.987 0.0703 .
b1 -0.0026368 0.0053523 -0.493 0.6312
Signif. codes: 0 '***' 0.001 '**' 0.01 '*' 0.05 '.' 0.1 ' ' 1
Residual standard error: 0.03317 on 12 degrees of freedom
Achieved convergence tolerance: 1.958e-06
Adjust. R-squared: [1] 0.6056474

Dichrostachys cinerea

SF = 1.028E-05xCA² + 0.0009xCA
R² = 0.9267

Parameters:
  Estimate Std. Error t value Pr(>|t|)
a1 1.028e-05 5.440e-06 1.890 0.1006
b1 9.458e-04 2.752e-04 3.437 0.0109 *
Signif. codes: 0 '***' 0.001 '**' 0.01 '*' 0.05 '.' 0.1 ' ' 1
Residual standard error: 0.008794 on 7 degrees of freedom
Achieved convergence tolerance: 1.087e-08

Adjust. R-squared: [1] 0.926743

Acacia erioloba

SF = 0.0094xCA² - 0.0178xCA
R² = 0.7835

Parameters:
  Estimate Std. Error t value Pr(>|t|)
a1 0.009428 0.001864 5.058 6.02e-05 ***
b1 -0.017780 0.008695 -2.045 0.0543 .
Signif. codes: 0 '***' 0.001 '**' 0.01 '*' 0.05 '.' 0.1 ' ' 1
Residual standard error: 0.03832 on 20 degrees of freedom
Achieved convergence tolerance: 4.795e-07
Adjust. R-squared: [1] 0.7835063

Figure 6.9 Upscaling functions for *Ochna pulchra, Dichrostachys cinerea* and *Acacia erioloba,*

Acacia luederitzii

$SD = -0.0107 \times CA^2 + 0.9741 \times CA$
$R^2 = 0.8786$

stem diameter (cm) vs *canopy area (m2)*

$SF = 0.001 \times SD^2 - 0.0077 \times SD$
$R^2 = 0.850$

sap flow [lt/h] vs *stem diameter (cm)*

Parameters:
  Estimate Std. Error t value Pr(>|t|)
a1 -0.01065 0.00119 -8.949 1.26e-07 ***
b1 0.97414 0.05666 17.193 9.71e-12 ***
Signif. codes: 0 '***' 0.001 '**' 0.01 '*' 0.05 '.' 0.1 ' ' 1
Residual standard error: 2.431 on 16 degrees of freedom
Achieved convergence tolerance: 2.777e-07
adjusted R2   [1] 0.8786113

Parameters:
  Estimate Std. Error t value Pr(>|t|)
a1 0.0009902 0.0001790 5.532 4.56e-05 ***
b1 -0.0077279 0.0034300 -2.253 0.0386 *
Signif. codes: 0 '***' 0.001 '**' 0.01 '*' 0.05 '.' 0.1 ' ' 1
Residual standard error: 0.05528 on 16 degrees of freedom
Achieved convergence tolerance: 7.568e-06
adjusted R2   [1] 0.8499744

Boscia albitrunca

$SD = -0.0538 \times CA^2 + 3.0524 \times CA$
$R^2 = 0.8709$

stem diameter (cm) vs *canopy area (m2)*

$SF = 0.026 \times SD$
$R^2 = 0.8589$

sap flow [lt/h] vs *stem diameter (cm)*

Parameters:
  Estimate Std. Error t value Pr(>|t|)
a1 -0.05376 0.03133 -1.716 0.124476
b1 3.05243 0.48838 6.250 0.000246 ***
Signif. codes: 0 '***' 0.001 '**' 0.01 '*' 0.05 '.' 0.1 ' ' 1
Residual standard error: 5.116 on 8 degrees of freedom
Achieved convergence tolerance: 1.454e-07
Adjusted -R2   [1] 0.87085

Parameters:
  Estimate Std. Error t value Pr(>|t|)
a1 0.026064 0.001852 14.08 1.96e-07 ***
Signif. codes: 0 '***' 0.001 '**' 0.01 '*' 0.05 '.' 0.1 ' ' 1
Residual standard error: 0.1458 on 9 degrees of freedom
Achieved convergence tolerance: 1.246e-07
Adjusted -R2   [1] 0.8588578

Terminalia sericea

$SA = 0.0524 \times CA^2 + 5.777 \times CA$
$R^2 = 0.8583$

stem area (cm2) vs *canopy area (m2)*

$SF = 2.54E\text{-}06 \times SA^2 + 0.0008 \times SA$
$R^2 = 0.9249$

sap flow (lit/h) vs *stem area (cm2)*

Parameters:
  Estimate Std. Error t value Pr(>|t|)
a1 0.05242 0.08329 0.629 0.5432
b1 5.77776 2.02078 2.859 0.0170 *
Signif. codes: 0 '***' 0.001 '**' 0.01 '*' 0.05 '.' 0.1 ' ' 1
Residual standard error: 30.25 on 10 degrees of freedom
Achieved convergence tolerance: 1.758e-07
Adjusted -R2   [1] 0.8583643

Parameters:
  Estimate Std. Error t value Pr(>|t|)
a1 2.546e-06 1.337e-06 1.904 0.0860 .
b1 8.256e-04 2.550e-04 3.238 0.0089 **
Signif. codes: 0 '***' 0.001 '**' 0.01 '*' 0.05 '.' 0.1 ' ' 1
Residual standard error: 0.03114 on 10 degrees of freedom
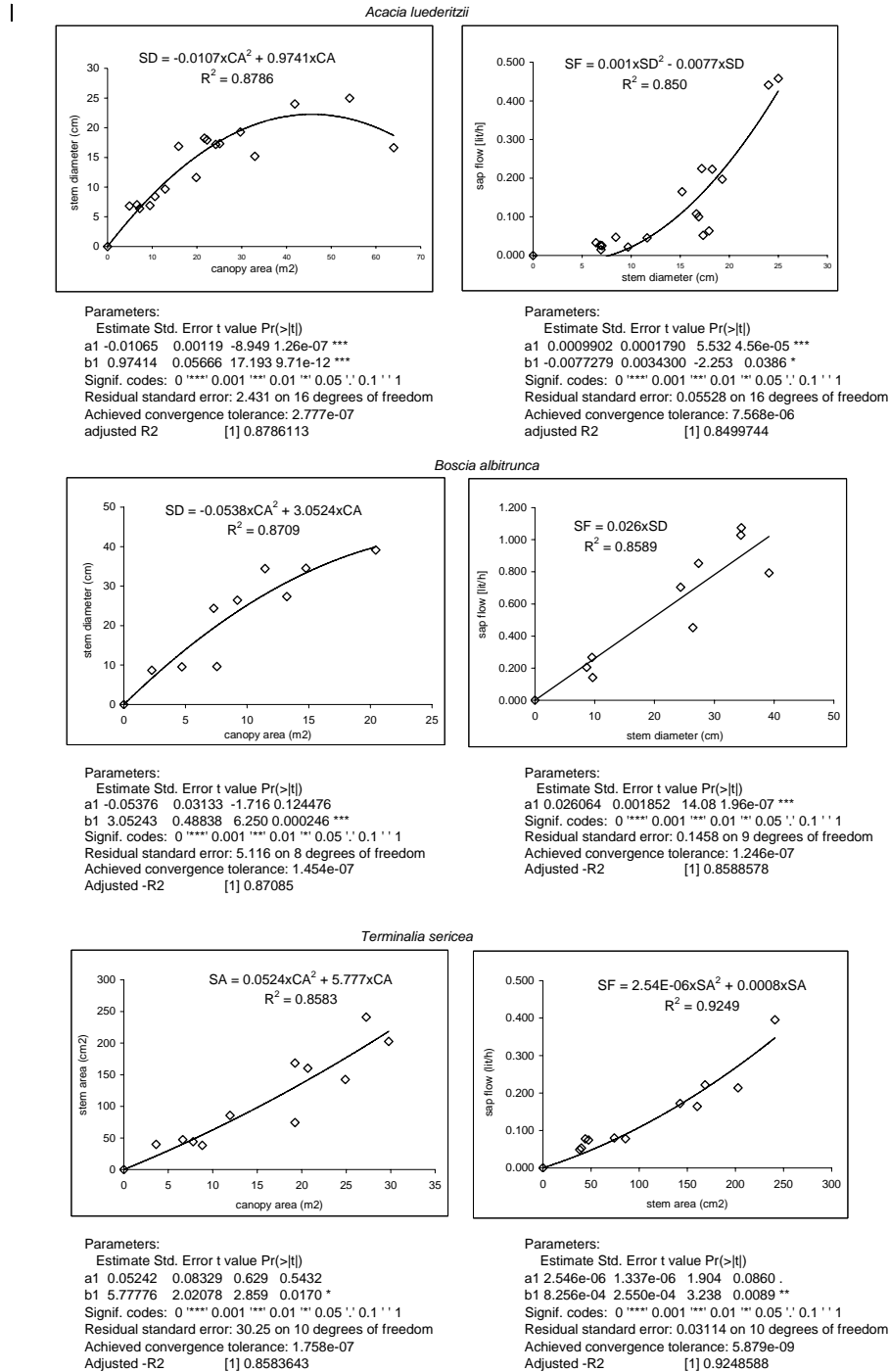Achieved convergence tolerance: 5.879e-09
Adjusted -R2   [1] 0.9248588

Figure 6.10 Upscaling functions *for Acacia luederitzii, Boscia albitrunca* and *Terminalia sericea*

c) tree-canopy transpiration map obtained after applying upscaling functions per species to classified image (the canopy transpiration map provides at a glance an idea of the high-water-consumption species distribution and d) plot transpiration map where sap flow is normalized as mm/day flux over a 25mx25m imaginary grid. The total transpiration flux per sub-area including the number of classified trees per species is presented in Table 6.2
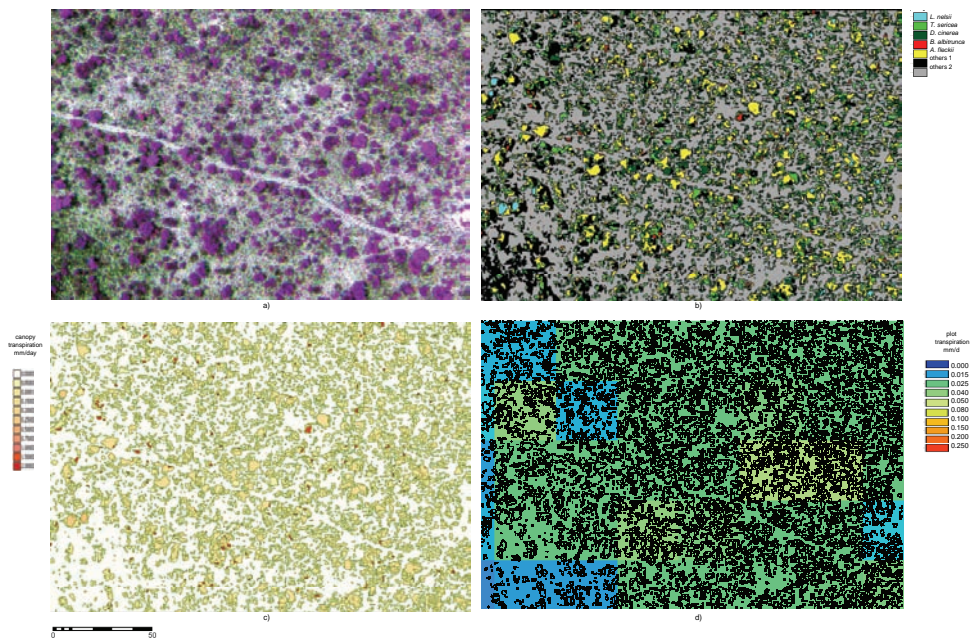

Figure 6.11 Sub-area 1: a) original airborne image 30cm resolution, b) classified image, c) canopy transpiration map and d) plot transpiration

Table 6.2 characteristics of the 5 sub-areas and resulting transpiration fluxes.

sub-area	area	number of classified trees *							tree density	transpiration flux
	m2	L. nelsii	A. fleckii	O. pulchra	D. cinerea	B. albitrunca	T. sericea	total	tree/(25mx25m)	mm/day
1	31998	271	1838		2213	196	2641	7159	140	0.0441
2	20427		131		527		682	1340	41	0.0374
3	21927		173		456			629	18	0.0206
4	14007		118	73	238		261	690	31	0.0220
5	17390		439		606	351		1396	50	0.1647

*Tree density as presented in Table 6.2 refers to the number of classified trees per an imaginary 25mx25m plot. These figures do not include the number of polygons non-classified in the selected categories (such as small shrubs or tree shadows and bare soil). As an additional check of the classification procedure it is worth noting that when tree densities from table 6.2 were converted to specimens per ha., the values are in the same order of magnitude as the tree density reported in the SAFARI 2000 project, corresponding to 400-450mm of precipitation (Caylor *et al.* 2003). The averaged-5 sub-areas tree density from table 6.2 is 895 specimens per ha compared with 972 specimens per ha reported in the referred study.
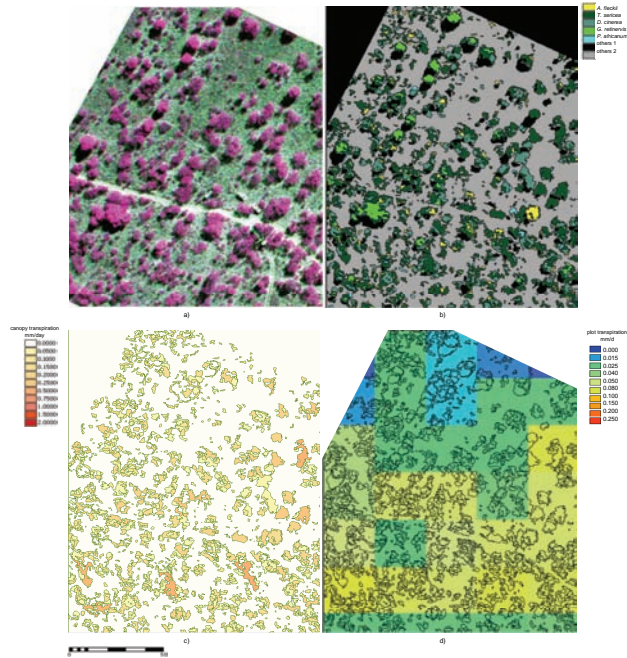
Figure 6.12. Sub-area 2: a) original airborne image 30cm resolution, b) classified image, c) canopy transpiration map and d) plot transpiration
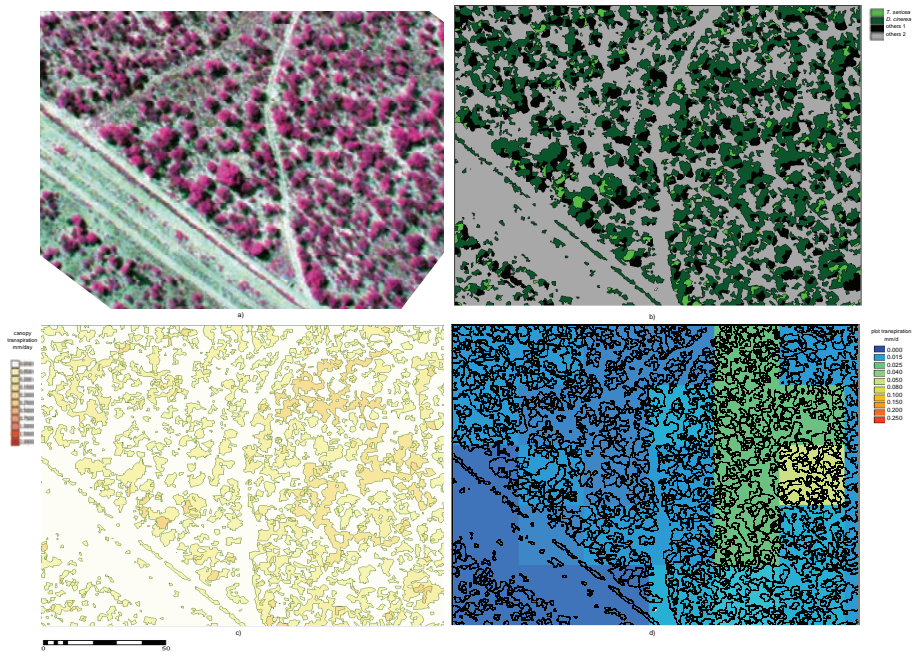

Figure 6.13. Sub-area 3: a) original airborne image 30cm resolution, b) classified image, c) canopy transpiration map and d) plot transpiration
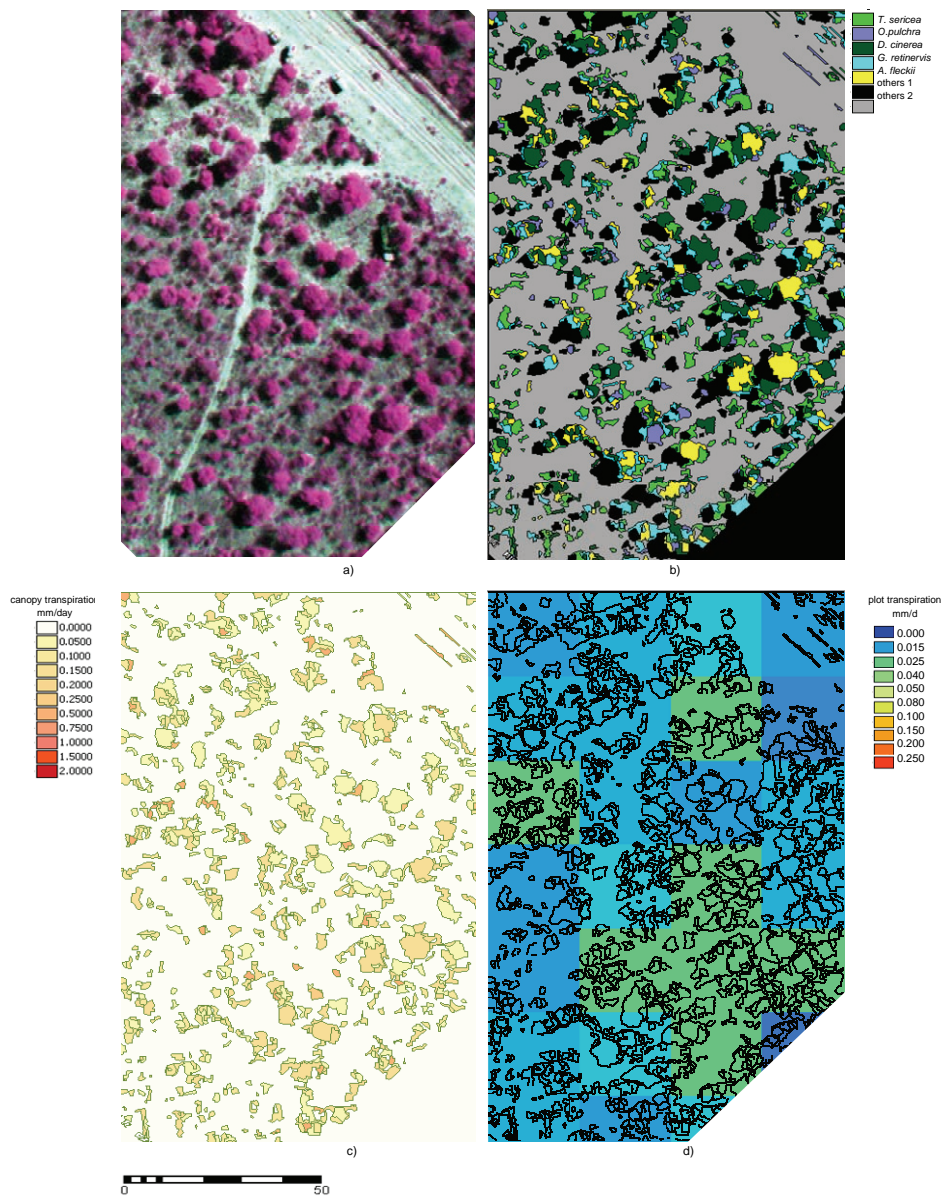
Figure 6.14. Sub-area 4: a) original airborne image 30cm resolution, b) classified image, c) canopy transpiration map and d) plot transpiration
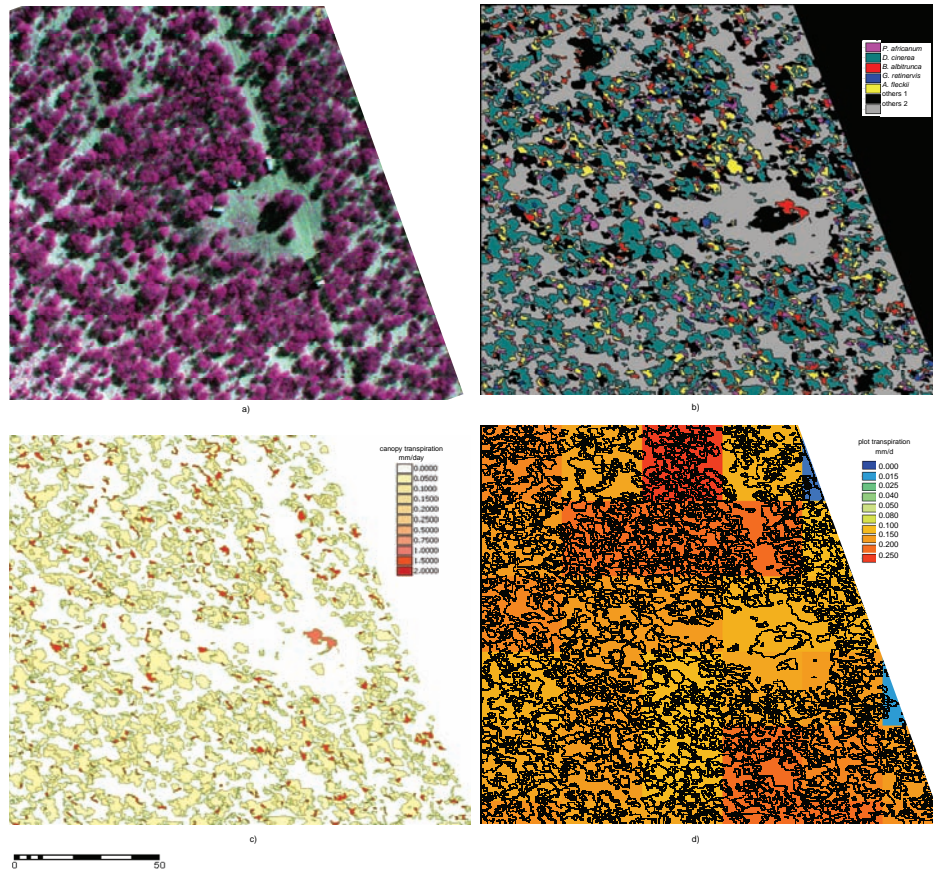
Figure 6.15. Sub-area 5: a) original airborne image 30cm resolution, b) classified image, c) canopy transpiration map and d) plot transpiration.

Transpiration fluxes presented in Table 6.2 confirm that the presence of *Boscia albitrunca* (196 specimens in sub-area1 and 351 in sub-area 5) largely influences the amount of transpiration flux. Careful consideration of the sap flow bimodal pattern described in Chapter 4 is thus critical

Finally, the spatial variability of tree transpiration fluxes in the IKONOS scene based on the sub-areas investigated is presented in Figure 6.16. The abundant presence of species with high sap flow e.g. *Boscia albitrunca* makes a clear differentiation between areas of low (less than 0.05 mm/day, sub-areas 1 to 4) and high (more than 0.1 mm/day, sub-area 5) transpiration.
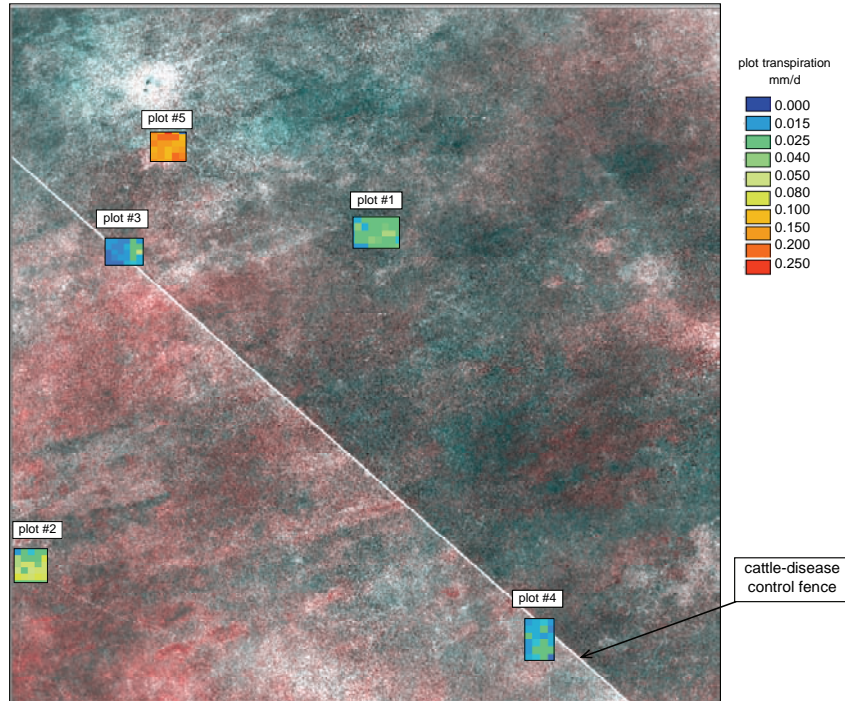
Figure 6.16. Partial spatial variation of tree transpiration in the IKONOS scene obtained from the five sub-areas investigated

6.4   Discussion and Conclusions

Sap flow measurements of some of the tree species measured in the Serowe area showed a bimodal behavior, *i*.e. normal daytime sap flow that can be expressed in terms of transpiration and nocturnal activity, possibly related to mechanisms of water redistribution. Under these circumstances, considerable overestimations of transpiration fluxes can occur if discrimination between these two processes is not considered when determining mean sap flux densities, S_f. For example, in *B. albitrunca* species, S_f was 7.703cm^3/ (cm^{2}xh) while day-time S_f was 5.081cm^3/(cm^{2}xh); this represents an overestimation of ~51%. In *T sericea*, the situation is more critical: 24h-mean S_f was 4.976cm^3/(cm^{2}xh) while daylight time S_f resulted in 2.288cm^3/(cm^{2}xh), i.e. an overestimation of ~117% (values taken from Figure 6.1). However, these conclusions must be taken with caution as they result from only 4 or 5-day continuous measurements of sap flow at the end of the dry season, and therefore they should not be considered representative of the entire vegetative year of the same species.

A further aspect for consideration when developing upscaling functions is the possible effect of clustering in the correlation of sap flow with any biometric parameter. *A. fleckii*, one of the most abundant species in the Serowe area, showed very poor correlation between sap flow and biometric parameters and even among biometric parameters, as described by the statistical indicators presented in Table 6.1. The degree of correlation improved substantially when the same trees were grouped in the original clusters. Similar behavior was observed in *B. albitrunca* trees, although in this case the 24 measured trees belonged to only 9 clusters. This resulted in a data almost one third shorter than the original, which favourably influenced the statistical indicators. On the other hand, the proximity among specimens inside *B. albitrunca* clusters, compared with the distance between clusters, explains the increased correlativity among biometric parameters and supports the resulting good correlation with sap flow estimations. A definite conclusion on the clustering effect of this species would require measurement over a much larger data set, taking care that the number of pairs of variables to be correlated does not decrease significantly after grouping in clusters.

The good correlation between SD and eventually SA with SF has been discussed in similar studies (Hatton *et al.* 1995; Kumagai *et al.* 2005; Vertessy *et al.* 1995; Vertessy *et al.* 1997; Wullschleger and King 2000; Wullschleger *et al.* 1998). In these studies however, the upscaling from tree to stand level is implemented by means of tree inventorying and allometric sampling of the whole stand. In contrast, the upscaling method presented in this thesis exploits the capability of GIS/RS techniques for tree species separation and canopy delineation, therefore reducing the time and resources needed for large areas sampling. The disadvantage of the method is that it has to rely on the correlativeness of ground-projected canopy area as a direct or indirect scalar. The results presented in this chapter confirm that such correlativeness exists and that tree transpiration can be mapped in relatively large plots without a detailed tree inventory.

Among the nine woody species investigated with regards to sap flow, only six were identified in the five mapped sub-areas. Species such as *A. erioloba, A. luederitzii* and *B. africana* grow abundantly in other spots inside the IKONOS-reference area, but a field campaign for these spots was not possible with the resources available for this study. Nevertheless, the five transpiration maps obtained in this study provide some insight into the spatial variation of transpiration fluxes and the most influential species inside the reference area.

Sub-area 5 yielded transpiration fluxes in proportion between 4 to 10 times higher than in the other four sub-areas (0.1647mm/day in sub-area 5 compared with *e.g.* 0.0206 mm/day in sub-area 3) in spite of having tree density similar to sub-areas 2 to 4, and almost three times lower than sub-area 1 as inferred from Table 6.2. The presence of the evergreen *B. albitrunca* species constitutes the determining factor for such high transpiration fluxes. 352 specimens were classified in sub-area 5 and 196 in sub-area 1. In sub-areas 2 to 4 there was no evi-

dence of the existence of this species. Evidence of high transpiration fluxes during the dry season in *B. albitrunca* tree has been highlighted in published studies of the Kalahari (Alias and Milton 2003; Obakeng 2007; Wand et al. 1999). In contrast, in sub-areas in which species such as *D. cinerea* and *T. sericea* are predominant, resulting transpiration fluxes were very low, *e.g.* 0.0206mm/day in sub-area 3 in spite of having a tree density similar to sub-area 5.

Dry-season transpiration maps obtained for 5 sub-areas of the Serowe experimental site resulted in values ranging from almost zero to ~0.25mm/day over an imaginary 25m-cell grid (section d- in Figures 6.11 to 6.15); the total transpiration in the same sub-areas ranged from 0.0206mm/day to 0.1647mm/day.

Although these results should be taken prudently as they inevitably involve the cumulated error of the sap flow measurements, the classification procedure and the upscaling itself, they fall into the range of fluxes correspondent to the dry-season presented by Obakeng (2007). After a continuous sap flow monitoring at seven sites (5-6 tree per site) inside the KRP study area, Obakeng (2007) concluded that the multi-annual plot transpiration rate varied from 3 to 71mm/year during the years 2001 to 2003. During the same years, the dry-season plot transpiration ranged from nearly zero to 0.4mm/day. From another perspective, the general groundwater balance presented in the same study concluded that from the 15mm/year groundwater recharge in the KRP area, only 4mm corresponds to observed discharge and 10mm/year (*i.e.* a multi-species average of 0.027mm/day) are extracted by deep rooting vegetation such as *B. albitrunca*. More detailed information about *B. albitrunca* root morphology and water extraction patterns is presented in Chapter 4 of this thesis.

The suitability of the transpiration mapping based on upscaled sap flow in environments such as the Kalahari can also be assessed by comparison of the results of this approach with the results obtained in previous studies based on energy balance algorithms. To exemplify, applying SEBAL algorithm Bastiaanssen *et al.* (1998), and Timmermans and Meijerink (1999) obtained rates of actual evapotranspiration (AET) ranging from 1.5 - 3 mm/day during the dry season in the Botswana Kalahari. These results were debated by Obakeng (2007), who argued that on average annual scale such values of AET exceed the annual rainfall and therefore cannot be realistic. The same author found fluxes up to 6.1mm/d in the same area when applying temperature profiles surface energy balance (TSEB), which were also found over-scaled. Transpiration fluxes from upscaled sap flow proved to be more realistic and constitute a valid approach, provided that aspects related to sensors functioning, sapwood area determination, careful observation of sap flow patterns and appropriate GIS/RS tools are considered. Discussion of these key aspects is presented in Chapters 2 to 5 of this thesis.

Finally, it should be noted that the mapping of tree transpiration from upscaled sap flow requires the availability of high resolution RS data in addition to a field campaign, to allow accurate species differentiation. The vegetation structure and composition of African savannas such as the Kalahari can often result in the need for very high resolution, *e.g.* less than 1m, airborne images. As discussed in Chapter 5, canopy delineation and classification inside acceptable ranges of accuracy can be only obtained from high resolution RS data. With this constraint, the RS upscaling method could be regarded as unaffordable for low-budget studies. However, the use of simple multi-spectral cameras e.g. TETRACAM as used for this study, properly attached in a small aircraft, can provide individual shots of the tree canopies suitable for small-scale studies. The execution of airborne campaigns with these characteristics must be affordable for small to medium size organizations. When large-scale studies are required, the use of a multi-spectral sensor that can guarantee acceptable levels of radiometric and geometric correctness is advisable. Likewise, the degree of accuracy of transpiration maps generated with the method presented in this thesis depends on the appropriateness of RS data and classification algorithms, as well as the careful acquisition and interpretation of sap flow measurements.

From a financial perspective, an additional advantage of this method is that a single RS image and a single classification procedure can be combined with upscaling functions derived from different seasons of the vegetative year and from several years. In this way, multi-temporal transpiration maps can be created by different sap flow campaigns optimizing the initial investment in an airborne campaign.

References

Alias, D. and S. Milton 2003. A collation and overview of research information on *Boscia albitrunca* (Shepherd's tree) and identification of relevant research gaps to inform protection of the species. Department of Water Affairs and Forestry, South Africa, Pretoria.

Baldocchi, D. and Vogel 1996. Energy and CO_2 flux densities above and below a temperate broad-leaved forest and a boreal pine forest. Tree Physiol. 16:5-16.

Bastiaanssen, W., M. Meneti, R. Feddes and A. Holtslag 1998. The Surface Energy Balance Algorithm for Land (SEBAL): Part 1 formulation. Journal of Hydrology. 212-213 198-212.

Bastiaanssen, W.G.M. and K.M.P.S. Bandara 2001. Evaporative depletion assessments for irrigated watersheds in Sri Lanka. In: Irrigation Science, 21(2001)1, pp. 1-15.

Caylor, K., H. Shugart, P. Dowty and T.M. Smith 2003. Tree spacing along the Kalahari transect in southern Africa. Journal of Arid Environment. 54:281-296.

Granier, A. 1985. Une nouvelle méthode pour la mesure du flux de sève brute dans le tronc des arbres Annales des Sciences Forestières 42:193-200

Granier, A. 1987. Evaluation of transpiration in a Douglas-fir stand by means of sap flow measurement. Tree Physiol. 3:309-320.

Hatton, T.J., S.J. Moore and P.H. Reece 1995. Estimating stand transpiration in a Eucalyptus populnea woodland with the heat pulse method: measurement errors and sampling strategies. Tree Physiol. 15:219-227.

Kumagai, T., H. Nagasawa, T. Mabuchi, S. Ohsaki, K. Kubota, K. Kogi, Y. Utsumi, S. Koga and K. Otsuki 2005. Sources of error in estimating stand transpiration using allometric relationships between stem diameter and sapwood area for *Cryptomeria japonica* and *Chamaecyparis obtusa*. For Ecol Manag. 206:191-195.

Meijerink, A.M.J., A.S.M. Gieske and Z. Vekerdy 2005. Surface energy balance using satellite data for the water balance of a traditional irrigation - wetland system in SW Iran. Irrigation and drainage systems : an international journal. 19

Obakeng, O.T. 2007. Soil moisture dynamics and evapotranspiration at the fringe of the Botswana Kalahari. Vrije Universiteit, Amsterdam, NL.

Privette, J., Y. Tian, R. Roberts, R.J. Scholess, Y. Wang, K. Caylor, P. Frost and M. Mukelabai 2004. Vegetation structure characteristics and relationships of Kalahari woodlands and savannas. Global Change Biology. 10:281-291.

Scholes, R., P. Dowty, K. Caylor, D. Parsons, P. Frost and H. Shugart 2002. Trends in savanna structure and composition along the aridity gradient in the Kalahari. Journal of Vegetation Sciences. 13:419-428.

Timmermans, W. and A. Meijerink 1999. Remotely sensed actual evapotranspiration: implications for groundwater management in Botswana. Interna-

tional Journal of Applied Earth Observations and Geoinformation. 1:222-233.

Vertessy, R.A., R.G. Benyon, S.K. O'Sullivan and P.R. Gribben 1995. Relationships between stem diameter, sapwood area, leaf area and transpiration in a young mountain ash forest. Tree Physiol. 15:559-567.

Vertessy, R.A., T.J. Hatton, P. Reece, S.K. O'Sullivan and R.G. Benyon 1997. Estimating stand water use of large mountain ash trees and validation of the sap flow measurement technique. Tree Physiol. 17:747-756.

Wand, S., K. Esler, P. Rundel and H. Sherwin 1999. A preliminary study of the responsiveness to seasonal atmospheric and rainfall patterns of wash woodland species in the arid Richterveld. Plant Ecology. 142:149-160.

Wullschleger, S.D., P.J. Hanson and D.E. Todd 2001. Transpiration from a multispecies deciduous forest as estimated by xylem sap flow techniques. For Ecol Manag. 143:205-213.

Wullschleger, S.D. and A.W. King 2000. Radial variation in sap velocity as a function of stem diameter and sapwood thickness in yellow-poplar trees. Tree Physiol. 20:511-518.

Wullschleger, S.D., F.C. Meinzer and R.A. Vertessy 1998. A review of whole-plant water use studies in trees. Tree Physiol. 18:499-512.

Chapter 7

Summary and Conclusions

7.1 Introduction and Problem Statement

The Botswana Kalahari is characterised by low rainfall and high evapotranspiration rates. Despite these conditions which contribute towards cataloging the area as a *desert*, the Botswana Kalahari embraces numerous vegetation types including trees, shrubs and grasses. The extent of vegetation in the area has granted the Kalahari the label '*dry savanna*' which appears to be more appropriate than desert. This dichotomy between water shortages and the wide range of vegetation in the Kalahari provides unique opportunities to study vegetation water-use and coping mechanisms.

Previous studies in the Kalahari showed that in its harsh conditions, the survival of vegetation is ensured only if individual species (or co-existent associations of species) are able to implement local mechanisms to overcome regional water scarcity. The results obtained in the KRP provides examples of such mechanisms: the study found that some of the Kalahari species can develop roots as deep as 70m enabling them to make use of deep groundwater reserves. The same study reveals that most of the tree species in the Botswana Kalahari made predominant use of soil water from depths of more than 3m, *i.e.* below the root zone of shrubs and grasses. These findings shed light on how certain species remain green during the critical dry season. However, many uncertainties remain: Do these tree species use *only* groundwater during the dry season? Is the water removed from deep soil layers actually *lost* by transpiration? How do sap flow and transpiration patterns vary throughout the vegetative year and how they are related to hydro-climatic conditions? These uncertainties confirm that the survival mechanisms of Kalahari species are neither completely understood nor fully identified, partly because they are variable in space and time.

This study attempts to identify transpiration patterns and quantify the water abstraction of the predominant species in the eastern Botswana Kalahari, based on

127

upscaled sap flow measurements. The study focuses on the eco-hydrological conditions at the end of the critical dry season in the experimental Serowe site of the KRP.

To accomplish the objective of this study *i.e.* quantification and mapping of transpiration fluxes of the predominant Kalahari species, two major steps were followed: *i)* Field collection and statistical analysis of sap flow measurements and *ii)* RS and GIS processing to produce transpiration maps. The method was developed for the particular conditions of the Kalahari but it can be used in its general form in other water-limited environments where tree transpiration constitutes an unidentified component of the water balance. It is the aim of the author that the results presented in this thesis make a contribution towards a greater understanding of intriguing environments such as the Kalahari.

7.2   Study Area

The area is located in the Central District region of Botswana, at the eastern fringe of the Kalahari basin. The investigation of transpiration patterns was concentrated in a 100km^2-polygon (S 22°20', E 26°20') inside the KPR area, approximately 40km west of Serowe

The area is characterised by permeable sands with high infiltration rates, high retention capacity and negligible surface runoff. The sand mantle of the Kalahari reaches depths ranging from of 0-5m on the eastern fringe to 60-100 m towards the center. The climate is semi-arid with a mean annual temperature of 20°C. The main seasonal contrasts in the study area result from variations in precipitation rather than in temperature, making it more appropriate to talk in terms of wet and dry seasons rather than summer and winter seasons. The area receives a mean annual precipitation (MAP) of 400mm. Rainfall is seasonal, occurring mainly in summer (November to March) and transitional autumn (April to May). Potential evapotranspiration (PET) ranges from 0.1 to 6.3mm/day and show more temporal than spatial variability. The estimated mean annual PET for the years 2002 to 2004 was 1035mm. Perennial surface water streams in the area are non-existent, making groundwater reserves the main source of water supply. Groundwater is mainly found in the Karoo rocks below the thick layer of Kalahari sands. The Ntane formation is considered the main aquiferous unit, replenished principally by the high-intensity summer rainfall. According to the KRP, the groundwater table in the study area can be found at depths between 60 and 100m. A detailed description of the study area is presented in Chapter 1.

The vegetation cover of the study area constitutes open savanna grassland and low thorny trees. Some of these tree species are recognized as having both large tap roots and well developed lateral rooting systems which enable them to

make full use of available soil moisture. This characteristic was confirmed during the KRP. Another important feature related to the water-use habits of the studied species is related to their phenological variation during the vegetative year. Previous studies reveal that moisture availability and air temperature variations are the main environmental cues to their schedule of pheno-phases.

7.3 Sap Flow Measurements

Sap measurements were acquired during the dry season (July to September) of 2004 in the Serowe study area, using thermal dissipation probes (TDP) (UP Gmbh, Germany). Nine tree species were selected based on their frequency of occurrence, namely: *Acacia fleckii, Acacia erioloba, Acacia luederitzii, Boscia albitrunca, Lonchocarpus nelsii, Terminalia sericea, Burkea africana, Ochna pulchra* and *Dichrostachys cinerea*. Continuous records of sap flux densities were collected simultaneously in groups of 18 to 24 individuals of each species during 3 or 4 consecutive days, which allowed the determination of sap flow patterns.

Previous studies show that sap flow measurements with TDP (or any sap flow thermal-based method) conducted in similar climates with large diurnal temperature variations, in sparse vegetation and under low sap flow ranges, are particularly vulnerable to the distorting effect of natural thermal gradients (NTG). With this antecedent and motivated by the observations of the 2004 campaign, a second survey was carried out in May 2005. During this campaign, a new multi-step scheme for the correction of NTG in TDP sensors was tested in four of the nine species measured in 2004. The proposed method introduced an intermittent ON-OFF power mode (commutated signal), while simulating the constant heating conditions in which the TDP method was originally developed. First, the existence of NTG in the studied species was confirmed; next, the commutated power mode was implemented, and finally the TDP raw signal was corrected by modeling it to steady-state to allow the use of the original calibration. Although the corrective method was not available at the time of the 2004 campaign, it was later developed and tested in the same species and therefore it is available for further sap flow measurements. A detailed explanation of the method for NTG correction is presented in Chapter 2.

7.4 Sapwood Area Determination

The estimations of sap flow using TDP in the Kalahari species, highlighted the need to assess current methods of sapwood area evaluation. The hardness of the stem wood in the studied species obviated the use of common methods such as the increment borer. As an initial approach, *cut&dye* method was used whereby cut trees were submerged in a staining solution and thin colored disks were visually analyzed. However, the contradictory sapwood patterns obtained with this

approach motivated the investigation of other methods. Firstly, X-ray computed tomography (CT) was used, from which xylem sectoring in some species was revealed. CT scanning provided a different sapwood boundary compared with the wood staining. Secondly, a more comprehensive approach was implemented, namely nuclear magnetic resonance (NMR), also called magnetic resonance imaging (MRI). The MRI results showed that only a relatively small percentage of the xylem is active in which high to slow speed channels exist. Another important finding related to sapwood delimitation is that the active portion of the xylem varies with time and therefore the *cut&dye* approach reveals only the sap channels active at the moment of the measurement. A review of the principles behind the TDP method led to the conclusion that it is the potential sap conductive area rather than the real-time flowing area that has to be combined with TDP sap flux densities. Although MRI is not yet available for field sapwood determination, it provides valuable insight on xylem (sapwood tissue) functioning. A laboratory experiment using simultaneously MRI, TDP and a volumetric method for sap flow estimations offered not only an accurate estimation of sapwood area for the tree under investigation, but also the possibility of analyzing the advantages and limitation of these methods. In terms of sapwood area estimations, the main conclusion is that wood staining is not an efficient approach as it can mislead the quantification of conductive tissue. Methods such as portable CT or visual observation of fresh wood cores or stem disks can provide more reliable sapwood determination. The subject of sapwood area determination is discussed in detail in Chapter 3.

7.5 Transpiration Patterns in the Kalahari

The ability of Kalahari tree species to survive the eventual stress and pressure of their environment, as described in published literature, results from two main physiological features. First, the existence of convenient root morphology and habits enabling the trees to obtain precious moisture and second, the adjustment of their phenological schedule to reduce periods of transpiration. The way the studied species combine these two physiological characteristics to survive xeric conditions was inferred from the sap flow patterns obtained from the 2004 sap flow campaign. Careful analysis of these survival strategies reflected in the sap flow data set provide important clues for the quantification of transpiration.

As an illustration of some of the survival strategies in the area, species such as *Lonchocarpus nelsii* prevent or reduce transpiration by partial or total defoliation, entering into a state of dormancy throughout the dry season. Remarkable reduction in sap flow magnitude takes place as the dry season progresses compared with earlier periods. Correlation with micro-climatic variables simultaneously measured, suggested that an increase in air temperature might be the environmental cue for defoliation. In species with this behaviour, net transpiration was obtained directly from mean measured sap flow, under the assumption that

all the sap activity recorded at stem level can be expressed in terms of transpiration. Contrastingly, in species maintaining their foliage partly or completely during the dry season, special strategies to acquire the moisture needed for the transpiration process were observed. In species such as *Boscia albitrunca, Terminalia sericea, and Dichrostachys cinerea* a modified concept of hydraulic redistribution was identified based on their sap flow patterns. Under this concept, it is theorized that during part of the day a bi-directional sap flow process takes place. In the case of deep rooted species (*e.g. Boscia albitrunca*), this bi-directional process allows water tapped from deep soil layers to be brought upwards through the stem, branches and leaves for the transpiration process. Water non-transpired is allowed to go downwards (downwards sap flow, DSF) through the same channels to the roots located in the driest soil layers. Moreover, another process is identified where air moisture is collected by tree foliage and twigs in a process termed air moisture harvesting (AMH). Moisture thus collected is channelled through the xylem conduits and flows downwards to the roots and adjacent soil. In species in which DSF was identified (mainly at nighttime) care was taken to subtract these volumes of sap in the transpiration accounts.

Processes such as DSF and AMH observed in this study are species-dependent and occur under specific environmental and tree physiological factors, not yet fully identified. In order to completely understand and quantify the partitioning of moisture stored and sent downwards to different soil layers, additional measurements of sap flow of stem and roots together with soil moisture and water potential profiles are needed. Although sap flow measurements with TDP cannot directly determine and quantify DSF, careful observation of sap flow patterns combined with micro-climatic variables allowed, in this case, the discrimination between periods of transpiration and internal sap flow (hydraulic re-circulation). A comprehensive analysis of sap flow patterns of the species investigated is presented in Chapter 4. This chapter concludes that the monitoring of sap flow provides valuable information about the internal functioning of the tree as it reproduces its schedule of activity or stillness. Moreover, quantification of sap flow allows the identification of tree water-use strategies without going into the complexity of soil moisture dynamics, which are highly influenced by the scale of consideration.

7.6   *GIS/RS to Upscale Sap Flow*

High spatial resolution airborne images (G, R and NIR) and satellite IKONOS imagery of the Serowe experimental area were used to map vegetation as a complementary step to transpiration mapping. Airborne images were acquired using a digital TETRACAM camera mounted on a small aircraft to collect data in 30cm, 60cm and 1m spatial resolution. The classified airborne images were compared with the classification of the 1m pansharpened IKONOS image using eCognition®, an object-oriented classification tool. In environments such as the

Kalahari, such an object-oriented approach proved to be more suitable than previously applied pixel-based methods for species differentiation. The results suggested that due to the clustered composition of some of the Kalahari species, very high resolution images are needed to succeed in individual canopy delineation and classification. After comparing accuracy indicators of the classification using a satellite IKONOS image and airborne TETRACAM images at three spatial resolutions, 30cm resolution TETRACAM images were chosen as the best option to map transpiration. Details of the classification process and accuracy assessment are presented in Chapter 5.

Once RS images inside the experimental 100km^2-polygon were classified, the focus turned to the development of upscaled functions based on the ground measurements of sap flow in the nine species investigated. After analyzing the sap flow patterns (as presented in Chapter 4), mean sap flow (SF) values were correlated with biometric measurements of the same trees for the development of species-specific upscaling functions. Given the capability of GIS/RS techniques for canopy area (CA) determination in the classified images, the upscaling functions used CA as a main scalar. The suitability of different upscaling approaches was investigated in each species, in which CA was directly correlated with SF, or indirectly correlated using as intermediary scalar stem area (SA) or sapwood area (SW). Simple GIS operations were applied to five classified sub-areas of the experimental 100km^2-polygon to obtain maps of transpiration.

The results confirmed that among the nine species investigated, namely *A .fleckii, A. erioloba, A. luederitzii, B. albitrunca, L. nelssi, B. africana, O. pulchra* and *D. cinerea,* the presence of the evergreen *B. albitrunca* defines areas of high water extraction. The total transpiration fluxes in the five images ranged from 0.021mm/day for the image with predominant occurrence of *Dichrostachys cinerea and Terminalia sericea,* to 0.165mm/day for the image where *B. albitrunca* was abundant. The results also highlighted the importance of identifying periods of reverse sap flow before the implementation of upscaling functions. Considering that the TDP sensor does not provide direct information of flow direction and that downward volumes of sap can be substantially high, misinterpretation of the sap flow patterns can result in large overestimations of transpiration. Transpiration fluxes obtained from the RS-based upscaling approach yielded more realistic values than energy balance methods previously applied in the same area. Details on the determination of upscaling functions and GIS procedure for transpiration mapping are presented in Chapter 6.

7.7   Final Conclusions and Further Research

Mapping of transpiration fluxes and identification of species with enhanced sap flow provide valuable information for natural resource management. At a plot

or regional level, transpiration mapping supplies important inputs to regional water balances. In open natural savannas such as the Kalahari, the same information can create awareness at the population level of the effect of high water-consumption species proliferation. In agroforestry systems within water-limited environments, such information can result in constraints on afforestation of certain species due to their effect on groundwater yields.

The results presented in this study show that the combination of ground measurements, laboratory experiments and GIS/RS procedures constitute a robust approach to the mapping of natural processes such as tree transpiration. Sap flow measurements with TDP sensors offers a simple and affordable method for transpiration mapping, provided that sap flow patterns are carefully analyzed and correlated with micro-climatic variables in order to identify processes related to vegetation water-use. The low cost of TDP sensors allows simultaneous measurements of several specimens of each species to facilitate the characterization of sap flow dynamics.

Further research carried out in the Kalahari should include long-term sap flow monitoring of the critical tree species from the water-use point of view. Sap flow measurements must be collected in stems and roots, and ideally rooting depths per individual tree should be investigated. Sap flow sensors should include a flow-direction scheme in at least one individual per site. Additionally, soil moisture and water potential profiles should be obtained. Water-vegetation-climate interactions thus monitored throughout the vegetative (or hydrological year) will provide insight on the vegetation water-use in intriguing environments such as the Kalahari.

Fieldwork and Laboratory Scenes

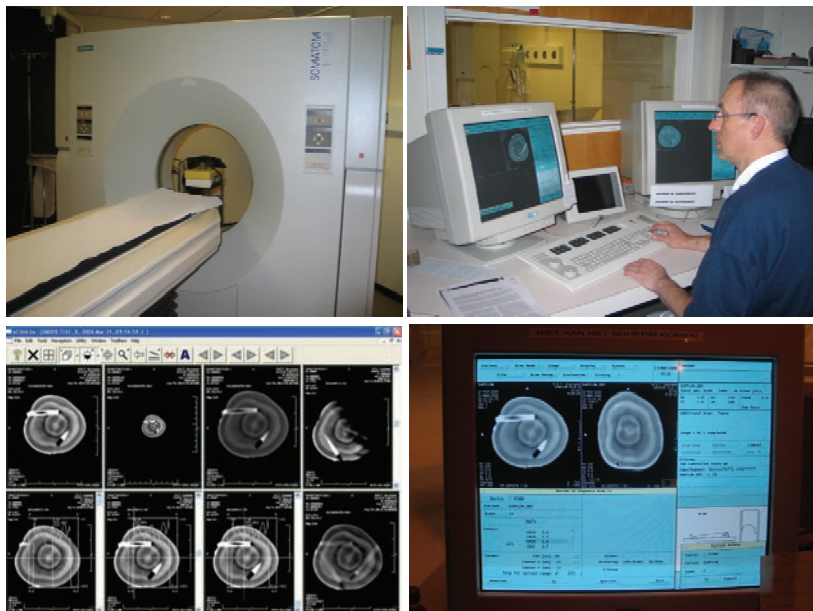Airborne campaign, ground spectral measurements and vegetation sampling. Serowe area, Boswana 2004

2004 and 2005 sap flow campaigns. Serowe area, Botswana.

NMR experiment. Wageningen NL, 2005

X-ray CT scanning. Enschede NL, 2006.

Samenvatting

In droge en woestijnomgevingen zoals de Kalahari, waar het grondwater de belangrijkste bron van water vormt, moet waterextractie door vegetatie uit de onverzadigde en verzadigde zone van de bodem zorgvuldig worden vastgesteld. Uit eerdere studies in deze omgeving is gebleken dat het grondwater kan worden opgevoerd van meer dan 60 m diepte door diepgewortelde boomvegetatie in de vorm van transpiratie. Onderzoeken uitgevoerd door de overheid van Botswana concluderen dat het merendeel van de boomsoorten in de oostelijke Kalahari overheersend gebruik maken van grondwater van een diepte van meer dan 3 m, d.w.z. beneden de wortelzone van struiken en grassen. Deze bevindingen werpen een licht op hoe bepaalde soorten groen blijven tijdens het droge seizoen, maar dragen ook bij tot de bezorgdheid over de invloed van de boomtranspiratie, in vergelijking tot het potentieel behoud van grondwater voor andere doeleinden.

In deze studie wordt een methode voorgesteld voor het in kaart brengen van boom transpiratie door middel van ruimtelijke schaalvergroting van sapstroommetingen. Voor dat doel werden negen boomsoorten van de Kalahari onderzocht, namelijk *Acacia fleckii*, *Acacia erioloba*, *Acacia luederitzii*, *Boscia albitrunca*, *Lonchorcarpus nelsii*, *Terminalia sericea*, *Burkea Africana*, *Ochna pulchra* en *Dichrostachys cinerea*. De selectie van deze soorten was gebaseerd op hun frequentie van voorkomen in het studiegebied. De methodiek wordt gepresenteerd in twee grote stappen: i) sapstroom onderzoek en ii) schaalvergroting en kartering. Het eerste deelonderzoek was gebaseerd op metingen in het veld, gevolgd door laboratorium experimenten. Voor de schaalvergroting en kartering werd gebruik gemaakt van geoinformatie en aardobservatie technieken. Deze aanpak blijkt geschikt voor savanne ecosystemen waarin verschillende soorten naast elkaar bestaan, en waarbij het mogelijk wordt om soorten te identificeren die afhankelijk zijn van deze vorm van transpiratie. Tevens kon de dynamiek van de inherente sapstroom patronen op basis van het onderzoek vastgesteld worden. De methode werd ontwikkeld voor de specifieke omstandigheden van de Kalahari, maar kan ook worden gebruikt in zijn algemene vorm in andere omgevingen.

In de eerste stap, werden sapstroommetingen uitgevoerd door middel van thermische dissipatie sondes (TDP). Hierbij werd het effect van de natuurlijke thermische gradiënten (NTG) grondig geanalyseerd. Complementair werd de kwestie van het watergeleidende spinthout herzien in het licht van de laboratoriumexperimenten met röntgen tomografie en nucleaire magnetische resonantie (NMR). Sapstromen werden berekend als het product van de flux dichtheden gemeten met de TDP in het spinthout, in groepen van 18 tot 24 exemplaren per soort. De verkregen sapstroompatronen in combinatie met microklimaat indicatoren lieten zeer ongewone watergebruikgewoontes van sommige boomsoorten zien, zoals nachtelijke sapstromen, neerwaartse sapstromen in de stam en captatie van wa-

terdamp uit de lucht. Dit werd waargenomen in vier van de negen onderzochte soorten. Dergelijke bevindingen moesten ook worden meegenomen in het ruimtelijke schaalvergrotingsproces.

In de tweede stap, werden de sapstroom van elke gemeten boom direct of indirect gecorreleerd met een door aardobservatie waarneembare en meetbare parameter, namelijk het kroonlaag oppervlak van de boom (CA), voor de opstellen van soortspecifieke ruimtelijke schaalfuncties. Vijf multispectrale beelden opgenomen vanuit de lucht in drie verschillende ruimtelijke resoluties, samen met een IKONOS satellietbeeld van het studiegebied werden ingedeeld met behulp van een object georiënteerde modelbenadering voor beeld interpretatie. De juistheid van deze classificatie bepaald de optimale resolutie waarin boomsoorten kunnen worden gediscrimineerd. Boomsoortspecifieke schaalfuncties, gebaseerd op de correlatie tussen CA en sapstroom werden toegepast op de geclassificeerde beelden, wat resulteerde in kwantitatieve boomtranspiratiekaarten.

De resultaten toonden aan dat onder de negen gemeten soorten, de aanwezigheid van de evergreen boomsoort *Boscia albitrunca,* gebieden van hoge grondwaterextractie definieert. De totale transpiratie flux tijdens het droge seizoen, bepaald in de vijf beelden varieerden van 0,021 mm / dag voor gebieden met overheersende aanwezigheid van *Dichrostachys cinerea* en *Terminalia sericea*, en tot 0.165 mm / dag voor gebieden waar *Boscia Albitrunca* overheersend aanwezig was. Transpiratiefluxen van vegetatie, door middel van aardobservatie gebaseerde ruimtelijke schaalvergroting geeft meer realistische waarden dan de energiebalans methode, eerder toegepast in hetzelfde gebied en tijdens hetzelfde seizoen. De gepresenteerde resultaten in deze studie tonen verder aan dat de combinatie van grondmetingen, laboratoriumexperimenten met geoinformatie en aardobservatie procedures een robuuste aanpak vormen voor het in kaart brengen van natuurlijke processen, zoals waterverbruik door bomen in droge gebieden.

Trefwoorden: geoinformatie, aardobservatie, sapstromen, TDP, boomtranspiratie flux, schaalvergroting.

ITC Dissertation List

http://www.itc.nl/research/phd/phd_graduates.aspx